University of Sussex

Multi-photon processes in cavity QED

Moteb M Alqahtani

Submitted for the degree of Doctor of Philosophy

University of Sussex

January 2014

Declaration

I hereby declare that this thesis has not been and will not be submitted in whole or in part to another University for the award of any other degree.

Signature:

Moteb M Alqahtani

UNIVERSITY OF SUSSEX

MOTEB M ALQAHTANI, Doctor of Philosophy

Multi-photon processes in cavity QED

ABSTRACT

Based on a multi-mode multi-level Jaynes-Cummings model and multi-photon resonance theory, a set of universal two-qubit and three-qubit gates has been realized where dual-rail qubits are encoded in cavities. In this way, the information has been stored in cavities and the off-resonant levels have been eliminated by the theory of an effective two-level Hamiltonian. A further model, namely the spin-J model, has been introduced so that a complete population inversion for levels of interest has been achieved and periodic multi-level multi-photon models have been performed. The combination of the two models has been employed to address two-level, three-level, four-level, and even five-level configurations.

Considering the present cavity-QED experiments, several numerical simulations have been designed in order to check the robustness of the logic gates to variations in experimentally important parameters including the coupling constants and the detunings. Finally, based on Liouville's equation, and the wave-function treatments, the impact of decoherence processes on the fidelity of the qubit states in the iSWAP and the Fredkin gates has been studied.

This thesis may have applications to quantum information processing, involving logic with simple quantum bits, with the possible application to the building of a quantum computer.

Acknowledgments

Of course, thanks to my supervisor Barry Garraway for giving me this studentship. We have had a close collaboration, always running smoothly. As any Professor he has been busy, but I have never felt that I have stood on the same old spot. Thanks to German and Kathryn for their friendship and many interesting chats in the office. Thanks for all the emotional support from all my friends in Brighton.

A special and very deep thanks to my huge family. My mother and father, my sisters and brothers, and many thanks to my wife. This work would not have been possible without your support, in you I feel safe and secure. Thanks to all friends at home, and finally thanks to all those people who I may have missed out.

Contents

List of Tables

List of Figures

Preface

Cavity quantum electrodynamics, or cavity QED, has long been a very preferred area for the study of different phenomena in quantum optics [1]. This field, historically, started when Purcell showed that the spontaneous emission rates were enhanced inside a cavity [2, 3]. The interactions between compound systems inside high-quality cavities can dominate those of the surrounding environment, providing a high degree of coherence [1]. The strong coupling between a two-level "atom" and a single mode of the electromagnetic (or shortly the EM) field is one of the most important properties in cavity-QED: such a property can be very useful for applications in quantum computation [4].

A cavity QED based scheme is the central topic in this thesis. We divide this thesis into three main parts. In the first part, we introduce the standard Jaynes-Cummings model and discuss, in brief, the dynamics of the atom-field system when the initial cavity field is either a Fock state, coherent state, or thermal state. Then, some basic fundamentals in the field of quantum computing have been presented in chapter 2, heavily concentrating on the implementation of quantum computation in the cavity QED field. The theory of periodic multi-photon resonance in a cavity is the main topic in chapter 3. This theory consists of two models, namely the effective two-level Hamiltonian and the spin-J model. Based on this theory and cavity QED, a set of universal gates have been proposed as shown in the following part.

In part II, based on dual-rail qubits encoded in cavities, two-qubit and three-qubit gates have been studied. The iSWAP gate is the main subject in chapter 4. The multi-photon resonance theory developed in part I is employed to analyse several multi-level multi-photon configurations, and then we consider only models being able to obey the truth table of the iSWAP gate. A similar procedure has been repeated in the case of the Fredkin gate in chapter 5. In both cases, numerical simulations have been designed to examine the performance of these operations when variations in some experimentally important parameters have been undertaken. In these simulations, we consider the results provided by the recent cavity-QED experiments (such experiments made by the groups of Prof. G.

Rempe [5], Prof. S. Haroche [6], Prof. H. Kimble [4], and Prof. H. Walther [2]).

In the third part of the thesis, the effects of atomic and photonic relaxations on the proposed gate operations have been investigated. The treatment is first based on Liouville's equation which is solved numerically. The wave-function approach, on the other hand, has been employed to introduce analytical solutions. Here, the influence of the decoherence processes in a qubit state in the iSWAP gate, and in another qubit state in the Fredkin gate, have been addressed. The expressions provided by the wave-function approach give more details and then more understanding on the impact of the dissipation processes on the iSWAP and Fredkin gates.

In this thesis, we realize some photonic logics that may be useful for applications in photonic quantum information processing. Building photonic logics, generally speaking, is an attractive choice since photons form a natural interface with optical telecommunications and existing telecoms technology.

Part I

Background

Chapter 1

Cavity-atom interaction

In 1963, a fully quantized description for light-matter interaction became possible after the appearance of the Jaynes-Cummings model (or shortly JCM). Later, experiments showed that the model is realizable and is able to provide correct predictions and explanations for the observed results (see e.g. [7, 8, 4] and references therein). Recently, this model has been a cornerstone for many applications in the field of quantum optics. For instance, JCM is the starting point for much fruitful research ranging from ultra-cold atoms [9] to quantum information processing [10, 11]. In this thesis, based on a generalisation of the Jaynes-Cummings model, a set of quantum logic gates has been realized for the applications in quantum information processing. In this chapter, we introduce the Hamiltonian describing the interaction between a two-level atom and a quantized field inside the cavity, i.e. the simple JCM.

In Sec. 1.1 we introduce the general Hamiltonian which describes a two-level atom interacting with a single mode under the electric dipole approximation. In the following section, the rotating-wave approximation is assumed and then the Jaynes-Cummings model is produced. The quantized field inside a cavity can be initially in several different states: the number state, the coherent state, or the thermal state. With the main focus on Fock states, we provide a brief introduction for each state in Sec. 1.3. Then, we conclude this chapter in Sec. 1.4.

1.1 The interaction of a single atom with a quantized field

The most simple situation in the JCM is the interaction between a single atom with a single-mode cavity. In this case, the total Hamiltonian can be written as [7, 12, 13, 14]

$$\hat{H} = \hat{H}_A + \hat{H}_F + \hat{H}_{int} \ , \tag{1.1}$$

where $\hat{H}_{\rm A}$ and $\hat{H}_{\rm F}$ are the free atom and the free field Hamiltonians, and $\hat{H}_{int}$ is the atom-field interaction Hamiltonian.

1.1.1 The uncoupled Hamiltonian

For a single atom with the ground and excited states $|a\rangle$ and $|b\rangle$, we define the following atomic operators

$$\begin{aligned} \hat{\sigma}_3 &= |b\rangle\langle b| - |a\rangle\langle a| \ , \\ \hat{\sigma}_{ba} &= |b\rangle\langle a|, \\ \hat{\sigma}_{ab} &= |a\rangle\langle b| \ . \end{aligned} \tag{1.2}$$

The operator $\hat{\sigma}_3$ is nothing but the Pauli operator known for the atomic inversion, and $\hat{\sigma}_{ba}$ and $\hat{\sigma}_{ab}$ are the raising and lowering operators for the atom related to the Pauli operators $\hat{\sigma}_1$ and $\hat{\sigma}_2$ through $\hat{\sigma}_{ba} = \frac{1}{2}(\hat{\sigma}_1 + \mathrm{i}\hat{\sigma}_2)$ and $\hat{\sigma}_{ab} = \frac{1}{2}(\hat{\sigma}_1 - \mathrm{i}\hat{\sigma}_2)$ [15, 16]. It is easy to find that these operators satisfy the commutation relations

$$[\hat{\sigma}_3, \hat{\sigma}_{ba}] = +2\hat{\sigma}_{ba} \ , \ [\hat{\sigma}_3, \hat{\sigma}_{ab}] = -2\hat{\sigma}_{ab} \ , \ [\hat{\sigma}_{ba}, \hat{\sigma}_{ab}] = \hat{\sigma}_3 \ . \tag{1.3}$$

By setting the zero point of energy half-way between the atomic levels $|a\rangle$ and $|b\rangle$ to be the zero-point energy, one can express the atomic Hamiltonian $\hat{H}_A$ as

$$\hat{H}_{\rm A} = \frac{1}{2}\hbar\omega_{ba}\hat{\sigma}_3 \ , \tag{1.4}$$

where $\omega_{ba} = \omega_b - \omega_a$ represents the atomic transition frequency. The second term in Eq. (1.1) is the field Hamiltonian which is nothing but the energy of the harmonic oscillator [15] and can be represented as (see appendix *A* for more details)

$$\hat{H}_{\rm F} = \hbar\omega\left(\hat{a}^\dagger\hat{a} + \frac{1}{2}\right) \ . \tag{1.5}$$

This Hamiltonian considers a single mode whose frequency is ω. The operators $\hat{a}$ and $\hat{a}^\dagger$ are the annihilation and the creation operators for the field mode. These operators are non-Hermitian and satisfy the following commutation relations

$$[\hat{a}, \hat{a}^\dagger] = 1 \ , \quad [\hat{a}, \hat{a}] = [\hat{a}^\dagger, \hat{a}^\dagger] = 0 \ . \tag{1.6}$$

The combination of the previous atom and field Hamiltonians can be denoted as $\hat{H}_0 = \hat{H}_A + \hat{H}_F$ representing the non-interacting terms. The atomic operators $\hat{\sigma}_{ba}$ and $\hat{\sigma}_{ab}$ and the field operators $\hat{a}$ and $\hat{a}^\dagger$ all have no explicit time dependence and can be transformed

into the Heisenberg picture [3]. The Heisenberg's equation for an arbitrary operator $\hat{A}$ having no explicit time dependence is [3, 15, 16]

$$\frac{d}{dt}\hat{A} = \frac{\mathrm{i}}{\hbar}[\hat{H}, \hat{A}] \ . \tag{1.7}$$

For applying this equation to the atomic operators, we simply replace the operator $\hat{A}$ by $\hat{\sigma}_{ba}$ or $\hat{\sigma}_{ab}$ and the Hamiltonian $\hat{H}$ by $\hat{H}_A$; likewise, in the case for the field operators we use $\hat{H}_F$ and $\hat{a}$ and $\hat{a}^\dagger$. One then finds that (with the help of the commutation relations in Eqs. (1.3, 1.6))

$$\hat{\sigma}_{ab}(t) = \hat{\sigma}_{ab}\ e^{-\mathrm{i}\omega_{ba}t} \ , \quad \hat{a}(t) = \hat{a}\ e^{-\mathrm{i}\omega t} \ , \tag{1.8}$$

while the operators $\hat{\sigma}_{ba}$ and $\hat{a}^\dagger$ are the hermitian conjugate of $\hat{\sigma}_{ab}$ and $\hat{a}$. Alternatively, the previous transformations for the atomic and the field operators can be obtained by considering suitable unitary transformations. That is, by using the unitary operators $\hat{U}_\mathrm{A} = e^{-\mathrm{i}\hat{H}_A t/\hbar}$ for atom and $\hat{U}_\mathrm{F} = e^{-\mathrm{i}\hat{H}_\mathrm{F} t}$ for the field, we can obtain the previous time-dependence operators as

$$\hat{\sigma}_{ab}(t) = \hat{U}_\mathrm{A}^\dagger\ \hat{\sigma}_{ab}\ \hat{U}_\mathrm{A}, \quad \hat{a}(t) = \hat{U}_\mathrm{F}^\dagger\ \hat{a}\ \hat{U}_\mathrm{F} \ . \tag{1.9}$$

1.1.2 The interaction Hamiltonian

For a single mode confined within a cavity whose volume is V, the electric field operator $\hat{E}$ at the atomic position z for a standing-wave mode can be given as (see appendix *A*)

$$\hat{E}(z,t) = \sqrt{\frac{\hbar\omega}{\epsilon_0 V}}[\hat{a}(t) + \hat{a}^\dagger(t)]\sin(kz) \ , \tag{1.10}$$

where ω and k are the mode frequency and wavevector. Since the field has, for example, in the visible light a wavelength in order $\lambda \sim 500$nm (longer for microwaves and infrared regions), and the atom radius $a_0 \sim 0.05$nm then $\frac{a_0}{\lambda} \sim 10^{-4}$, we can consider the interaction between the atom and the field to be of the electric dipole form [16]. This implies that the interaction Hamiltonian $\hat{H}_{int}$ in Eq. (1.1) can be expressed as

$$\hat{H}_{int} = -\hat{\mu} \cdot\ \hat{E}(z,t) \ . \tag{1.11}$$

Note that the electric field, under the electric dipole approximation, is no longer spatial dependent. The atomic dipole operator $\hat{\mu}$, on the other hand, can be written as [16]

$$\hat{\mu} = \mu_{ba}^*\ \hat{\sigma}_{ba} + \mu_{ab}\ \hat{\sigma}_{ab} \ . \tag{1.12}$$

For simplicity we can assume that $\mu_{ba}^* = \mu_{ab}$, i.e. it has a real value.

1.2 The Jaynes-Cummings model

By substituting Eqs. (1.10, 1.12) into the interaction Hamiltonian defined by Eq. (1.11), one can find that

$$\hat{H}_{\text{int}} = \hbar g(\hat{\sigma}_{ab} + \hat{\sigma}_{ba})(\hat{a}^{\dagger} + \hat{a}) \ , \tag{1.13}$$

where $g = -\mu_{ab}\sqrt{\frac{\omega}{\hbar\epsilon_0 V}}\ \sin(\kappa z)$ is the coupling strength which has a frequency unit. Once again, under the dipole approximation, we further assume that the coupling strength g is a good approximation independent of z.

The unitary operator $\hat{U} = e^{-\mathrm{i}\hat{H}_0 t/\hbar}$ has been employed to transform the interaction Hamiltonian in Eq. (1.13) into the interaction picture as $\hat{H}'_{int} = \hat{U}^{\dagger}\hat{H}_{int}\hat{U}$. This transformation will produce the atomic and field operators in Eq. (1.8). Consequently, in the interaction picture the Hamiltonian $\hat{H}_{int}$ can be given as

$$\hat{H}'_{\text{int}} = \hbar g(\hat{a}^{\dagger}\hat{\sigma}_{ab}\ e^{-\mathrm{i}(\omega_{ba}-\omega)t} + \hat{\sigma}_{ba}\hat{a}\ e^{\mathrm{i}(\omega_{ba}-\omega)t} + \hat{a}\hat{\sigma}_{ab}\ e^{-\mathrm{i}(\omega_{ba}+\omega)t} + \hat{\sigma}_{ba}\hat{a}^{\dagger}\ e^{\mathrm{i}(\omega_{ba}+\omega)t}) \ . \tag{1.14}$$

Under the condition $\omega \approx \omega_{ba}$ (i.e. the frequency of the mode is near to the corresponding atomic transition frequency), the third and fourth terms in Eq. (1.14) oscillating with the frequencies $\pm(\omega_{ba} + \omega)$ correspond to the process of the atom and the field, which are simultaneously de-excited or excited, respectively. The first two terms, on the other hand, describe the near resonant process in which a photon is emitted as the atom moves from the excited to the ground state (as shown by the term of the form $\hat{\sigma}_{ab}\hat{a}^{\dagger}$), while the term $\hat{a}\hat{\sigma}_{ba}$ corresponds to the inverse process. Moreover, the last two terms vary much more rapidly than the other terms [3, 15, 16, 17]. Jaynes and Cummings [12] neglected the fast oscillating terms in Eq. (1.14), such a procedure is well-known as the rotating-wave approximation (or shortly RWA).

Under the RWA, the interaction Hamiltonian (1.14), therefore, can be reexpressed as

$$\hat{H}'_{int} = \hbar g(\hat{a}^{\dagger}\hat{\sigma}_{ab} + \hat{\sigma}_{ba}\hat{a}) \ . \tag{1.15}$$

The total Hamiltonian $\hat{H}$ in Eq. (1.1) can be, then, rewritten as

$$\hat{H} = \frac{1}{2}\ \hbar\ \omega_{ba}\ \hat{\sigma}_3 + \hbar\ \omega\ \hat{a}^{\dagger}\hat{a} + \hbar g(\hat{a}^{\dagger}\hat{\sigma}_{ab} + \hat{\sigma}_{ba}\hat{a}) \ . \tag{1.16}$$

This Hamiltonian is the Jaynes-Cummings model (JCM) [12]. The Hamiltonian $\hat{H}$ describes a single mode interacting with a single atom. In chapters 4 and 5, where multi-mode cavities interact with a multi-level atom, this simple JC model has been extended to include multiple JC models.

1.3 Dynamics of the atom+field for different initial states of the cavity field

In this section, we consider the JC model above and study the dynamics of the atom-field system in different initial states of the electromagnetic field.

1.3.1 Fock (number) state

Beginning with the Fock (number) state, the actions of the field Hamiltonian $\hat{H}_F$ and the field operators $\hat{a}$ and $\hat{a}^\dagger$ in a single mode number state $|n\rangle$ can be defined as

$$\hat{H}_F|n\rangle = \hbar\omega(n+1/2)|n\rangle, \quad \hat{a}|n\rangle = \sqrt{n}\ |n-1\rangle\ , \quad \hat{a}^\dagger|n\rangle = \sqrt{n+1}\ |n+1\rangle\ . \tag{1.17}$$

It is clear that the states $|n\rangle$ are eigenstates of $\hat{H}_F$ alone, one then can write the eigenvalue equation $\hat{H}_F|n\rangle = E_n|n\rangle$, where $E_n = \hbar\omega(n+1/2)$ is the energy eigenvalue of the energy eigenstate $|n\rangle$. The action of the number operator $\hat{n} = \hat{a}^\dagger\hat{a}$ is another eigenvalue equation as $\hat{a}^\dagger\hat{a}|n\rangle = n|n\rangle$. By multiplying the eigenvalue equation in Eq. (1.17) by either the operator $\hat{a}$ or $\hat{a}^\dagger$ (note that we replace n by $\hat{n} \equiv \hat{a}^\dagger\hat{a}$), it is easy to find (with the help of Eq. (1.6)) that [18]

$$\begin{aligned} \hat{H}(\hat{a}|n\rangle) &= (E_n - \hbar\omega)\hat{a}|n\rangle\ , \\ \hat{H}(\hat{a}^\dagger|n\rangle) &= (E_n + \hbar\omega)\hat{a}^\dagger|n\rangle\ . \end{aligned} \tag{1.18}$$

The physical meaning of Eq. (1.18) is that a quanta of energy $\hbar\omega$ can be generated by the operator $\hat{a}^\dagger$, and a quanta of $\hbar\omega$ is destroyed by the operator $\hat{a}$. The operators $\hat{a}$ and $\hat{a}^\dagger$, therefore, are called the annihilation and creation operators. Furthermore, the zero-point energy in number state $|0\rangle$ has an energy $E_{\text{Z-P}} = \hbar\omega/2$, and it is possible to generate any number state $|n\rangle$ from this state as

$$|n\rangle = \frac{1}{\sqrt{n!}}(\hat{a}^\dagger)^n\ |0\rangle\ . \tag{1.19}$$

Considering the JC model above, we seek now to study the dynamics of a compound system (atom+field) in the case of Fock state being the initial state of the field. Assuming a two-level atom in the ground state $|a\rangle$ passing through a cavity with a single mode in the number state $|n\rangle$, the initial state of the atom-field system is then $|\Psi(0)\rangle = |a,n\rangle$. The interaction part in the Hamiltonian $\hat{H}$ (1.16) tells us that this state is only allowed to couple the state $|b,n-1\rangle$. In the interaction picture, the statevector of the compound system, consequently, can be a superposition

$$|\Psi(t)\rangle = c_1(t)\ |a,n\rangle + c_2(t)\ |b,n-1\rangle\ . \tag{1.20}$$

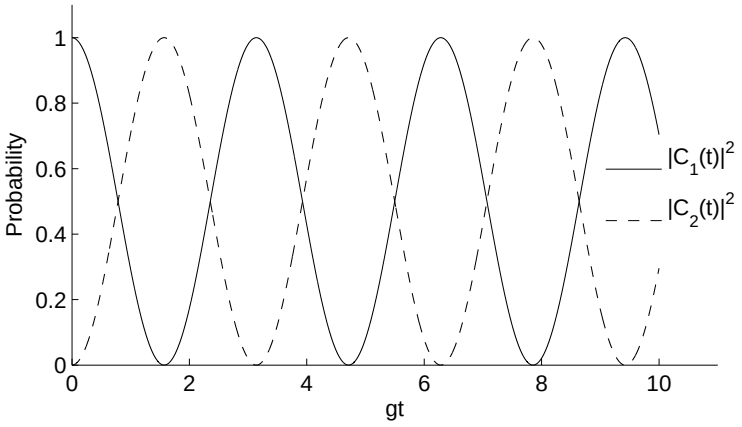

Figure 1.1: Rabi oscillations between the states $|a, n\rangle$ and $|b, n-1\rangle$ at the Rabi frequency $g\sqrt{n}$ with the cavity field initially in the number state and $n = 1$. $|c_1(t)|^2 = \cos^2 g\ t$ and $|c_2(t)|^2 = 1 - |c_1(t)|^2$.

Given the basis states $\{|a, n\rangle, |b, n-1\rangle\}$, in this space the Hamiltonian describing the system can be written, in the matrix form, as

$$\hat{H}' = \begin{pmatrix} 0 & g\sqrt{n} \\ g\sqrt{n} & \Delta \end{pmatrix} , \tag{1.21}$$

where $\Delta = \omega_{ba} - \omega$ is the detuning. Note that we set the initial state $|1, n\rangle$ to be the zero-point energy. By substituting the initial state $|\Psi(0)\rangle$, the system wavefunction $|\Psi(t)\rangle$, and the time-independent Hamiltonian $\hat{H}'$ into Schrödinger's equation $|\Psi(t)\rangle = \exp(-\mathrm{i}\hat{H}'t)\ |\Psi(0)$, the time evolution of the initial state, at the resonance case $\Delta = 0$ and with the initial conditions $c_1(0) = 1$ and $c_2(t) = 0$, can be expressed as

$$|\Psi(t)\rangle \mapsto \cos(g\sqrt{n}\ t)\ |a, n\rangle - \mathrm{i}\sin(g\sqrt{n}\ t)\ |b, n-1\rangle\ . \tag{1.22}$$

This system oscillates between the basis states with Rabi frequency $2g\sqrt{n}$ (see Fig. 1.1). In the case of the atom being initially excited, we can find directly that the initial state $|b, n\rangle$ is coupled to $|a, n+1\rangle$ with a Rabi frequency $2g\sqrt{n+1}$. If the cavity is initially empty (i.e. the field is initially in the vacuum number state $|0\rangle$), the system is still able to oscillate between the basis states, such oscillations are well-known as vacuum Rabi oscillations [15]. The observation of these oscillations require that the coupling strength between the atom and the field inside a cavity is much larger than the coupling to the surrounding environment. We will see in subsequent sections that these requirements can be efficiently met in the field of cavity QED.

In this thesis, we employ the number (Fock) state in the realization of a set of quantum

logic gates, namely the iSWAP and the Fredkin gates. For completeness, we below briefly introduce another two important states for the cavity field: the coherent and the thermal states.

1.3.2 Coherent and thermal states

A cavity field can be described by the coherent state [19]. This state is a right eigenstate of the annihilation operator $\hat{a}$, and a left eigenstate of the creation operator $\hat{a}^\dagger$ [16]. The action of $\hat{a}$ in this state can be defined as

$$\hat{a}\ |\alpha\rangle = \alpha\ |\alpha\rangle\ , \tag{1.23}$$

where α is a complex number. This state can be generated from the number states above. That is, by exploiting the orthonormality ($\langle n|n'\rangle = \delta_{n,n'}$) and the completeness ($\sum_{n=0}^{\infty} |n\rangle\langle n| = I$) for the number state, one can easily expand the coherent state in terms of the number state (with the help of the completeness theory $|\alpha\rangle = (\sum_{n=0}^{\infty} |n\rangle\langle n|)|\alpha\rangle$ and the expressions [1.19, 1.23]) as

$$|\alpha\rangle = e^{-\frac{1}{2}|\alpha|^2} \sum_{n=0}^{\infty} \frac{\alpha^n}{\sqrt{n!}}\ |n\rangle\ . \tag{1.24}$$

Once again we assume an atom in ground state $|a\rangle$ interacts with a field initially now in a coherent state $|\alpha\rangle$ (i.e. $|\Psi(0)\rangle = |a, \alpha\rangle$. As we have seen previously the state $|a, n\rangle$ is coupled only to $|b, n-1\rangle$ and then the atom-field wavefunction in the interaction picture can be expressed as

$$|\Psi(t)\rangle = e^{-\frac{1}{2}|\alpha|^2} \left[|a,0\rangle + \sum_{n=1}^{\infty} \frac{\alpha^n}{\sqrt{n!}}\ [c_1(t)|a,n\rangle + c_2(t)\ |b,n-1\rangle]\right]\ . \tag{1.25}$$

Note that the uncoupled state $|1,0\rangle$ is included in the summation above, and the amplitudes $c_1(t)$ and $c_2(t)$ can be found in Eq. (1.22). Revivals and collapses of the Rabi oscillations (firstly observed by [20]) can be produced by the coherent state, as shown by the time-dependence of the excited state probability $|\langle b, n-1|\Psi(t)\rangle|^2$ in Fig. 1.2.

Unlike the previous states, thermal state (as another possible state for a quantized single-mode) can not be represented by a statevector but alternatively by a density matrix ρ. Once again, in the number state basis, thermal state can be defined as

$$\rho = \sum_{n=0}^{\infty} P_n |n\rangle\langle n|\ . \tag{1.26}$$

The probability P_n of finding n photons in the field is [3, 16]

$$P_n = \frac{\bar{n}^n}{(1+\bar{n})^{1+n}}\ , \tag{1.27}$$

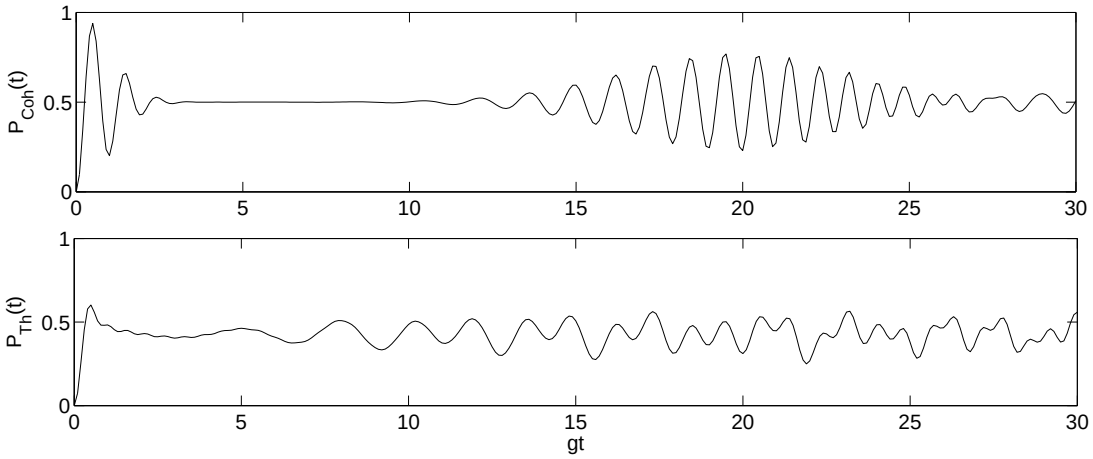

Figure 1.2: The probability of the excited state in the Jaynes-Cummings model with the cavity field initially in: (top) a coherent state where the photon number distribution $P_n = \exp(-\bar{n})\bar{n}^n/n!$ with $\bar{n} = |\alpha|^2$, (down) a thermal state with $P_n = \frac{\bar{n}^n}{(1+\bar{n})^{1+n}}$. The mean photon $\bar{n}$ is set to $\bar{n} = 10$.

where the average photon number is $\bar{n} = \mathrm{Tr}(\rho\ \hat{\mathrm{n}}) = (\mathrm{e}^{\hbar\omega/\mathrm{k_B T}} - 1)^{-1}$ with k_B as the Boltzmann constant and T is the absolute temperature. This expression for $\bar{n}$ shows that the number of thermal photons increases with longer wavelengths λ, implying that lower temperatures for the cavity are required more in the microwave cavity-QED experiments than in those experiments in the optical regime (further examples will be given in subsequent chapters).

Under the same initial conditions in the previous states and with the help of Eq. (1.22), we can find that the excited state probability is

$$\langle b, n-1|\rho|b, n-1\rangle = P_b(t) = \sum_{n=0}^{\infty} \frac{\bar{n}^n}{(1+\bar{n})^{1+n}}\ \sin^2(g\sqrt{n}\ t)\ . \tag{1.28}$$

In Fig. 1.2, it is clear that the quantized field in a thermal state follows a chaotic behaviour.

1.4 Summary

In this chapter, a simple Jaynes-Cummings model, as a fully quantized model for the atom-light interaction, is introduced. This soluble model is the starting point for many investigations in the field of quantum optics. Considering the electric dipole and the rotating-wave approximations, the JC Hamiltonian has been given. Then, examples of the dynamics of the atom-field system with the JC model and for different initial states for a cavity field have been, in brief, discussed.

In chapters 4 and 5, multiple JC models are considered for the study of the interactions

of multi-mode cavities with few atom systems. The decoherence properties of the systems will be the subject of chapter 6 and so will the dissipation process in the previous JC model. For the applications in quantum information processing, we only consider Fock state as the initial state for the cavity field.

Chapter 2

Elements of quantum computation

In 1985, Deutsch [21] employed the fundamental concepts in quantum mechanics, namely superposition and entanglement, to propose a quantum computer. Furthermore, Deutsch in [22] showed that the processing of information can be more efficient than in the case of conventional computers. He compared classical and quantum algorithms solving problems in which many repetitions of some task were required. Classical computers then have to look through all entries and make many repetitions of the simple task, whereas in quantum computers, fewer steps are needed. These steps may include preparing a well-defined initial state, establishing a superposition of all possible states, applying some transformations to this superposition, and then reading out.

Moreover, the quantum factoring and searching algorithms represented by Shor [23] and Grover [24] strongly confirmed, in principle, that quantum computers can manipulate difficult computation tasks in a way that is faster and simpler than any known classical algorithms. More precisely, on the one hand, the quantum computation in those quantum algorithms solves a class of problems with certainty in exponentially less time compared to any classical computation. On the other hand, by working out an example of quantum algorithm that is based on Hadamard transform (see Table 2.1), Grover found that quantum mechanical algorithms are likely to be much simpler to implement than classical algorithms which are based on large scale Fourier transform. These findings and others shown later all contribute to the birth of a new field known as quantum information processing (QIP), which in turn has many subfields such as cryptography and teleportation, quantum simulation, and quantum computation.

In subsequent sections, the basic unit in QIP (qubit) is introduced in Sec. 2.1. Then, quantum logic gates and some well-known one- and multi-qubit gates are discussed in Sec. 2.2. The implementation of quantum computation in a physical system such as

cavity-QED is considered in Sec. 2.3, and finally we conclude in Sec. 2.5.

2.1 Quantum bits

In quantum information theory [15], a system with only two energy levels conventionally denoted as $|0\rangle$ and $|1\rangle$ can be described by a state $|\Psi\rangle$ as

$$|\Psi\rangle = c_1|0\rangle + c_2|1\rangle \ , \tag{2.1}$$

where c_1 and c_2 are complex numbers and $|c_1|^2 + |c_2^2| = 1$. This implies that the quantum system can be in the level $|0\rangle$ or $|1\rangle$ or in a combination "superposition" of the two. In this theory, quantum information can be stored and manipulated in $|\Psi\rangle$. In classical devices, in contrast, the elementary unit of information is a bit which has two states and can store 0 or 1. It is then clear that in the quantum view, information can be stored and manipulated in infinitely many quantum states compared to only one value in a classical bit. In analogy to classical information theory, a quantum state $|\Psi\rangle$ can be considered as a quantum bit (or qubit) and $|0\rangle$ and $|1\rangle$ can replace the values 0 and 1.

The previous qubit $|\Psi\rangle$ may describe only a single quantum system, so $|\Psi\rangle$ is a single qubit. Quantum mechanics allows, on the other hand, a system to contain two or more correlated quantum systems, so two- or many-qubit systems can be considered. For example, Bell states [15] represent the well-known double-qubit states

$$\begin{aligned} B_{00} &= \frac{1}{\sqrt{2}}(|00\rangle + |11\rangle), \ B_{01} = \frac{1}{\sqrt{2}}(|01\rangle + |10\rangle), \\ B_{10} &= \frac{1}{\sqrt{2}}(|00\rangle - |11\rangle), \ B_{11} = \frac{1}{\sqrt{2}}(|01\rangle - |10\rangle) \ . \end{aligned} \tag{2.2}$$

Greenberger-Horne-Zeilinger (GHZ) states [25] (with $|\mathrm{GHZ}\rangle = \frac{1}{\sqrt{2}}(|000...0\rangle \pm |111...1\rangle)$) and the W states [15] (where $|\mathrm{W}\rangle = \frac{1}{\sqrt{N}}(|000...1\rangle + |001...0\rangle + |010...0\rangle + |100...0\rangle)$) are examples of three or more qubit states.

In the previous examples of n qubits (with $n > 1$), the states are said to be entangled; the states can not be written as a product of states (i.e. $\rho \neq \sum_i \ p_i \ \rho_1^i \otimes \rho_2^i \otimes \cdots \otimes \rho_n^i$).

In atom-cavity interactions (see Sec. 1.2), quantum information can be stored in either atoms or cavity modes, producing atomic or photonic qubits, respectively. Encoding qubits in either atoms or photons can be employed in significant applications in quantum information processing and quantum computing (see for example [4]). In chapters 4 and 5, we discuss a theoretical scheme for building n-qubit gates (with $n = 1, 2,$ and 3) in which information is stored in photonic qubits.

Logic gate U	$\|0\rangle$	$\|1\rangle$
X	$\|1\rangle$	$\|0\rangle$
Y	$\mathrm{i}\,\|1\rangle$	$-\mathrm{i}\,\|0\rangle$
H	$\frac{1}{\sqrt{2}}(\|0\rangle + \|1\rangle)$	$\frac{1}{\sqrt{2}}(\|0\rangle - \|1\rangle)$
G	$\|0\rangle$	$e^{i\theta}\|1\rangle$

Table 2.1: Actions of some important single-qubit gates in the computation basis $\{|0\rangle, |1\rangle\}$. These gates include Pauli X and Y, Hadamard H, and the Phase gates G. Setting the value of the phase θ as $\theta = 0,\ \pi/4,\ \pi/2,\ \pi$, the operation G represents the unity I, the phase shift operations T and S, and Pauli-Z gate, respectively.

2.2 Logic gates

Only unitary operators (by definition an operator $\hat{U}$ is said to be unitary if it satisfies $\hat{U}^\dagger = \hat{U}^{-1}$) that preserve the normalization condition $\sum_\alpha |c_\alpha|^2 = 1$ of the register's wavevector $|\Psi_n\rangle$ are considered in quantum circuits [15, 25]. We have mentioned previously that for n-qubit state, n can have values $n \geq 1$. Therefore, for single-, double-, and multi-qubit states there are, respectively, single-, two-, and multi-qubit logic gates.

2.2.1 Single-qubit gates

Beginning with single qubit gates, actions of some important one-qubit gates can be found in table 2.1. For example, the Pauli X gate transforms the qubit state in $|A\rangle$ (where in the computation basis $A \in \{|0\rangle, |1\rangle\}$) according to $\mathrm{X}|0\rangle \mapsto |1\rangle$ and $\mathrm{X}|1\rangle \mapsto |0\rangle$.
Pauli X, Y, and Z gates are nothing but Pauli spin-1/2 operators $\hat{\sigma}_x$, $\hat{\sigma}_y$, and $\hat{\sigma}_z$, respectively. The exponential of Pauli operators produces very useful rotation operators $R_n(\theta) = \exp(-\mathrm{i}\theta\ \hat{n}\cdot\hat{\sigma}/2)$ where the vectors $\hat{\sigma} = (\sigma_x, \sigma_y, \sigma_z)$ and $\hat{n} = (n_x, n_y, n_z)$ [26]. In matrix form, these rotation operators can be explicity represented as

$$R_x(\theta) = \begin{pmatrix} \cos(\frac{\theta}{2}) & -\mathrm{i}\sin(\frac{\theta}{2}) \\ -\mathrm{i}\sin(\frac{\theta}{2}) & \cos(\frac{\theta}{2}) \end{pmatrix},\ R_y(\theta) = \begin{pmatrix} \cos(\frac{\theta}{2}) & -\sin(\frac{\theta}{2}) \\ \sin(\frac{\theta}{2}) & \cos(\frac{\theta}{2}) \end{pmatrix},\ R_z(\theta) = \begin{pmatrix} e^{-\mathrm{i}\frac{\theta}{2}} & 0 \\ 0 & e^{\mathrm{i}\frac{\theta}{2}} \end{pmatrix}.$$

In order to build a universal gate set, in addition to a multi-qubit gate, rotation operators are required [26]. In appendix B, we show that two rotation operators, namely $R_x(\theta)$ and $R_z(\theta)$ operations can be realized by our scheme.

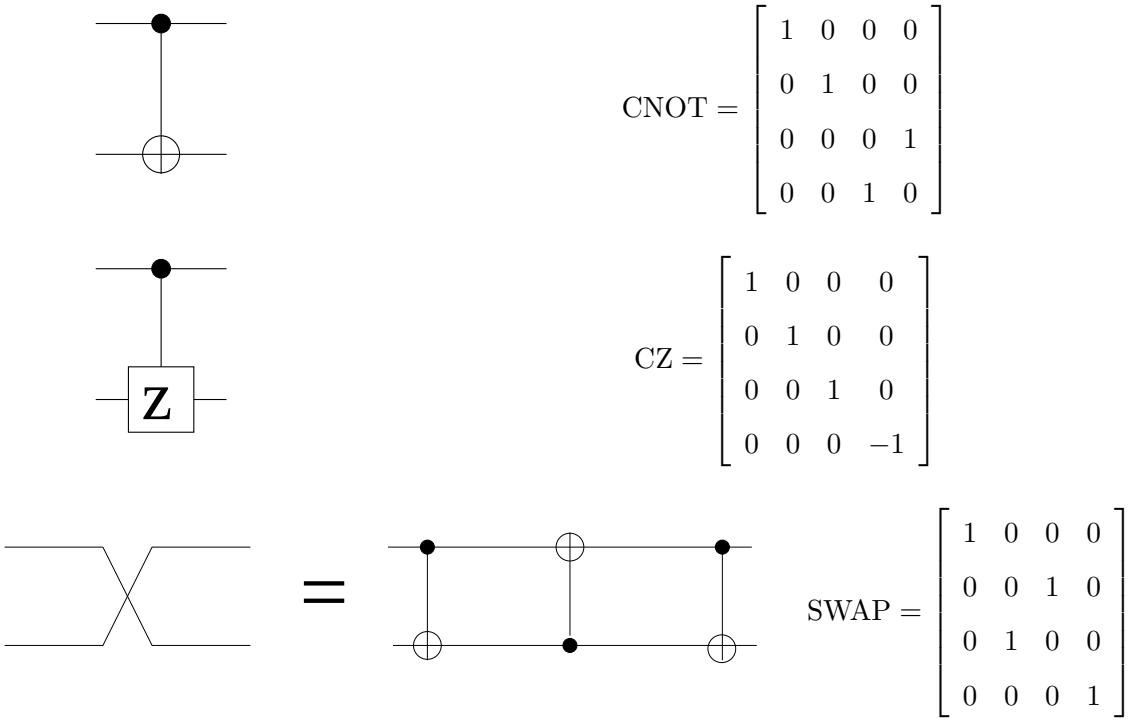

$$\text{CNOT} = \begin{bmatrix} 1 & 0 & 0 & 0 \\ 0 & 1 & 0 & 0 \\ 0 & 0 & 0 & 1 \\ 0 & 0 & 1 & 0 \end{bmatrix}$$

$$\text{CZ} = \begin{bmatrix} 1 & 0 & 0 & 0 \\ 0 & 1 & 0 & 0 \\ 0 & 0 & 1 & 0 \\ 0 & 0 & 0 & -1 \end{bmatrix}$$

$$\text{SWAP} = \begin{bmatrix} 1 & 0 & 0 & 0 \\ 0 & 0 & 1 & 0 \\ 0 & 1 & 0 & 0 \\ 0 & 0 & 0 & 1 \end{bmatrix}$$

Figure 2.1: Controlled-NOT (CNOT), controlled-Z (CZ), and the SWAP gates and their associated unitary matrices. It is shown that the quantum circuit of three CNOT gates is equivalent to the SWAP gate.

2.2.2 Multi-qubit gates

Fig. 2.1 shows examples for two-qubit gates. For a two qubit state $|AB\rangle$, the first qubit A is considered to be the control qubit and the second qubit B is the target qubit with $A, B \in \{|0\rangle, |1\rangle\}$. In the prototypical two-qubit gate CNOT, for instance, this operation flips the target qubit if the control qubit is in $|1\rangle$; otherwise, $|AB\rangle$ remains unchanged. The SWAP gate exchanges the states of two qubits; the two-qubit phase gate CZ introduces a phase only when both control and target qubits are $|1\rangle$(see Fig. 2.1).

Controlled-controlled operation are examples of a three-qubit gate. That is, controlled-CNOT, controlled-CZ, and controlled-SWAP are equivalent to the three-qubit Toffoli, phase, and Fredkin gates, respectively. For a three qubit state $|ABC\rangle$, Toffoli gate works if the first and the second qubits (i.e. qubits A and B, respectively) are in the state $|1\rangle$, whereas in the three-qubit phase gate a phase is introduced only when all qubits are $|1\rangle$. In Fredkin gate, if $|A\rangle$ is set to $|1\rangle$ the gate interchanges qubits B and C.

Remarkably, any double- and multi-qubit gates can be decomposed into a number of CNOT gates plus several single-qubit gates [27, 28]. In other words, the two-qubit CNOT gate is universal. Moreover, the two-qubit gates such as CZ and $\sqrt{\text{SWAP}}$ are as good

as the CNOT gate and can be considered as universal gates [15, 29]. More generally, an entangling two-qubit gate with a set of single-qubit gates is universal [30].

As demonstrated in Fig. 2.1, the SWAP gate can be realized by three CNOT gates [25]. The measurement realized by these operations can be determined by the action of this circuit on the input qubits $|00\rangle$, $|01\rangle$, $|10\rangle$, $|11\rangle$ as follows

$$\begin{aligned} |00\rangle &\mapsto |00\rangle \mapsto |00\rangle \mapsto |00\rangle \\ |01\rangle &\mapsto |01\rangle \mapsto |11\rangle \mapsto |10\rangle \\ |10\rangle &\mapsto |11\rangle \mapsto |01\rangle \mapsto |01\rangle \\ |11\rangle &\mapsto |10\rangle \mapsto |10\rangle \mapsto |11\rangle \ . \end{aligned} \tag{2.3}$$

In chapters 4 and 5, the two- and three-qubit SWAP gates are in the centre of our scheme.

2.3 Quantum computing in cavity-QED

In quantum computing, the coupling between quantum information units (qubits) must be much stronger than the coupling between qubits and the surrounding environment. This helps to isolate these qubits from its environment and highly control them [4]. It is reported that a number of physical systems can meet to some extent such requirements. These systems include, for instance, Nuclear magnetic resonance (or shortly NMR) [31], Linear optics with single photons [32], Semiconductor quantum dots [33, 34], Linear ion-traps [35], and Cavity-QED [10].

In cavity-QED, a strong coupling between information carriers (qubits) has been recently achieved. We have seen previously that for a single atom interacting with a single mode, the coupling energy can be given by $\hbar g = \hat{\mu} \cdot \hat{E}$. From Eq. (1.10) the field per photon expressed as $\sqrt{\frac{\hbar\omega}{\epsilon_0 V}}$ within a very small cavity V can be very large with ω being either in optical or microwave regions. Indeed, a very small V in current cavities in either optical or microwave cavity-QED experiments is reported. For example, in the microwave regime the cavity dimensions are generally in millimeter order [8], and they can be in μm scale in the optical domain [4]. Moreover, in experiments for semiconductor quantum dots, nanocavities are fabricated [36]. Consequently, a large value for the coupling strength g compared to the dissipative mechanisms (such as atomic and photonic decay rates) is reached in the present cavity-QED experiments.

Recent experiments in cavity-QED provide a very weak coupling to the surrounding environment. We will see in chapter 6 that dissipative mechanisms such as the spontaneous emissions Γ or the cavity decays κ are highly reduced, and the strong coupling regime

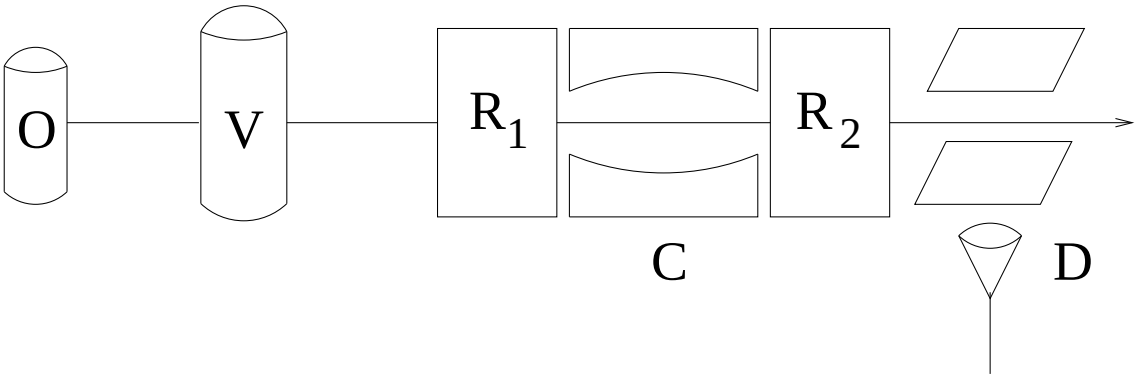

Figure 2.2: Sketch of the main apparatus in CQED experiments. Velocity-selected Rydberg atoms excited to desirable atomic states and one by one cross cavity C and are classically manipulated by Ramsey zones R_1 and R_2. The atomic state is finally measured by a detector D.

(i.e. $g >> \Gamma,\ \kappa$) is dominant in most CQED techniques. This shows that cavity-QED is probably one of the suitable systems for quantum computer implementations.
Depending on the wavelength of the EM field prepared inside a cavity, cavity-QED in a strong coupling regime can be reached in optical or microwave domains. With a smaller volume of cavity, coupling constants in optical CQED can be larger, but trapping and addressing atoms inside cavities would be more difficult [4]. In a microwave regime, on the other hand, cavity dimensions are larger and, then, easier to control atoms inside the cavity, but experiment apparatus must be cooled to very low temperatures to eliminate excited photons (see Sec. 1.3.2). So, both regimes have advantages and difficulties.

2.4 General set-up for cavity-QED experiments

We now describe in brief the main stages in a cavity-QED experiment. Generally speaking, in the optical and microwave cavity-QED experiments three main stages can be considered: the preparation of the initial atomic state, the photon-atom interaction, and the detection of the atomic state outside the cavity.
In the preparation stage, atoms are emitted by an oven O, and then, by a set of classical fields, the initial state of the atoms can be prepared and their velocity can be selected. Then, the atomic state for the atoms can be rotated (i.e. we can prepare atoms in superpositions) inside a classical Ramsey field R_1. Rydberg atoms are the standard atoms in such experiments. This is because of the large radius of the circular orbit in these atoms which then gives a very large dipole moment and then a very strong coupling with the

EM field. Furthermore, the long lifetime of the atomic state as a result of the high orbital angular momentum is another reason and is considered to be a very important property for QIP applications [37, 38].

Atoms then traverse to a high-Q cavity. An open Fabry-Perot resonator is a standard cavity for many optical and microwave CQED experiments as in [5, 39, 40], but a closed cylindrical cavity is another form of practical resonators as illustrated by [41]. The initial state of the field inside the cavity is prepared by different methods varying from cavity-laser interactions, preparing the cavity at a low temperature, or from cavity-atom interactions. For many quantum information processing applications, the number (Fock) state is the target state. It is reported that different experiments can be employed to generate this state such as experiments in one-atom maser [41, 42] and in solid-state systems [43].

To determine the atomic state of atoms outside the cavity, atoms have been sent to a detector D. Another classical Ramsey field R_2 may be used before that in order to add further phases to the atomic state superposition. For Rydberg atoms, field ionization is the standard technique for detection [8, 44].

The previous setup is not only the scheme used in cavity-QED experiments, but it may show the main and common processes which have taken place in other possible setups. Even in a cavity-QED, an atom can be replaced by, for example, a trapped ion [45], and in this thesis we focus our attention on a case in which a multi-level atom interacts with multi-mode cavity in the strong regime.

2.5 Summary

In this chapter, some basic principles in quantum computing have been introduced. These principles are useful when discussing the construction of a set of universal gates in chapters 4, and 5. Loss of information stored in qubits due to dissipative processes such as atomic and photonic relaxations will be the central topic of chapter 6.

Chapter 3

Multi-photon resonance

Based on Green's function and the projection operators, Shore [46] developed a theoretical method which is, in general, able to treat multi-photon resonance systems. This theory predicts the locations of sharp resonances from the use of effective two-level, three-level, and even more complex Hamiltonians. This method, however, does not ensure a full transfer for populations in the truncated systems, in particular for effective systems with more than three levels.

A further model, namely the spin-J model [47], can be employed in order to produce a complete population inversion. At the heart of quantum mechanics, this model is soluble, periodic, and able to proceed an entire population transfer. The spin-J model can be used to provide the proper values for the effective coupling constants in multi-level multi-photon systems so that the population inversion can take place.

Based on these two treatments, a theory for periodic multi-photon cavity-atom interactions has been developed, and then a set of universal quantum gates has been proposed (see chapters 4, 5). This chapter is organized as follows. In Sec. 3.1 we introduce the effective two-level theory. Then, the spin-J model is discussed in Sec. 3.2. Finally, we conclude in Sec. 3.3.

3.1 Effective two-level behaviour

Generally speaking, time evolution of a quantum system described by the time-independent Hamiltonian H in the RWA is governed by Schrödinger's equation ($\hbar = 1$)

$$|\Psi(t)\rangle \quad = \quad e^{-\mathrm{i}\hat{H}\ t}\ |\Psi(0)\rangle\ , \tag{3.1}$$

where $|\Psi(0)\rangle$ is the initial state at $t = 0$. Alternatively, the dynamics of the system can be addressed by an integral transform rather than the previous exponential form [48]. That

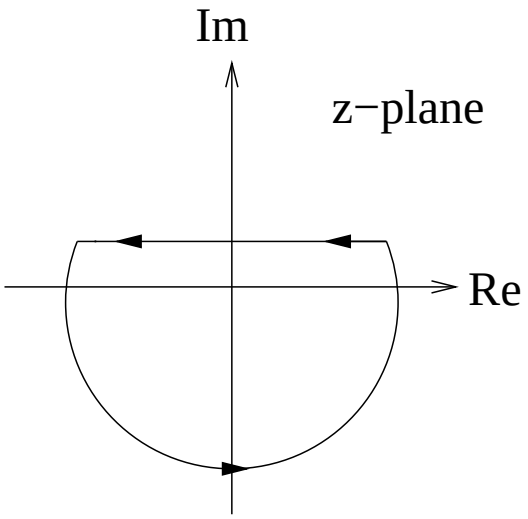

Figure 3.1: Integration contour for the complex integral (3.3).

is, we reexpress the previous wavefunction $|\Psi(t)\rangle$ in terms of Laplace transform. This transform shows that [49]

$$\mathcal{L}(|\Psi(t)\rangle) = \int_0^\infty |\Psi(t)\rangle \; e^{-pt} \; dt = \frac{1}{p\hat{I} + \mathrm{i}\hat{H}} \; |\Psi(0)\rangle \; , \tag{3.2}$$

and then the inverse Laplace transform, with introducing the variable change $p = -\mathrm{i}z$ [48], is

$$|\Psi(t)\rangle = \frac{1}{2\pi\mathrm{i}} \int_{\mathrm{i}\epsilon+\infty}^{\mathrm{i}\epsilon-\infty} e^{-\mathrm{i}zt} \; \frac{1}{z\hat{I} - \hat{H}} \; dz \; |\Psi(0)\rangle \; . \tag{3.3}$$

This transform is equivalent to Eq. (3.1). As proof, the previous integral can be solved by the Residue theorem [49] as follows. To enclose all singularities of the transform (all poles lie on the real z-axis), the counter-clockwise contour of this integral consists of a straight line that is shifted just above the real z-axis and is extended between $\pm\infty$, and finally closed with a semicircular path in the lower-half of the imaginary z-axis [48] (see Fig. 3.1). Assuming $\mathrm{f}(z) = e^{-\mathrm{i}zt}/(z\hat{I} - \hat{H}) = \mathrm{h}(z)/\mathrm{g}(z)$, the residues of $\mathrm{f}(z)$ (or shortly Res $\{\mathrm{f}(z)\}$) can be given by Res $\{\mathrm{f}(z)\} \equiv \mathrm{h}(\hat{H})/\frac{d}{dz}(\mathrm{g}(\hat{H})) = e^{-\mathrm{i}\hat{H}t}$, which is nothing but the exponential in Eq. (3.1).

The operator $\hat{G}(z) = \frac{1}{(z\hat{I}-\hat{H})}$ in Eq. (3.3) can be considered as Green's function for $(z\hat{I}-\hat{H})$ [48], which implies that

$$(z\hat{I} - \hat{H}) \; \hat{G}(z) = 1 \; . \tag{3.4}$$

Now we assume that the basis states in the superposition $|\Psi(t)\rangle$ can be partitioned into two subsystems spanned by the orthogonal projection operators $\mathbb{P}$ and $\mathbb{Q}$ [50], and these

projectors own the following properties [46] $\mathbb{P}\mathbb{P} = \mathbb{P}$, $\mathbb{Q}\mathbb{Q} = \mathbb{Q}$, $\mathbb{P}\mathbb{Q} = \mathbb{Q}\mathbb{P} = 0$, and $\mathbb{P} + \mathbb{Q} = 1$. Consequently, one finds that $|\Psi(t)\rangle = \mathbb{P}|\Psi(t)\rangle + \mathbb{Q}|\Psi(t)\rangle$. This implies that for a system $|\Psi(t)\rangle$ containing m possible states, the subspace $\mathbb{P}$ can include $N \leq m$ states, leaving $(m - N)$ states for the $\mathbb{Q}$-space. This may indicate that the effective two-level Hamiltonian in [46] can be valid for $m \geq N \geq 2$. Indeed, we have expanded this theory to include more than two states in the subspace $\mathbb{P}$, as we will see in subsequent chapters. Throughout this thesis, we assume "the states of interest" to be always spanned by $\mathbb{P}$, so we need to find the time evolution of the subsystem $\mathbb{P}|\Psi(t)\rangle$ alone. Recalling the transform in Eq. (3.3), one obtains that

$$\mathbb{P}|\Psi(t)\rangle \quad = \quad \frac{1}{2\pi i}\int dz\; e^{-izt}\; \mathbb{P}\hat{G}(z)\; |\Psi(0)\rangle\; . \tag{3.5}$$

In order to find $\mathbb{P}\hat{G}(z)$, we follow the traditional operator algebra in appendix C. After a few lines of algebra, the expression for the effective Hamiltonian describing the subsystem $\mathbb{P}|\Psi(t)\rangle$ can be given by $\hat{H}_{\text{eff}}$ as

$$\hat{H}_{\text{eff}} = \hat{H}_0 + \hat{B}\; \frac{1}{(z\hat{I} - \hat{A})}\; \hat{B}^{\dagger}\; , \tag{3.6}$$

where $\mathbb{P}\hat{H}\mathbb{P} = \hat{H}_0$, $\mathbb{P}\hat{H}\mathbb{Q} = \hat{B}$, and $\mathbb{Q}\hat{H}\mathbb{Q} = \hat{A}$. Assuming the operator $\hat{A}$ has larger eigenvalues λ_k (k represents the dimension of the space $\mathbb{Q}$) than the eigenvalues z of the effective Hamiltonian $\hat{H}_{\text{eff}}$ (i.e. under the limit $|\lambda_k| >> |z|$), we can introduce the approximation

$$\frac{1}{(z\hat{I} - \hat{A})} \approx \frac{-1}{\hat{A}}(1 + \frac{z\hat{I}}{\hat{A}})\; . \tag{3.7}$$

Indeed, in many cases the approximation $z\hat{I} - \hat{A} \approx -\hat{A}$ is valid (several examples have been provided in chapters 4, and 5), but in others (see for example Sec. 5.4.2) the formula (3.7) (i.e. the 2nd-order corrections) must be taken into account.

The condition that the eigenvalues of $\hat{A}$ are much larger than the eigenvalues of the effective Hamiltonian $\hat{H}_{\text{eff}}$ can be applicable in two different situations [46]. In the case of non-resonance systems, this condition produces multiphoton resonance systems. That is, we allow large detunings for the states in the $\mathbb{Q}$-space and find out the resonance conditions for the states in the $\mathbb{P}$ space. In the following two chapters, N-photon resonance models (with $N = 2, 3, 4$, and 5) have been successfully performed.

On the other hand, in a completely resonant system and with the $\mathbb{Q}$ space containing at least two states, the coupling constant(s) linked the states in the space $\mathbb{Q}$ must be much larger in magnitude than the coupling strengths in the subsystem $\mathbb{P}|\Psi\rangle$. A couple of examples have been discussed in Secs. 4.6, 5.6. Large detunings and large coupling

constants can be used together to reduce a large system into further lower dimensions (an example can be found in 5.6).

Although the previous derivation for the effective Hamiltonian $\hat{H}_{\text{eff}}$ deals with Hermitian Hamiltonians $\hat{H}$, this restriction is certainly not essential. The effective Hamiltonian theory can be applied to the systems described by non-Hermitian Hamiltonians, and such cases when the dissipation processes are considered. Further details and examples can be found in Chapter 6.

3.2 Spin-J model

The preceding theory of the effective N-level Hamiltonian predicts the resonance conditions for the states in the subsystem $\mathbb{P}|\Psi(t)\rangle$ so that the probabilities can be largely confined to only the states belonging to $\mathbb{P}$ space. For $N \leq 3$ (where N is the number of possible states in $\mathbb{P}$-space) the effectively lossless two- and three-state systems, with fixed coupling strengths, are certainly periodic (examples can be found in Secs. 4.3, 4.4, 5.4). On the other hand, effective systems with $N > 3$ may require additional control for the values of effective couplings $g^{(n)}$ in order to produce an entire population transfer.

The well-known spin-J model in a constant magnetic field owns important properties which include the periodicity and the ability to conduct a complete population inversion [15, 18]. This model, therefore, can be employed to address the proper values of the coupling constants in the effective Hamiltonian $\hat{H}_{\text{eff}}$ in order that periodic systems can be constructed [47, 51]. Further models, in contrast, have been suggested to express the sequence coupling strengths by some special functions [52, 53]. Except the spin-J model, all these models fail to produce a full inversion of the population in systems with $N > 3$ [47].

As a brief reminder for the spin-J model, the angular momentum operator $\hat{J}$ in the Cartesian coordinates can be written as [18, 47, 54]

$$\hat{J} = a\hat{J}_z + b\hat{J}_x + c\hat{J}_y \ , \tag{3.8}$$

where a, b, and c are constants for a certain $\hat{J}$. By defining the raising and lowering operators $\hat{J}_\pm = \hat{J}_x \pm \mathrm{i}\hat{J}_y$, one can express $\hat{J}_x = \frac{1}{2}(\hat{J}_+ + \hat{J}_-)$ and $\hat{J}_y = -\frac{\mathrm{i}}{2}(\hat{J}_+ - \hat{J}_-)$. The operator $\hat{J}$, hence, can be reexpressed as

$$\hat{J} = a\hat{J}_z + \frac{1}{2}(b - \mathrm{i}c)\hat{J}_+ + \frac{1}{2}(b + \mathrm{i}c)\hat{J}_- \ . \tag{3.9}$$

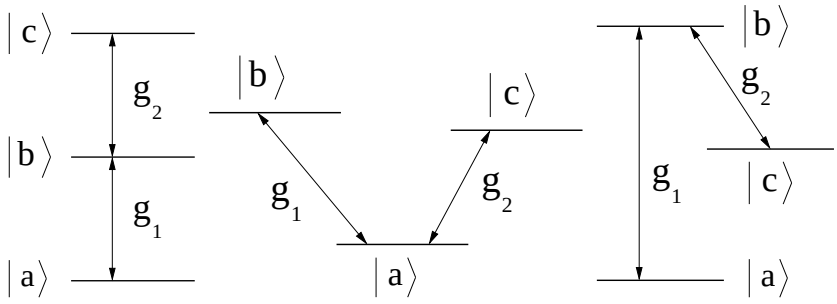

(a) Ξ (b) V (c) Λ

Figure 3.2: Possible systems described by tridiagonal Hamiltonians.

In the basis of the angular momentum $|J, M\rangle$

$$a\hat{J}_z|J,M\rangle = aM|J,M\rangle, \tag{3.10}$$

$$\frac{1}{2}(b \mp \mathrm{i}c)\hat{J}_\pm|J,M\rangle = \frac{1}{2}(b \mp \mathrm{i}c)\sqrt{(J \mp M)(J \pm M + 1)}|J, M \pm 1\rangle \ . \tag{3.11}$$

It is clear that $\hat{J}$ produces a tridiagonal matrix, where the on- and off-diagonal elements can be given by the eigenvalues aM and $\frac{1}{2}(b \mp \mathrm{i}c)\sqrt{(J \mp M)(J \pm M + 1)}$, respectively.

Considering the RWA time-independent $\hat{H}$ in (3.1) to be always tridiagonal, the operators $\hat{J}$ and $\hat{H}_{\text{eff}}$ (3.6) both produce tridiagonal matrices in their basis. Moreover, the number of the magnetic sub-levels $2J+1$ in $\hat{J}$ meets the number of the basis states N in $\hat{H}_{\text{eff}}$, and the specific eigenvalue M of the component $\hat{J}_z$ corresponds to the specific atomic level nth. Consequently, the analogy between these operators can be exploited as following

$$N = 2J + 1, \quad n_\pm = J \pm M + 1 \ . \tag{3.12}$$

Note that the sign in the expression of n depends on the operator $\hat{J}_\pm$. Therefore, the eigenvalues in Eqs. (3.10, 3.11) can be represented in terms of N and n as

$$\pm aM \mapsto \pm[a\ n - \frac{1}{2}a\ (N-1)] \ , \tag{3.13}$$

$$\frac{1}{2}(b \mp \mathrm{i}c)\sqrt{(J \mp M)(J \pm M + 1)} \mapsto \frac{1}{2}(b \mp \mathrm{i}c)\sqrt{n(N-n)} \ . \tag{3.14}$$

In the effective system described by $\hat{H}_{\text{eff}}$ all states have been set to be on- or near- resonance, which means the parameter a in the last equations can be safely set to zero, i.e. $a = 0$. Furthermore, the values of the effective coupling constants $g^{(n)}$, which are the off-diagonal elements in $\hat{H}_{\text{eff}}$, can follow the formula

$$g^{(n)} = g_0\sqrt{n(N-n)} \ , \tag{3.15}$$

where $g_0 = \frac{1}{2}(b \mp \mathrm{i}c)$. Note that in chapter 1 we assume that the coupling constant to be always real and spatial-independent. This expression for $g^{(n)}$ ensures that a complete

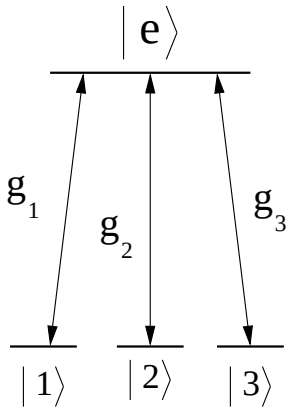

Figure 3.3: A degenerate F-pod system with F $>$ 2 (in this example F = 3)[55]. This system does not form a tridiagonal Hamiltonian.

population transfer takes place. Generally, the system requires $|g_0|t = \pi/2$ to proceed the population inversion (note that g_0 remains unchanged for a certain value of N). In the following chapters, we will see that the interaction time plays a crucial role in the realization of our gates. From the previous expression for the effective coupling constant (see eq.(3.15)), the interaction time can be theoretically determined by

$$|g^{(n)}\ t_{th}| = \sqrt{n\ (N-n)}\ \pi/2\ , \tag{3.16}$$

where $g^{(n)}$ is the nth effective coupling, N is the dimension of the effective system (i.e. N is the dimension of $\mathbb{P}$ space), and $n = 1, 2, ..., N-1$.
When considering the decoherence processes, i.e. $a \neq 0$, the spin$-J$ model can be applied as well (more details can be found in chapter 6).

3.3 Summary

In this chapter, we have developed theory for multi-photon atom-cavity interactions based on off-resonant interactions with multiple single photons. This theory consists of two models. In the first model, the effective N-level Hamiltonian procedure developed by Shore in [46] can be applied by following two different methods. On the one hand, in a system $\hat{H}$ with non-vanishing detuning(s) a subset of virtual states can be efficiently isolated by allowing large detunings to those states, such a method is sometimes known as the adiabatic elimination. The fully resonant systems, on the other hand, can be reduced into effective N-level behaviour by setting large values for the coupling constants linked the states in the space of $\mathbb{Q}$. Both methods lead to the situation in which the eigenvalues of $\hat{H}_{\text{eff}}$ are much smaller than the eigenvalues of $\hat{A}$. The spin-J model, as a second model

in this theory, predicts the properly abstract values for the effective coupling constants to produce a complete population transfer.

The theory of two-level dynamics developed by Shore does not introduce any limitation to the time-independent RWA Hamiltonians. The spin-J model, however, requires that the RWA Hamiltonians to be tridiagonal. By definition, the RWA tridiagonal Hamiltonians describe the interactions between states which are linked to no more than a couple of the nearest states, and they do not make any loop [51] (see e.g. Figs. 3.2, 3.3).

Part II

Quantum logic gates in multi-level and multi-mode interaction

Chapter 4

The iSWAP gate

Based on cavity-QED and the effective N-level Hamiltonian theory in chapter 3, a set of universal gates, namely the iSWAP and the Fredkin gates, has been investigated [56]. In this scheme, quantum information units (qubits) are carried by photons, and atoms are used to mediate interactions between photonic qubits. Considering the present cavity QED techniques, the iSWAP gate briefly discussed in [56] is slow and probably not feasible (the authors found that the operation time in this gate is only an order of the magnitude smaller than the photon lifetime in a microwave cavity). In order to be a practical candidate for the implementation of a quantum computation, the gate operation time must be much shorter than the decoherence times (see e.g. [57]). The first aim in this chapter, therefore, is to improve the operation time of this gate. Based on the multi-photon resonance theory developed in chapter 3, we have found that by building further configurations for the iSWAP gate, the gate speed can be significantly improved. In the second part of this chapter, and in the absence of any decoherence process, the sensitivity of the gate fidelity to variations in experimentally characteristic parameters has been numerically simulated. The Fredkin gate, on the other hand, is left to be the main subject in chapter 5.

It is demonstrated that more complex quantum gates can be created by the iSWAP gate [58]. In [59], the combination of the CNOT and the SWAP gates produces the iSWAP gate (see Fig. 4.1). Furthermore, two iSWAP gates together with several one-qubit rotation gates can construct the CNOT gate, which is considered as a universal two-qubit gate [26, 27, 28].

The iSWAP gate can be represented by the operator (as in Fig. 4.1)

$$\text{iSWAP} \equiv |00\rangle\langle 00| + \mathrm{i}|01\rangle\langle 10| + \mathrm{i}|10\rangle\langle 01| + |11\rangle\langle 11| \ .$$

Recently, it has been shown that the iSWAP gate can be very useful for applications in

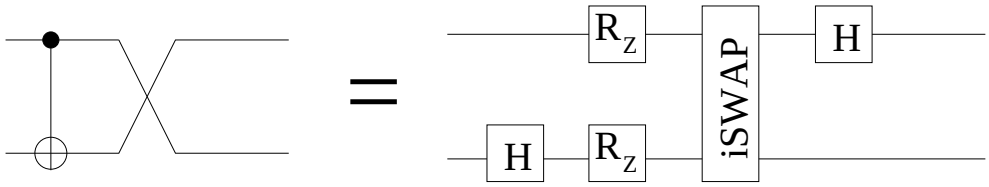

C	T	C	T
$\|0\rangle$	$\|0\rangle$	$\|0\rangle$	$\|0\rangle$
$\|0\rangle$	$\|1\rangle$	$i\,\|1\rangle$	$\|0\rangle$
$\|1\rangle$	$\|0\rangle$	$i\,\|0\rangle$	$\|1\rangle$
$\|1\rangle$	$\|1\rangle$	$\|1\rangle$	$\|1\rangle$

$$\text{iSWAP} \equiv \begin{pmatrix} 1 & 0 & 0 & 0 \\ 0 & 0 & i & 0 \\ 0 & i & 0 & 0 \\ 0 & 0 & 0 & 1 \end{pmatrix}$$

Figure 4.1: This figure includes (top) the quantum circuit generating the iSWAP gate as in [59], (left-down) the truth table of the iSWAP gate with C stands for the control qubit and T refers to the target qubit, and the iSWAP operator in the corresponding matrix representation (right-down).

quantum information process QIP and quantum computing. For example, it is reported that the replacement of the standard CNOT gate by the iSWAP gate provides a more efficient, simpler, and faster way of generating cluster states [60]. Cluster states (such states can be experimentally created by optical lattices [61]) are highly entangled states playing a crucial role in the so-called one-way quantum computation approach [62, 63]. Experimentally, it has been demonstrated that this new approach gives practical promises for realization of a universal set of one- and two-qubit operations and for implementation of Grover's algorithm [64].

In [56], the iSWAP gate is realizable in the dual-rail photonic qubits encoded on cavities. Subsequently, we discuss further configurations forming the gate by employing the treatment based on multi-photon resonances and the spin-J models. These two theoretical models can be used to predict the resonance conditions and the proper values for the coupling strengths in a system, respectively.

The chapter is organised as follows. The general Hamiltonian describing the model is analysed in Sec. 4.1. Subsequently, in Secs. 4.2, 4.6 possible configurations that exchange the qubits $|10\rangle$ and $|01\rangle$ have been realized. Then, we numerically investigate the fidelity in these configurations when considering variations in experimentally important parameters (Sec. 4.7). All configurations have been considered for the remaining qubits $|00\rangle$ and $|11\rangle$ in Sec. 4.8. Finally, the chapter concludes with Sec. 4.9.

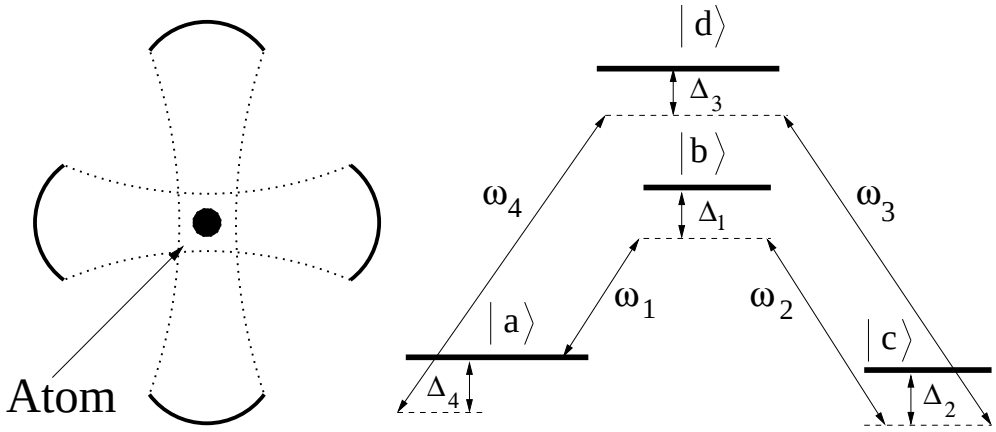

(a) (b)

Figure 4.2: This figure shows a possible schematics of the iSWAP gate with two identical cavities (as given in (a)) holding four modes and interacting with a double-lambda atom (as depicted in (b)). We require four modes for the gate operation; however, these modes could be set up as pairs of cavity modes as shown in (a).

4.1 The model

Following [56], we consider a de-excited atom in a double-lambda configuration interacting with high-Q cavities containing four modes with frequencies ω_i (where $i = 1, 2, 3, 4$). As shown by Fig. 4.2a, we assume these modes are generated by two cavities. Given each cavity represented by a dual-rail qubit (i.e. the EM mode in the one cavity can be either $|10\rangle$ or $|01\rangle$ and the EM mode in the other cavity is either $|10\rangle$ or $|01\rangle$), the initial field states, therefore, can be either $|1010\rangle$, $|1001\rangle$, $|0101\rangle$, or $|0110\rangle$.

Generally speaking, photonic qubits with a single excitation can be primarily encoded in a single or a double mode, such encodings defined as single- or dual-rail representation. The latter representation where two modes containing a single photon is the encoding considered in our scheme. As mentioned above, we assume each cavity contains two modes and a single photon. Given the dual-rail qubit $|01\rangle$ (where the excitation is in the second mode) this qubit encodes the basic $|0\rangle$ qubit state. Likewise, the dual-rail qubit $|10\rangle \equiv |1\rangle$. The initial field states in the previous two-mode cavities then can be represented as $|1010\rangle \equiv |10\rangle$, $|1001\rangle \equiv |11\rangle$, $|0101\rangle \equiv |01\rangle$, and $|0110\rangle \equiv |00\rangle$. In linear optical quantum computing, on the other hand, this sort of encoding has been introduced in theoretical and experimental proposals such as in [32, 65, 66, 67].

Considering the general set-up for cavity-QED experiments in Sec. 2.4, an atom prepared in the ground state passes through a group of cavities, and then the atomic state of this

atom outside the cavities is measured by a detector (see Fig. 2.2). Given the atom in Λ-Λ configuration, we consider an atom with the energies of the levels a, b, c, and d satisfying $E_b, E_d >> E_a, E_c$ and $E_c > E_a$ (see Fig. 4.2b). The atom before and after the cavities must be in the ground state, but inside the cavities it has been used to mediate interactions between photonic qubits.

For the first time, this scheme introduces the dual-rail approach to the cavity field modes [56]. On the other hand, the adiabatic elimination, representing qubits by photons, and using atoms to mediate interactions between qubits all have been exploited in a number of cavity QED-based schemes (see for examples [68, 69, 70]). In the dual-rail representation, we expect at all times that a single excitation exists in either mode n_1 or n_2 in the qubit $|n_1, n_2\rangle$, but not both; likewise for modes n_3 and n_4 in $|n_3, n_4\rangle$. This interesting feature allows us to detect any information loss from the computer. That is, with correct input preparation, if the projective measurement shows that the atom outside the field is not in the atomic state $|a\rangle$, then somewhere a random process must be interacting with the qubits in the machine. The dual-rail approach, therefore, has the advantage of making the effective decoherence very protectable, because if there is no excitation the gate must be aborted. This feature for the dual-rail approach is observed as well in the case of flying qubits [65].

In our case, the general Hamiltonian H for the atom, the cavity field, and atom-field interaction can be given as

$$\hat{H} = \hat{H}_0 + \hat{H}_{int} \ . \tag{4.1}$$

On the one hand, $\hat{H}_0$ is a combination of the four-level atom Hamiltonian $\hat{H}_A$ and the four-mode cavity field Hamiltonian $\hat{H}_F$. The atomic Hamiltonian can be defined as $\hat{H}_A = \hbar \sum_{i=a,b,c,d} \omega_i \, \hat{\sigma}_{ii}$ (with $\hat{\sigma}_{ii}$ represents the corresponding atomic levels as shown by Fig. 4.2), and the field Hamiltonian $\hat{H}_F$ can be defined as $\hat{H}_F = \hbar \sum_{j=1}^{4} \omega_j \, \hat{a}_j^\dagger \hat{a}_j$ (where $\hat{a}$ and $\hat{a}^\dagger$ are the photon annihilation and creation operators). On the other hand, the Hamiltonian for the atom-field interaction $\hat{H}_{int}$ can be given, in the dipole approximation, as $\hat{H}_{int} = -\hat{\mu} \cdot \hat{E}(z,t)$. In the first case we can express $\hat{H}_{int}$ as

$$\begin{aligned} \hat{H}_{int} = \ & - \ \mu_{ab}(\hat{\sigma}_{ab} + \hat{\sigma}_{ba}) \cdot \hat{E}_1(z,t) - \mu_{bc}(\hat{\sigma}_{bc} + \hat{\sigma}_{cb}) \cdot \hat{E}_2(z,t) \\ & - \ \mu_{cd}(\hat{\sigma}_{cd} + \hat{\sigma}_{dc}) \cdot \hat{E}_3(z,t) - \mu_{da}(\hat{\sigma}_{da} + \hat{\sigma}_{ad}) \cdot \hat{E}_4(z,t) \ , \end{aligned}$$

where the operators $\hat{\sigma}_{\alpha\beta}$ can be defined as the lowering and raising operators in the atom subspace. The cavity field modes at the atomic position z can be given by $\hat{E}_m(z,t) =$

$\epsilon_{\omega_m}\left[\hat{a}_m^\dagger(t)+\hat{a}_m(t)\right]\sin(k_m z)$ (where $\epsilon_\omega=\sqrt{\frac{\hbar\omega}{\epsilon_0 V}}$ is the electric field amplitude per photon for the corresponding field mode). Note that we assume, without loss of generality, that $\mu_{\alpha\beta}=\mu_{\beta\alpha}$. Defining the atom-field coupling strength $g_m=-\mu_{\alpha\beta}\,\epsilon_{\omega_m}\sin(k_m z)/\hbar$, one then can rewrite the Hamiltonian $\hat{H}_{int}$ as

$$\begin{aligned} H_{int} &= \hbar[g_1(\hat{\sigma}_{ab}+\hat{\sigma}_{ba})(\hat{a}_1^\dagger+\hat{a}_1) \\ &+ g_2(\hat{\sigma}_{bc}+\hat{\sigma}_{cb})(\hat{a}_2^\dagger+\hat{a}_2) \\ &+ g_3(\hat{\sigma}_{cd}+\hat{\sigma}_{dc})(\hat{a}_3^\dagger+\hat{a}_3) \\ &+ g_4(\hat{\sigma}_{da}+\hat{\sigma}_{ad})(\hat{a}_4^\dagger+\hat{a}_4)]\ . \end{aligned}$$

In order to map $\hat{H}_{int}$ into the interaction picture we use the transformation $\hat{U}^\dagger\ \hat{H}\ \hat{U}$, where $\hat{U}=e^{-i\hat{H}_0 t/\hbar}$. The interaction picture for the atomic operators can be given as $\hat{U}^\dagger\,\hat{\sigma}_\pm^{\alpha\beta}\,\hat{U}=\hat{\sigma}_\pm\,e^{\pm i\omega_{\beta\alpha}t}$ (with $E_\beta>E_\alpha$) and for the cavity field operators can be expressed as $\hat{U}^\dagger\,\hat{a}_i\,\hat{U}=\hat{a}_i\,e^{-i\omega_i t}$ and $\hat{U}^\dagger\,\hat{a}_i^\dagger\,\hat{U}=\hat{a}_i^\dagger\,e^{i\omega_i t}$. Now in the limit of near-resonance, applying the rotating wave approximation yields that the rapidly oscillating terms (such terms oscillating with the sum frequencies $\pm(\omega_{\beta\alpha}+\omega_i)$) can be neglected; the slowly oscillating terms (i.e. terms containing $\exp(\pm\mathrm{i}(\omega_{\beta\alpha}-\omega_i)t)$) remain. One then can reexpress the Hamiltonian $\hat{H}_{int}$ as

$$\hat{H}'_{int}=\hbar[g_1\ \hat{a}_1\ \hat{\sigma}_{ba}+g_2\ \hat{\sigma}_{cb}\ \hat{a}_2^\dagger+g_3\hat{a}_3\ \hat{\sigma}_{dc}+g_4\ \hat{\sigma}_{ad}\ \hat{a}_4^\dagger+\text{h.c.}]\ .$$

where h.c. refers to the Hermitian conjugate. Thus, the total Hamiltonian $\hat{H}$ can be re-represented as

$$\begin{aligned} \hat{H}=\hbar\sum_{i=a,b,c,d}\omega_i\ \hat{\sigma}_{ii} &+ \hbar\sum_{j=1}^{4}\omega_j\ \hat{a}_j^\dagger\hat{a}_j \\ &+ \hbar\ [g_1\ \hat{a}_1\ \hat{\sigma}_{ba}+g_2\ \hat{\sigma}_{cb}\ \hat{a}_2^\dagger+g_3\hat{a}_3\ \hat{\sigma}_{dc}+g_4\ \hat{\sigma}_{ad}\ \hat{a}_4^\dagger+\text{h.c.}] \quad (4.2) \end{aligned}$$

We shall now set $\hbar=1$ for the rest of this chapter, as we always work in the quantum limitations. The energies, thus, have the dimension $(\text{time})^{-1}$.

4.2 Time evolution of the qubit states $|a\ 10\rangle$ and $|a\ 01\rangle$

In the case of the initial state to be either $|a\ 10\rangle$ or $|a\ 01\rangle$, the interaction part in the Hamiltonian $\hat{H}$ (4.2) can be used to determine the basis states for the atom-field system. We consider $|\Psi(0)\rangle=|a\ 10\rangle$, and make the ansatz

$$|\Psi(t)\rangle=c_1(t)|a\ 1010\rangle+c_2(t)|b\ 0010\rangle+c_3(t)|c\ 0110\rangle+c_4(t)|d\ 0100\rangle+c_5(t)|a\ 0101\rangle\ . (4.3)$$

The system dynamics is the same when setting the initial state to be $|a\ 01\rangle$. In the space $\mathbb{H} \equiv \{|a\ 1010\rangle, |b\ 0010\rangle, |c\ 0110\rangle, |d\ 0100\rangle, |a\ 0101\rangle\}$, the Hamiltonian $\hat{H}$, in the matrix representation and with $|a\ 10\rangle$ to be zero-point energy, becomes

$$\hat{H}' = \begin{pmatrix} 0 & g_1 & 0 & 0 & 0 \\ g_1 & \Delta_1 & g_2 & 0 & 0 \\ 0 & g_2 & \Delta_2 & g_3 & 0 \\ 0 & 0 & g_3 & \Delta_3 & g_4 \\ 0 & 0 & 0 & g_4 & \Delta_4 \end{pmatrix} , \tag{4.4}$$

where the system detunings Δ_i $(i = 1, 2, 3, 4)$ can be defined as

$$\begin{aligned} \Delta_1 &= (\omega_{ba} - \omega_1) , \\ \Delta_2 &= (\omega_{ba} - \omega_1) - (\omega_{bc} - \omega_2) , \\ \Delta_3 &= (\omega_{ba} - \omega_1) - (\omega_{bc} - \omega_2) + (\omega_{dc} - \omega_3) , \\ \Delta_4 &= (\omega_{ba} - \omega_1) - (\omega_{bc} - \omega_2) + (\omega_{dc} - \omega_3) - (\omega_{da} - \omega_4) . \end{aligned} \tag{4.5}$$

The previous definition for Δ_i (the detunings of the field from the corresponding transitions in atom) can be easily obtained by the extension of the standard JC model in a lambda configuration [54]. The truth table of the iSWAP gate shows that (see table 4.1) the qubit state $|a\ 10\rangle$ has to be transformed into the qubit state $|a\ 01\rangle$, and vice versa. To this end, we employ the effective Hamiltonian theory (i.e. Shore's method discussed in Sec. 3.1) to perform adiabatically eliminations for the unwanted basis states. It is clear (as this system contains several basis states) that many possible configurations can be generated by applying Shore's method. The terminal states (i.e. $|a\ 10\rangle$ and $|a\ 01\rangle$) are always set to be resonant or nearly resonant, which means the remaining states in the space $\mathbb{H}$ can be set to be far- or on-resonance. This implies that there are possibly 2^3 different models that can generate the operation.

In table 4.1, we set the values 0 and 1 for the off- and on-resonance states, respectively. Depending on the dimension N of the effective Hamiltonians $\hat{H}_{\text{eff}}$ in Eq. (3.6), one can classify the resultant models into an N-level system. In the model (10001), for example, the states $|a\ 10\rangle$ and $|a\ 01\rangle$ are assumed to be resonant. Then the remaining basis states (i.e. $|b\ 0010\rangle, |c\ 0110\rangle$, and $|d\ 0100\rangle$) all are adiabatically eliminated. The effective Hamiltonian for this system (as will be seen soon) acts in the subspace $\{|a\ 10\rangle, |a01\rangle\}$, and the populations of the system are confined between these states. Furthermore, in the model (10101) the unwanted states are the states $|b\ 0010\rangle$ and $|d\ 0100\rangle$. So, detunings in these states are set to be much larger than the couplings g_i (with $i = 1, 2, 3, 4$) and the detunings in states

N-level system	On-resonance state(s)	Label
2-level	Nil	(10001)
3-level	$\|b\ 0010\rangle$	(11001)
	$\|c\ 0110\rangle$	(10101)
	$\|d\ 0100\rangle$	(10011)
4-level	$\|b\ 0010\rangle$ & $\|c\ 0110\rangle$	(11101)
	$\|c\ 0110\rangle$ & $\|d\ 0100\rangle$	(10111)
	$\|b\ 0010\rangle$ & $\|d\ 0100\rangle$	(11011)
5-level	All	(11111)

Table 4.1: Configurations for the systems that are able to interchange the two qubit states $|a10\rangle$ and $|a\,01\rangle$. Note that qubit states $|a\ 10\rangle$ and $|a\ 01\rangle$ are always set to have vanishing or very sharp detuning values. N indicates the dimension of $\mathbb{P}$ space (such a space containing the resonant states alone).

$|a\ 1010\rangle$, $|c\ 0110\rangle$, and $|a\ 0101\rangle$.

4.3 Two-level behaviour: the model (10001)

The basis states given by $|\Psi(t)\rangle$ in Eq. (4.3) can be divided into a couple of subsystems $\mathbb{P}|\Psi(t)\rangle$ and $\mathbb{Q}|\Psi(t)\rangle$, where $\mathbb{P}$ and $\mathbb{Q}$ are orthogonal projection operators and $\mathbb{P}+\mathbb{Q}=1$. Assuming $\mathbb{P}$ consists of the states $|a10\rangle$ and $|a01\rangle$, one finds that the operators $\hat{H}_0=\mathbb{P}\hat{H}\mathbb{P}$, $\hat{A}=\mathbb{Q}\hat{H}\mathbb{Q}$, and $\hat{B}=\mathbb{P}\hat{H}\mathbb{Q}$ can be expressed, in the matrix formalism, as

$$\hat{H}_0=\begin{bmatrix}0 & 0\\ 0 & \Delta_4\end{bmatrix}\ ,\ \hat{B}=\begin{bmatrix}g_1 & 0 & 0\\ 0 & 0 & g_4\end{bmatrix}\ ,\ \hat{A}=\begin{bmatrix}\Delta_1 & g_2 & 0\\ g_2 & \Delta_2 & g_3\\ 0 & g_3 & \Delta_3\end{bmatrix}\ . \tag{4.6}$$

An effective two-level Hamiltonian $\hat{H}_{\text{eff}}$ can be constructed by $\hat{H}_{\text{eff}}=\hat{H}_0-\hat{B}\ \hat{A}^{-1}\ \hat{B}^{\dagger}$. One then finds that the effective two-photon coupling g_{eff} linked the states $|a10\rangle$ and $|a01\rangle$ can be given as (with $\Delta_{1,2,3} >> g_{1,2,3,4}$)

$$g_{\text{eff}} \quad = \quad -\frac{g_1g_2g_3g_4}{\Delta_1\Delta_2\Delta_3-\Delta_1g_3^2-g_2^2\Delta_3}\approx-\frac{g_1g_2g_3g_4}{\Delta_1\Delta_2\Delta_3}\ , \tag{4.7}$$

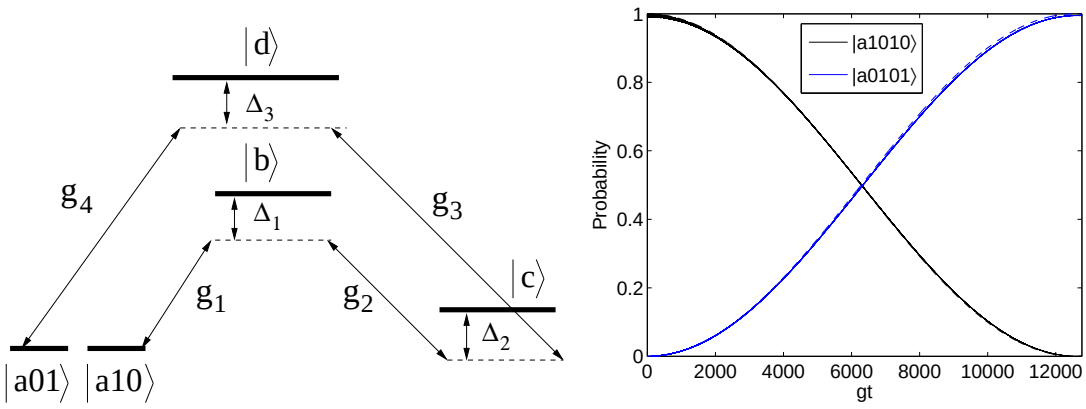

Figure 4.3: [Left] The sketch of the model (10001) as a two-level approximation. The state $|a01\rangle$ has been set to be on- or near-resonance, resulting in a two-photon resonance. [Right] The probability of the states $|a, 10\rangle$ and $|a, 01\rangle$. The dashed line shows the exact result in Eq. (4.9), and the solid line represents the numerical integration of the Hamiltonian [4.4]. The coupling constants g_1, g_2, g_3 and g_4 are all set to g and the detunings Δ_1, Δ_2, and Δ_3 are set to $\Delta = 20g$. The two-photon resonance condition [4.8] determines the value of Δ_4.

and the effective detuning Δ_{eff}, after setting the initial state as an energy reference point,

$$\begin{aligned}\Delta_{\text{eff}} &= \Delta_4 - \frac{g_4^2(\Delta_1\Delta_2 - g_2^2)}{\Delta_1\Delta_2\Delta_3 - \Delta_1 g_3^2 - g_2^2\Delta_3} + \frac{g_1^2(\Delta_2\Delta_3 - g_3^2)}{\Delta_1\Delta_2\Delta_3 - \Delta_1 g_3^2 - g_2^2\Delta_3} \\ &\approx \Delta_4 - \frac{g_4^2}{\Delta_3} + \frac{g_1^2}{\Delta_1} \ . \end{aligned} \tag{4.8}$$

In the resonance case ($\Delta_{\text{eff}} = 0$), the time evolution of the initial state $|\Psi(0)\rangle$, in our case the initial state can be either $|a, 10\rangle$ or $|a, 01\rangle$, can be easily given by Schrödinger's equation $\mathbb{P}|\Psi(t)\rangle = e^{-\mathrm{i}\hat{H}_{\text{eff}}\ t}\ |\Psi(0)\rangle$. One finds that

$$\begin{aligned}|a, 10\rangle &\mapsto \cos(g_{\text{eff}}t)|a, 10\rangle - \mathrm{i}\ \sin(\mathrm{g_{eff}t})|\mathrm{a}, 01\rangle \\ |a, 01\rangle &\mapsto \cos(g_{\text{eff}}t)|a, 01\rangle - \mathrm{i}\ \sin(\mathrm{g_{eff}t})|\mathrm{a}, 10\rangle \ . \end{aligned} \tag{4.9}$$

A complete population transfer takes place at $|g_{\text{eff}}t| = \pi/2$. A global phase can be considered so that no minus sign appears, and then the transformations $|a\ 10\rangle \mapsto \mathrm{i}|a\ 01\rangle$ and $|a\ 01\rangle \mapsto \mathrm{i}|a\ 10\rangle$ can be achieved.

This transformation, which is constructed by adiabatic elimination for three states, requires a long interaction time (see Fig. 4.3), and then results in a slow iSWAP operation. This slow gate was proposed by [56] as an example for a simple two-qubit gate for dual-rail cavity-QED, and the authors then concentrate heavily on constructing a fast three-qubit gate such as the Fredkin gate. For completeness, in the subsequent sections I show that the speed of the previous iSWAP gate can be significantly improved in order that a fast

double-qubit gate for dual-rail CQED can be performed as well.

4.4 Three-level system

The extension of the theory for the effective two-level Hamiltonian is possible in order that multi-photon resonances can be formed [46]. In this section, three-level approximations have been created in order to swap the qubit states $|a\ 10\rangle$ and $|a\ 01\rangle$. Since the states $|a10\rangle$ and $|a01\rangle$ in $|\Psi(t)\rangle$ are always set to resonance, this implies that three possible three-level configurations can be generated. Depending on the locations of far-resonance states in Fig. 4.2, these configurations include the models (10101), (11001), and (10011).
Generally, all previous effective three-level models can be described by the Hamiltonian $\hat{H}_{\text{eff}}$:

$$\hat{H}_{\text{eff}} = \begin{bmatrix} 0 & g_{(1)} & 0 \\ g_{(1)} & \Delta_{\text{eff}}^{(1)} & g_{(2)} \\ 0 & g_{(2)} & \Delta_{\text{eff}}^{(2)} \end{bmatrix} . \tag{4.10}$$

Note that we always set the initial state as a zero point of energy. The basis states of the Hamiltonian (4.4) can be partitioned into two subspaces spanned by the projection operators $\mathbb{P}$ and $\mathbb{Q}$. The on-resonance states $|a,10\rangle$, $|a,01\rangle$, and $|\Phi\rangle$ have been always set to lie on the $\mathbb{P}$ space, with $|\Phi\rangle$ can be either the state $|b,0010\rangle$, $|c,0110\rangle$, or $|d,0100\rangle$.
Further details about how exactly the previous effective systems behave can be provided by the following analytical study. For $t > 0$, the time evolution of the subsystem spanned by $\mathbb{P}$ can be governed by $\mathbb{P}|\Psi(t)\rangle = e^{-\mathrm{i}\hat{H}_{\text{eff}}t/\hbar}\ |\Psi(0)\rangle$. For the initial state, say $|a,1010\rangle$,

$$\begin{aligned} |a,10\rangle \longrightarrow \quad & [\frac{g_{(1)}^2}{\overline{g}^2} + \frac{g_{(2)}^2}{\overline{g}^2}\ \cos(\overline{g}t)]\ |a,1010\rangle \\ - \quad & \mathrm{i}\frac{g_{(1)}}{\overline{g}}\ \sin(\overline{g}t)\ |\Phi\rangle \\ + \quad & \frac{g_{(1)}g_{(2)}}{\overline{g}^2}\ [\cos(\overline{g}t) - 1]\ e^{i\eta t}\ |a,01\rangle\ , \end{aligned} \tag{4.11}$$

where $\overline{g} = \sqrt{g_{(1)}^2 + g_{(2)}^2}$. For all models (10011), (11001), and (10101) a complete population inversion, i.e. $|a,1010\rangle \rightarrow \mathrm{i}|a,0101\rangle$, can occur by setting $\overline{g}t = \pi$, $|g_{(1)}t| = |g_{(2)}t| = \pi/\sqrt{2}$ and $\eta t = \pi/2$.

4.4.1 The model (10101)

In the case of $\mathbb{Q} = |b, 0010\rangle\langle b, 0010| + |d, 0100\rangle\langle d, 0100|$, the operators $\hat{H}_0$, $\hat{A}$, and $\hat{B}$ can be given as

$$\hat{H}_0 = \begin{bmatrix} 0 & 0 & 0 \\ 0 & \Delta_2 & 0 \\ 0 & 0 & \Delta_4 \end{bmatrix}, \ \hat{B} = \begin{bmatrix} g_1 & 0 \\ g_2 & g_3 \\ 0 & g_4 \end{bmatrix}, \ \hat{A} = \begin{bmatrix} \Delta_1 & 0 \\ 0 & \Delta_3 \end{bmatrix} . \tag{4.12}$$

In the space $\{|a1010\rangle, |c0110\rangle, |a0101\rangle\}$, the effective Hamiltonian in Eq. (4.10) can be constructed with the effective couplings

$$g^{(1)} = -\frac{g_1\ g_2}{\Delta_1}, \quad g^{(2)} = -\frac{g_3\ g_4}{\Delta_3} , \tag{4.13}$$

and the effective detunings

$$\Delta_{\text{eff}}^{(1)} = \Delta_2 - \frac{g_2^2}{\Delta_1} - \frac{g_3^2}{\Delta_3} + \frac{g_1^2}{\Delta_1} , \tag{4.14}$$

$$\Delta_{\text{eff}}^{(2)} = \Delta_4 - \frac{g_4^2}{\Delta_3} + \frac{g_1^2}{\Delta_1} . \tag{4.15}$$

The vanishing detunings $\Delta_{\text{eff}}^{(1)}$ and $\Delta_{\text{eff}}^{(2)}$ in Eqs. (4.14, 4.15) give the resonance conditions for this model. The coupling constants $g^{(1)}$ and $g^{(2)}$ represent the effective couplings linking the terminal state $|a1010\rangle$ to the auxiliary state $|c0110\rangle$ and the terminal state $|a0101\rangle$ to the same auxiliary state, respectively.

The spin-J model (in this case $J = 1$) in chapter 3 shows that the sequence of the effective couplings $g^{(1)}$ and $g^{(2)}$ in Eq. (4.13) must follow the formula $g^{(n)} = g_0\sqrt{n(N-n)}$ (in this model $N = 3$ and $n = 1, 2$), so that full population transfer can be achievable. This implies that for effective three-state models $g^{(1)} = g^{(2)}$. At time $|g_0 t| = \pi/2$ the effective system is completely in level $N = 3$ (with the initial state $|a10\rangle$, the system terminates at the state $|a01\rangle$). Fig. 4.4 illustrates the probability as a function of time in the model (10101).

4.4.2 The models (10011) and (11001)

Replacing the state $|c, 0110\rangle$ in the model (10101) by either the state $|b, 0010\rangle$ or $|d, 0100\rangle$ can produce the effective three-state models (11001) or (10011), respectively. We here discuss in detail the model (11001). The parameters of the model (10011), on the other hand, can be found in Fig. 4.5. The resonant states in (11001) configuration include the states $|a\ 1010\rangle, |b\ 0010\rangle$ and $|a\ 0101\rangle$. Applying the effective two-level Hamiltonian yields

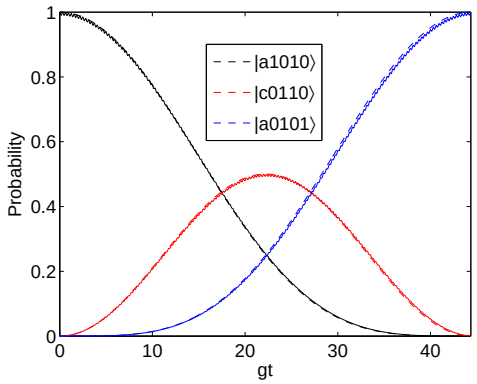

Figure 4.4: The three-level model (10101). The effective coupling constants are given by Eq. (4.13). The couplings g_1, g_2, g_3, and g_4 are set to g, and the detunings Δ_1 and Δ_3 are set to $\Delta = 20g$ so that $g^{(1)} = g^{(2)}$. Eqs. (4.14, 4.15) provide the resonance conditions for this model; therefore, the detunings Δ_2 and Δ_4 can be determined.

the following operators

$$\hat{H}_0 = \begin{bmatrix} 0 & g_1 & 0 \\ g_1 & \Delta_1 & 0 \\ 0 & 0 & \Delta_4 \end{bmatrix}, \ \hat{A} = \begin{bmatrix} \Delta_2 & g_3 \\ g_3 & \Delta_3 \end{bmatrix}, \ \hat{B} = \begin{bmatrix} 0 & 0 \\ g_2 & 0 \\ 0 & g_4 \end{bmatrix} . \tag{4.16}$$

One then finds that the effective couplings

$$g^{(1)} = g_1 \ , \quad g^{(2)} = \frac{g_2 g_3 g_4}{(\Delta_2\Delta_3 - g_3^2)} \approx \frac{g_2 g_3 g_4}{\Delta_2\Delta_3} \ , \tag{4.17}$$

and the effective detunings

$$\begin{aligned} \Delta^{(1)} &= \Delta_1 - \frac{g_2^2\Delta_3}{(\Delta_2\Delta_3 - g_3^2)} \approx \Delta_1 - \frac{g_2^2}{\Delta_2} \ , \\ \Delta^{(2)} &= \Delta_4 - \frac{g_4^2\Delta_2}{(\Delta_2\Delta_3 - g_3^2)} \approx \Delta_4 - \frac{g_4^2}{\Delta_3} \ . \end{aligned} \tag{4.18}$$

The numerical integration of the full Hamiltonian (4.4) shows that by setting $\Delta^{(1)} = \Delta^{(2)} = 0$ and $g_1 = \frac{g_2 g_3 g_4}{\Delta_2\Delta_3}$ the population of the initial state $|a\ 10\rangle$ can be entirely in the state $|a\ 01\rangle$ at $|g_0 t_{int}| = \pi/2$ (obviously the condition $\Delta_{2,3} >> g_{2,3,4}$ must be hold). Fig. 4.5 demonstrates the transformation of the qubit state $|a\ 10\rangle$ into $|a\ 01\rangle$ by considering both the analytical and the numerical results.

It is clear that the model (10101), where only a single state has been set to be near resonance (alongside the terminal states $|a10\rangle$ and $|a01\rangle$), introduces a significant improvement in the interaction time t_{int}, compared to the two-state system (see Figs. 4.3, 4.4). Moreover, the time needed to interchange the qubit states $|a\ 10\rangle$ and $|a\ 01\rangle$ in the three-level models (11001) and (10011) is still better than the corresponding time in the

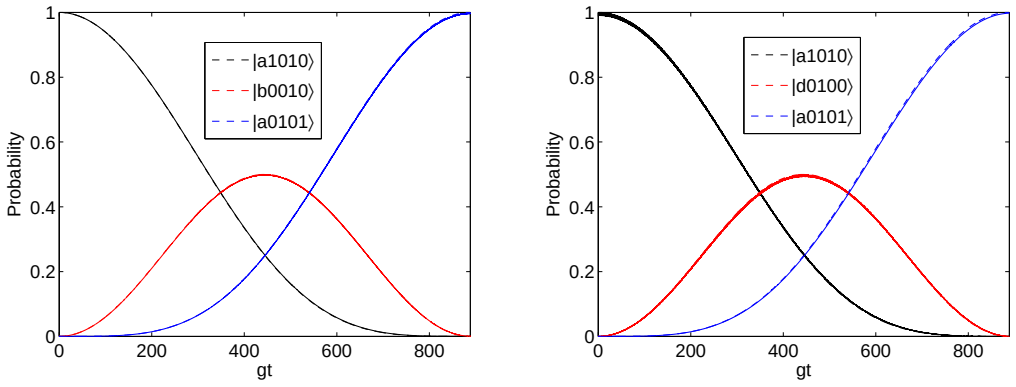

(a) (b)

Figure 4.5: The probability in the models (11001) and (10011). Note that the dashed line represents the theory (i.e. the dynamics of the system when the effective Hamiltonian (4.10) is considered), and the solid line shows the numerical simulation (the dynamics of the system by the full Hamiltonian in Eq. (4.4)). The numerical and theoretical results are in good agreement when the condition $\Delta >> g$ is satisfied. (a) The model (11001). The coupling strengths $g^{(1)}$ and $g^{(2)}$ are defined in Eq. (4.17), respectively. The coupling constants g_2, g_3, and g_4 are all set to g. The detunings Δ_2 and Δ_3 are set to Δ =20g and the detunings Δ_1 and Δ_4 are determined by the resonance conditions in Eq. (4.18). (b) The model (10011). The parameters are defined as $g^{(1)} = \frac{g_1 g_2 g_3}{\Delta_1\Delta_2 - g_2^2} \approx \frac{g_1 g_2 g_3}{\Delta_1\Delta_2}$, $g^{(2)} = g_4$, $\Delta_3 = \frac{g_3^2\Delta_1}{\Delta_1\Delta_2 - g_2^2} - \frac{g_1^2\Delta_2}{\Delta_1\Delta_2 - g_2^2} \approx \frac{g_3^2}{\Delta_2} - \frac{g_1^2}{\Delta_1}$, $\Delta_4 = -\frac{g_1^2\Delta_2}{\Delta_1\Delta_2 - g_2^2} \approx -\frac{g_1^2}{\Delta_1}$. The coupling constants g_1, g_2, and g_3 all are set to g and the detunings Δ_1 and Δ_2 are set to Δ =20g.

two-level model (10001).

It is observable that the interaction time in all configurations studied in this section is not the same, although all these configurations behave as effective three-level systems as illustrated by Figs. 4.4, 4.5. Indeed, the models (10011) and (11001) are slower than the model (10101). As a possible explanation, in these models we have found that the condition $g^{(1)} = g^{(2)}$ is required, which then sets $g^{(2)} = \frac{g_2 g_3 g_4}{\Delta_2\Delta_3}$ in the case of (11001) and $g^{(1)} = \frac{g_1 g_2 g_3}{\Delta_1\Delta_2}$ in the case (10011). In the model(10101), on the other hand, $g^{(1)} = -\frac{g_1\ g_2}{\Delta_1}$ and $g^{(2)} = -\frac{g_3\ g_4}{\Delta_3}$. Keeping in mind that $|g^{(1)}t| = |g^{(2)}t|$, it is clear that (under the condition $\Delta >> g$) the model (10101) is always faster.

4.5 Four-level behaviour

The next logical step is to find out whether or not the expansion of the $\mathbb{P}$-space would perform a faster iSWAP gate. In this section, we allow four states from the basis $\{|a, 1010\rangle, |b, 0010\rangle,$

$|c, 0110\rangle, |d, 0100\rangle, |a, 0101\rangle\}$ to be on- or near-resonance. Again we find three possible configurations can work as an effective four-level system. These models consist of the models (10111), (11011), and (11101).

A four-level effective Hamiltonian can be given, in general, by

$$\hat{H}_{\text{eff}} = \begin{bmatrix} 0 & g^{(1)} & 0 & 0 \\ g^{(1)} & \Delta^{(1)}_{\text{eff}} & g^{(2)} & 0 \\ 0 & g^{(2)} & \Delta^{(2)}_{\text{eff}} & g^{(3)} \\ 0 & 0 & g^{(3)} & \Delta^{(3)}_{\text{eff}} \end{bmatrix} . \tag{4.19}$$

By setting $\Delta^{(0)} = \Delta^{(1)} = \Delta^{(2)} = \Delta^{(3)} = 0$, a four-level four-photon configuration can be realized. Allowing a single state from the basis states $|\Psi(t)\rangle$ to be far resonant, can generate a four-level behaviour.

Generally speaking, the excitation dynamics for the effective four-level models above can be described by the wave vector

$\mathbb{P}|\Psi(t)\rangle = c_1(t)\ |a\ 1010\rangle + c_2(t)\ |\Phi\rangle + c_3(t)\ |\Theta\rangle + c_4(t)\ |a\ 0101\rangle$. The probability amplitudes $c_i(t)$ $(i = 1, 2, 3, 4)$ can be determined by solving Schrödinger's equation $\mathbb{P}|\Psi(t)\rangle = e^{-\mathrm{i}\hat{H}_{\text{eff}}\ t/\hbar}\ |\Psi(0)\rangle$. For this purpose, we use the traditional method of finding the corresponding eigenvectors for the eigenvalues of the effective Hamiltonian $\hat{H}_{\text{eff}}$ (4.19), and then we solve the resultant 1st-order ordinary differential equations. One can find, after setting all the effective detunings in the effective Hamiltonian to zero, that these eigenvalues λ can be represented by

$$\pm\lambda_{\pm} = \pm i g_{\pm}$$

where $g_{\pm} = \sqrt{(g/2) \pm \sqrt{(g/2)^2 - \tilde{g}^2}}$ (with $g = g^2_{(1)} + g^2_{(2)} + g^2_{(3)}$ and $\tilde{g} = g_{(1)} g_{(3)}$). The general solution for the probability amplitudes can, thus, be written as

$$c_i(t) = \alpha\ e^{+i\tilde{g}_+ t}|+\tilde{g}_+\rangle + \beta\ e^{-i\tilde{g}_+ t}|-\tilde{g}_+\rangle + \gamma\ e^{+i\tilde{g}_- t}|+\tilde{g}_-\rangle + \eta\ e^{-i\tilde{g}_- t}|-\tilde{g}_-\rangle\ , \tag{4.20}$$

where $|\pm\lambda_{\pm}\rangle$ are the eigenvectors corresponding to the eigenvalues $\pm\lambda_{\pm}$, and the coefficients α, β, γ, and η are constants which can be determined by the initial conditions.

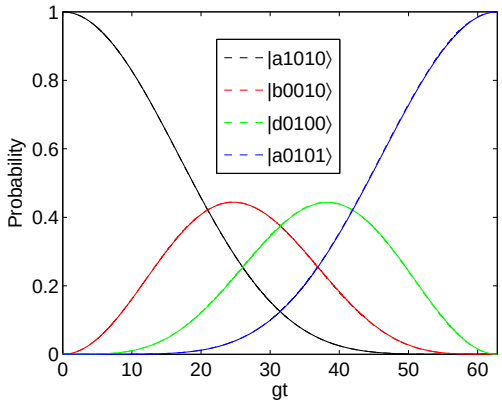

(a)

Figure 4.6: The configuration (11011) as a four-level behaviour. The effective couplings of the system can be provided by Eq. (4.23) and the coupling strengths g_2 and g_3 are set to g. The detuning Δ_2 is set to Δ =20g and the detunings Δ_1, Δ_3, and Δ_4 can be determined by the resonance conditions in Eq. (4.24). Note that the theory (dashed line) and the numerical calculations (solid line) show an efficient agreement.

Given the system initially in $|a1010\rangle$, the time evolution of this state can be written as

$$
\begin{aligned}
|a,10\rangle \longrightarrow \quad & [\frac{(g_{(1)}^2-g_-^2)}{(g_+^2-g_-^2)}\ \cos(g_+t)-\frac{(g_{(1)}^2-g_+^2)}{(g_+^2-g_-^2)}\ \cos(g_-t)]\ |a,10\rangle \\
+ \quad & \mathrm{i}[\frac{\mathrm{g}_+(\mathrm{g}_{(1)}^2-\mathrm{g}_-^2)}{\mathrm{g}_{(1)}(\mathrm{g}_+^2-\mathrm{g}_-^2)}\ \sin(\mathrm{g}_+\mathrm{t})-\frac{\mathrm{g}_-(\mathrm{g}_{(1)}^2-\mathrm{g}_+^2)}{\mathrm{g}_{(1)}(\mathrm{g}_+^2-\mathrm{g}_-^2)}\ \sin(\mathrm{g}_-\mathrm{t})]\ |\Phi\rangle \\
- \quad & [\frac{(g_{(1)}^2-g_+^2)(g_{(1)}^2-g_-^2)}{g_{(1)}g_{(2)}(g_+^2-g_-^2)}\ \cos(g_+t)+\frac{(g_{(1)}^2-g_-^2)(g_{(1)}^2-g_+^2)}{g_{(1)}g_{(2)}(g_+^2-g_-^2)}\ \cos(g_-t)]\ |\Theta\rangle \\
+ \quad & \mathrm{i}[\frac{\mathrm{g}_+(\mathrm{g}_+^2-\mathrm{g}_{(1)}^2-\mathrm{g}_{(2)}^2)(\mathrm{g}_{(1)}^2-\mathrm{g}_-^2)}{\mathrm{g}_{(1)}\mathrm{g}_{(2)}\mathrm{g}_{(3)}(\mathrm{g}_+^2-\mathrm{g}_-^2)}\ \sin(\mathrm{g}_+\mathrm{t}) \\
- \quad & \frac{g_-(g_-^2-g_{(1)}^2-g_{(2)}^2)(g_{(1)}^2-g_+^2)}{g_{(1)}g_{(2)}g_{(3)}(g_+^2-g_-^2)}\ \sin(g_-t)]\ e^{i\xi t}\ |a,01\rangle\ . \qquad (4.21)
\end{aligned}
$$

By setting the global phase $\xi \mapsto \pi$ and $|g_{(2)}t| \mapsto \pi$ (with the help of $g^{(n)} = g_0\sqrt{n(N-n)}$), one finds that $|a10\rangle \mapsto \mathrm{i}|a01\rangle$.

4.5.1 The model (11011)

Beginning with the model (11011), the $\mathbb{Q}$-space comprises just one state which is the state $|c,0110\rangle$. The operators required to construct the effective four-level Hamiltonian, which

is given by $\hat{H}_{\text{eff}} = \hat{H}_0 - \hat{B}\hat{A}^{-1}\hat{B}^{\dagger}$, can be written as

$$\hat{H}_0 = \begin{bmatrix} 0 & g_1 & 0 & 0 \\ g_1 & \Delta_1 & 0 & 0 \\ 0 & 0 & \Delta_3 & g_4 \\ 0 & 0 & g_4 & \Delta_4 \end{bmatrix}, \ \hat{B} = \begin{bmatrix} 0 \\ g_2 \\ g_3 \\ 0 \end{bmatrix}, \ \hat{A} = \Delta_2 \ . \tag{4.22}$$

The effective couplings in the Hamiltonian (4.19) can be expressed as

$$g^{(1)} = g_1 \ , \quad g^{(2)} = -\frac{g_2 g_3}{\Delta_2} \ , \quad g^{(3)} = g_4 \ , \tag{4.23}$$

and the resonance conditions of the system can be determined by

$$\Delta_{\text{eff}}^{(1)} = \Delta_1 - \frac{g_2^2}{\Delta_2} \ , \ \Delta_{\text{eff}}^{(2)} = \Delta_3 - \frac{g_3^2}{\Delta_2} \ , \ \Delta_{\text{eff}}^{(3)} = \Delta_4 \ . \tag{4.24}$$

Generally, it is observable that four-level systems require a couple of auxiliary states. In the model (11011), the states $|b\rangle$ and $|d\rangle$ work as auxiliary states, and have been linked to each other by the effective coupling $g^{(2)}$. The different effective couplings $g^{(1)}$, $g^{(2)}$, and $g^{(3)}$ can be related to each other by $g^{(n)} = g_0\sqrt{n(N-n)}$ (in our case $N = 4$, n= $1, 2, 3$). Setting the initial state of the system $|\Psi(0)\rangle = |a10\rangle$, a complete population inversion occurs at $|g_0 t| = \pi/2$, i.e. $|a10\rangle$ maps to $|a01\rangle$ (see Fig. 4.6).

4.5.2 The models (10111) and (11101)

Turning now to the four-level models (10111) and (11101), we simply replace the state $|c\ 0110\rangle$ in the model (11011) by either the states $|b\ 0010\rangle$ or $|d\ 0100\rangle$. Subsequently, we analyse the effective coupling constants and the resonance conditions for the model (11101), and the corresponding parameters for the model (10111) have been provided in Fig. 4.7. Setting the states $|a\ 1010\rangle, |d\ 0100\rangle$ and $|a\ 0101\rangle$ to be resonant, it is straightforward to find that

$$\hat{H}_0 = \begin{bmatrix} 0 & g_1 & 0 & 0 \\ g_1 & \Delta_1 & g_2 & 0 \\ 0 & g_2 & \Delta_2 & 0 \\ 0 & 0 & 0 & \Delta_4 \end{bmatrix}, \ \hat{B} = \begin{bmatrix} 0 \\ 0 \\ g_3 \\ g_4 \end{bmatrix}, \ \hat{A} = \Delta_3 \ . \tag{4.25}$$

The effective couplings in the Hamiltonian can be expressed as

$$g^{(1)} = g_1 \ , \quad g^{(2)} = g_2 \ , \quad g^{(3)} = -\frac{g_3 g_4}{\Delta_3} \ , \tag{4.26}$$

and the detunings Δ_1, Δ_2, and Δ_4 can be determined by

$$\Delta_{\text{eff}}^{(1)} = \Delta_1 \ , \quad \Delta_{\text{eff}}^{(2)} = \Delta_2 - \frac{g_3^2}{\Delta_3} \ , \quad \Delta_{\text{eff}}^{(3)} = \Delta_4 - \frac{g_4^2}{\Delta_3} \ . \tag{4.27}$$

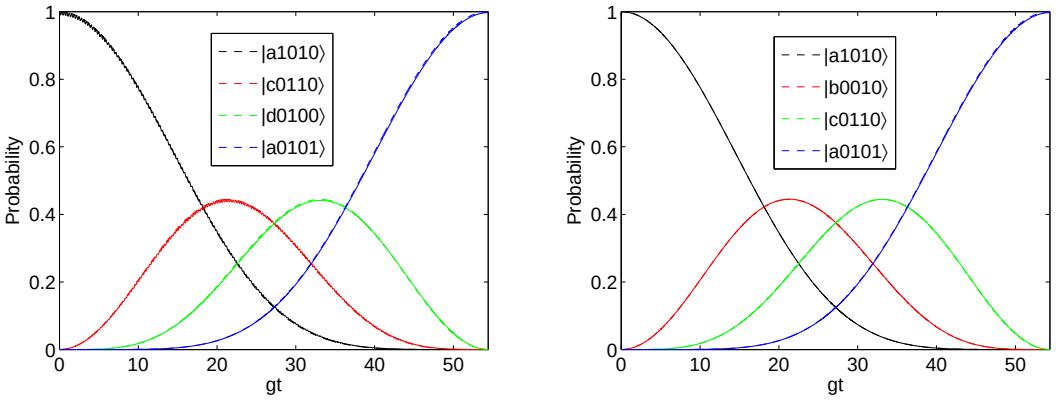

(a) (b)

Figure 4.7: (a) The populations in the model (10111). Parameters: the effective couplings of the system can be defined as $g^{(1)} = -\frac{g_1 g_2}{\Delta_1}$, $g^{(2)} = g_3$, and $g^{(3)} = g_4$. The coupling constants g_1 and g_2 are set to g and the detuning Δ_1 is set to $\Delta = 20g$. The resonance conditions can be given by $\Delta_2 = \frac{g_2^2}{\Delta_1} - \frac{g_1^2}{\Delta_1}$, and $\Delta_3 = \Delta_4 = -\frac{g_1^2}{\Delta_1}$. (b) The probability in the model (11101). The couplings g_3 and g_4 are set to g, and $\Delta_3 = \Delta = 20\ g$. The resonance conditions are given by Eqs. (4.27).

Fig. 4.7 demonstrates that the theory in (4.21) and the numerical simulation of (4.4) match in good agreement.

Compared to the model (10101), Figs. (4.6, 4.7) display that, unexpectedly, no improvement in the speed of the mapping $|a\ 10\rangle \mapsto |a\ 01\rangle$ can be attained. This result, however, is reasonable when recognizing that double auxiliary states are required, instead of a single auxiliary state in the case of the three-level approximations. Additionally, the condition of the effective couplings given by $g^{(n)} = g_0\sqrt{n(N-n)}$ keeps these effective couplings nearly equalized. This means that the operation by the model (10101) is still faster.

4.6 Five-level approximation: Model (11111)

If the basis states in (4.3) all are set to be resonant, this implies that the subspace spanned by $\mathbb{P}$ coincides completely with the space of the Hamiltonian $\hat{H}$ (4.4), and then $\mathbb{P}|\Psi(t)\rangle \mapsto |\Psi(t)\rangle$, i.e. the operator $\mathbb{P}$ acts as an identity operator. This means that the effective Hamiltonian of the system is nothing but the full Hamiltonian in Eq. (4.4), and it is easy to find that

$$g^{(1)} = g_1\ ,\quad g^{(2)} = g_2\ ,\quad g^{(3)} = g_3\ ,\quad g^{(4)} = g_4\ . \tag{4.28}$$

In order to ensure that a complete population transfer has taken place, these effective couplings must follow the formula $g^{(n)} = g_0\sqrt{n(N-n)}$. This effective system, therefore, is nothing but the system represented by the spin-J model (with $J = 2$) where the frequencies of modes match exactly with the corresponding atomic frequencies. By setting $|g_0 t| = \pi/2$, a very fast model can be generated, as expected (see Fig. 4.8).

A second approximation can be conducted on the model (11111) in order that the previous five-level system behaves as an effective three-state system. Following the procedure in [47], we create a subspace spanned by the operator $\mathbb{P}$ where the subsystem $\mathbb{P}|\Psi(t)\rangle$ contains the states $|a1010\rangle$, $|\Phi\rangle$, and $|a0101\rangle$. We are free to choose either the state $|b, 0010\rangle$ or $|d, 0100\rangle$ to represent the state $|\Phi\rangle$. Assuming the state $|b, 0010\rangle$ represents $|\Phi\rangle$, the operators $\hat{H}_0 = \mathbb{P}\hat{H}\mathbb{P}$, $\hat{A} = \mathbb{Q}\hat{H}\mathbb{Q}$, and $\hat{B} = \mathbb{P}\hat{H}\mathbb{Q}$ can be expressed as

$$\hat{H}_0 = \begin{bmatrix} 0 & g^{(1)} & 0 \\ g^{(1)} & 0 & 0 \\ 0 & 0 & 0 \end{bmatrix}, \ \hat{A} = \begin{bmatrix} 0 & g^{(3)} \\ g^{(3)} & 0 \end{bmatrix}, \ \hat{B} = \begin{bmatrix} 0 & 0 \\ g^{(2)} & 0 \\ 0 & g^{(4)} \end{bmatrix}. \tag{4.29}$$

The effective Hamiltonian $\hat{H}_{\text{eff}}$ can be constructed by $\hat{H}_{\text{eff}} = \hat{H}_0 - \hat{B}\ \hat{A}^{-1}\ \hat{B}^{\dagger}$. The corresponding effective couplings, hence, can be written as

$$G^{(1)} = g^{(1)}\ , \quad G^{(2)} = -\frac{g^{(2)}g^{(4)}}{g^{(3)}}\ . \tag{4.30}$$

The main point in the theory of the effective two-level Hamiltonian is that the eigenvalues of $\hat{A}$ are always much larger than the eigenvalues of $\hat{H}_{\text{eff}}$. In this particular three-level system, this condition can be met by allowing the coupling constant linked the states in the subsystem $\mathbb{Q}|\Psi(t)\rangle$ to be far stronger. That is, we assume $g^{(3)} >> g^{(1)}, g^{(2)}$, and $g^{(4)}$. It is observable now that the state $|c, 0110\rangle$ can not be a potential state in the subsystem $\mathbb{P}|\Psi(t)\rangle$.

Assuming the system initially in $|a\ 10\rangle$, the qubit states exchange (i.e. $|a\ 10\rangle \mapsto \mathrm{i}|a\ 01\rangle$) can be realized, by setting $\overline{g}t = \pi$ (with $\overline{g} = \sqrt{G^2_{(1)} + G^2_{(2)}}$), $|G^{(1)}t| = |G^{(2)}t| = \pi/\sqrt{2}$, and $\eta t = \pi/2$ (see Eq. (4.11)).

4.7 The impact of variations in couplings and detunings

Previously, we figured out possible configurations for swapping the qubit states $|a\ 10\rangle$ and $|a\ 01\rangle$. In what follows, we numerically test the impact of variations in significant parameters such as the coupling constant g and the detunings Δ and Δ_4 on the fidelity of different configurations.

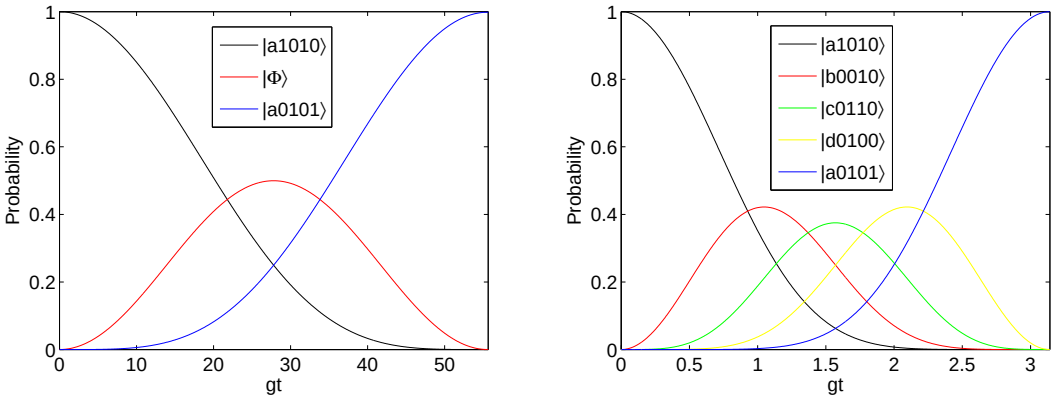

(a) (b)

Figure 4.8: A completely resonant system reduced into a three- or a five-level approximation. (a) a three-level system with the coupling strengths g_2 and g_4 are set to g, whereas the coupling strength g_3 is set to $25g$. The state $|\Phi\rangle$ can be either $|b0010\rangle$ or $|d0100\rangle$, in our example we use $|b0010\rangle$, and g_1 is determined by Eq. (4.30). (b) a five-level behaviour with the coupling constants g_1 and g_4 are set to g, and g_2 and g_3 are given by $\sqrt{3/2}\ g$.

4.7.1 Fidelity and conditional measurements

Generally speaking, fidelity is considered as a very useful tool for measuring the distance between quantum states in Hilbert space [26, 71]. For two quantum systems given by the density matrices ρ_1 and ρ_2 the fidelity $F(\rho_1, \rho_2)$ can be defined as [25, 71]

$$F(\rho_1, \rho_2) = \left(\mathrm{Tr}\sqrt{\rho_1^{1/2}\ \rho_2\ \rho_1^{1/2}} \right)^2 . \tag{4.31}$$

Previously, we have seen that the configurations in Secs. $4.2 - 4.6$ are able to interchange the qubit states $|a\ 10\rangle$ and $|a\ 01\rangle$. Here we aim to measure the fidelity in these models. The formula of fidelity above can be further simplified for special cases. In our case both of the wavefunction $|\Psi\rangle$ describing the system in Eq. (4.3) and the target $|a\ 01\rangle$ are pure states; consequently, one can set $\rho_1 = |\Psi\rangle\langle\Psi|$ and $\rho_2 = |a\ 01\rangle\langle a\ 01|$. The fidelity $F(\rho_1, \rho_2)$ then is nothing but the probability of the system to be in the state $|a\ 01\rangle$, i.e.

$$F(|\Psi\rangle\langle\Psi|, |a\ 01\rangle\langle a\ 01|) = |\langle a\ 01|\Psi\rangle|^2 . \tag{4.32}$$

In Fig. 4.9 the fidelity for some configurations has been plotted. It is clear that as much as we reduce the number of detuned states in the system (in other words the number of states spanned by $\mathbb{P}$ has been increased) a higher fidelity can be achievable at shorter interaction times. This feature is important in many CQED QIP applications as high fidelity operations with interaction times which are much shorter than the lifetime of photons in

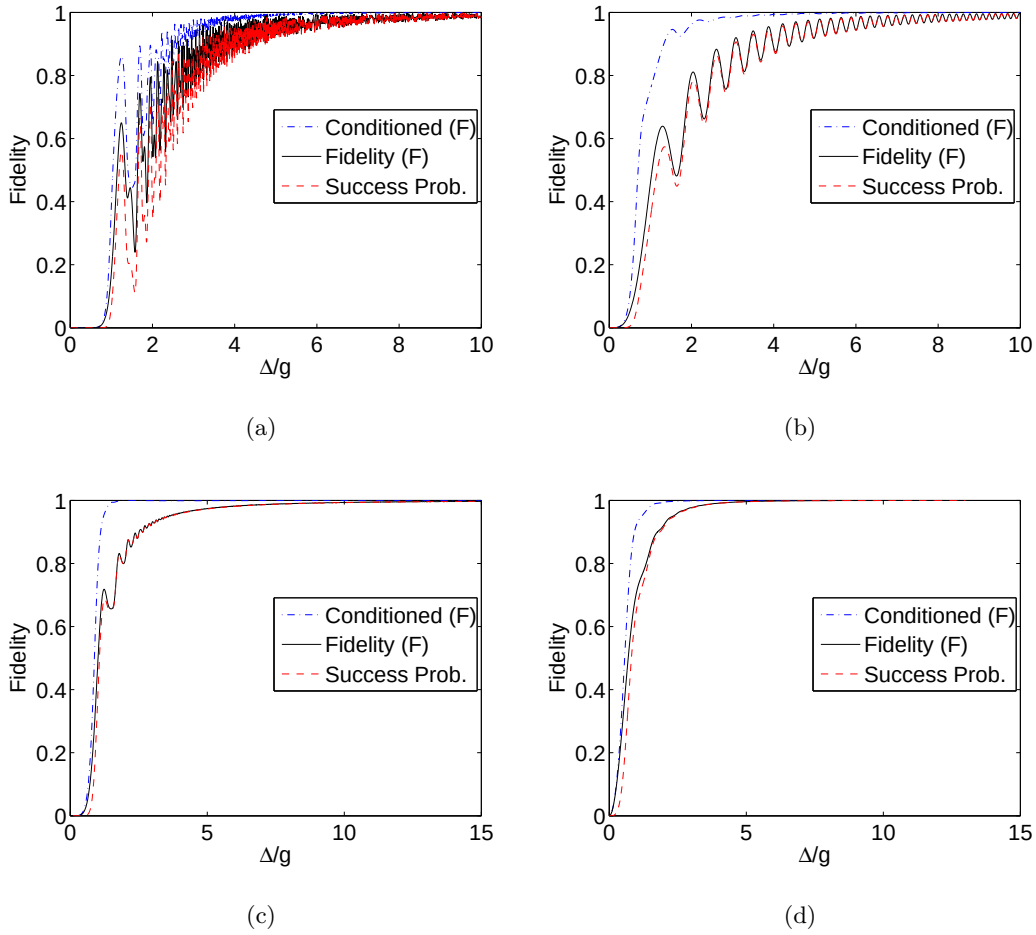

Figure 4.9: Fidelity (black solid line), the conditional measurement (blue dotted-dashed line), and success probability (red dashed line) in the configurations (a) (10001), (b) (10101), (c) (11001), and (d) (11011). Parameters can be found in Figs. 4.3, 4.4, 4.5, 4.6. Note that success probability is defined as the product of the fidelity with the conditional measurement.

the cavity is required.

With information being stored in the cavity, the atom in our scheme must be in the atomic state $|a\rangle$ before and after the cavity; otherwise, the operation does not work. Considering the conditional measurements on the atom, we allow the action of the projection operator $\Pi \equiv |a\rangle\langle a|$ on the state in Eq. (4.3). That is, by applying the previous projective measurement and renormalizing the resultant state, one finds that the post-measurement (see e.g. [15]) is $|\Psi^{PM}\rangle = \frac{\Pi\,|\Psi\rangle}{\sqrt{\langle\Psi|\Pi|\Psi\rangle}}$. The conditional fidelity $F(|\Psi^{PM}\rangle\langle\Psi^{PM}|, |a\ 01\rangle\langle a\ 01|)$ can be then defined as

$$F_{cond} = \frac{|\langle a\ 01|\Psi\rangle|^2}{\langle\Psi|\Pi|\Psi\rangle}\ , \tag{4.33}$$

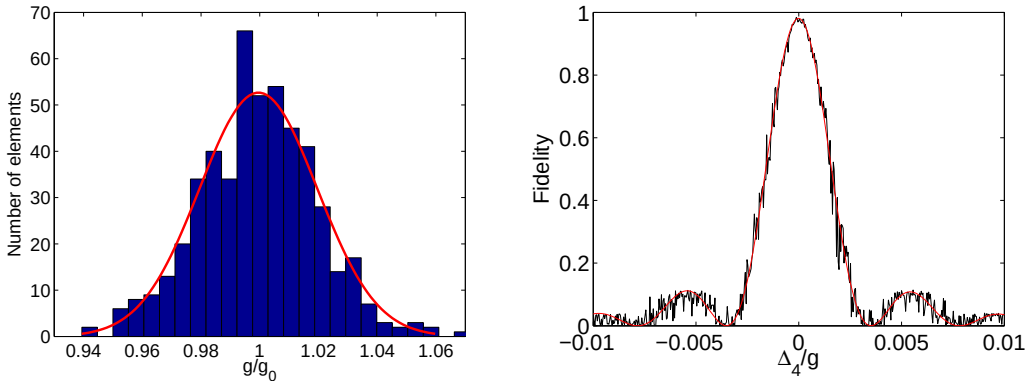

(a) (b)

Figure 4.10: (a) Histogram of the atom-field coupling strength with a Gaussian distribution fit, where the standard deviation is set to $\sigma = 0.02$. (b) Fidelity in (10001) with g given by (a) (black line) and with the theoretical value g_0 (red line). Parameters of resonance conditions and the system coupling constants can be found in Fig. 4.3, with $\Delta = 10\ g$.

where $\langle\Psi|\Pi|\Psi\rangle = |\langle a\ 10|\Psi\rangle|^2 + |\langle a\ 01|\Psi\rangle|^2$. In Fig. 4.9 the blue dashed lines represent the conditional fidelity for different models. It is illustrated that an enhancement in the configuration fidelity can be achieved when considering the conditional measurements on the atom, and such a result is reported in [56]. Practically, in the case of Rydberg atoms interacting with a cavity, for example, conditional measurements on atoms can be carried out by allowing Rydberg atoms to directly move into a detector D. Since different circular levels in the Rydberg atom ionize in different electric fields [8, 44], the electric field inside D can be chosen carefully so that the atomic level of interest can be ionized, and then D is state selective [8]. As a final line in this section, it is reported that conditional measurements on atoms can be used as an efficient method to generate and detect Fock states [72].

4.7.2 Sensitivity to variations in the coupling constants and detunings

Previously, the coupling strength g between the atom and the cavity was assumed to be perfect, i.e. the value of g has been assumed to be completely equal to the theoretical coupling g_0 during the interaction time. In reality, however, this is not the case. Even in the recent cavities, there is always uncertainty in values of parameters. For example, it is reported in [8] that the uncertainty in atom velocity ranges between ± 2 m/s, and then the atomic position of each atom can be determined with a ± 1 mm precision. Moreover, in the one-atom maser experiment [44], it is found that the variation of the atom-field

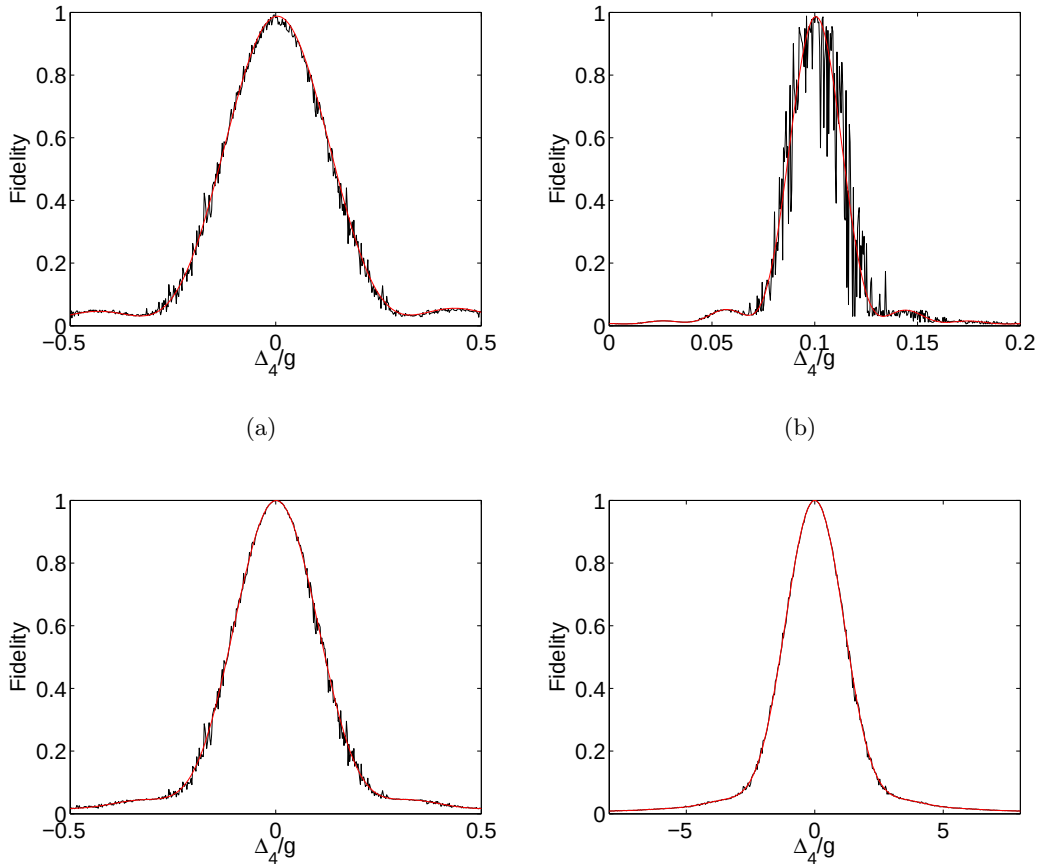

Figure 4.11: Plots (a)-(d) represent the fidelity of the models (10101), (11001), (11011), and (11111), respectively, with the theoretical coupling constant $g = g_0$ (red line) or g given by Gaussian distribution in Fig. 4.10 (a) (black line). Parameters: values of coupling constants and resonance conditions can be found in Figs. 4.4, 4.5, 4.6, 4.8, respectively, with $\Delta = 10\ g$.

strength over the cross section of the atomic beam (0.5 mm) is in order 2%.

Assuming the practical coupling constant to be g and the theoretical value to be g_0, one then can allow the value of g to vary slightly around g_0 , as shown in Fig. 4.10(a). Figs. 4.10(b), 4.11 show that the sensitivity of configurations differ between each other. For all models, the general tendency refers to the number of resonant states (i.e. the number of states spanned by $\mathbb{P}$) increases as the model becomes less sensitive to the changes in g. It is clear from figures, furthermore, that the fidelity of the models at the proper value of Δ_4 (the detuning of the last state $|a\ 01\rangle$) remains at the highest limit, such a result reflecting the robustness of the models.

Using the same Figs. 4.10(b),4.11, we can address the sensitivity of the previous models

to changes in Δ_4. The appropriate values of Δ_4 can be determined by the corresponding resonance condition in each model (see Secs. 4.3-4.6). However, allowing this detuning to vary around its proper value shows that the completely resonant system (11111) has the largest width amongst the models, whereas the narrowest width has been found in the model (10001). In more details, numerical calculations show that for models (10001), (10101), (11001), (11011), and (11111) full width at half maximum FWHM are, respectively, FWHM $= (3.2,\ 287,\ 28.7,\ 238.3,\ 2707) \times 10^{-3}$. It is clear then that faster models are less sensitive to variations in Δ_4 (the speed of each model can be found in Secs. 4.3-4.6).

To outline this section, we have checked the response of different configurations in Secs. 4.3-4.6 to variations in parameters such as Δ, g, and Δ_4. Generally, we have observed that the sensitivity of the system whose N is larger is less compared to other systems.

4.8 Time evolution of the qubit states $|a\ 11\rangle$ and $|a\ 00\rangle$

So far, several multi-photon resonance models transforming the qubit state $|a\ 1010\rangle$ to $|a\ 0101\rangle$, and vice versa, have been formed. Following the truth table 4.1 for the iSWAP gate, the qubit states $|a\ 1001\rangle$ and $|a\ 0110\rangle$ must be in their initial state. It is easy to find that the qubit state $|a\ 0110\rangle$ has not been affected by the Hamiltonian $\hat{H}$ in 4.2, i.e. $\hat{H}|a\ 0110\rangle \mapsto 0$, meaning that this state remains unchanged. On the other hand, the situation is nontrivial when considering the action of H in the qubit state $|a\ 1001\rangle$. So we need to find a way to keep this qubit in its initial state at the appropriate interaction time.

Recalling the Hamiltonian $\hat{H}$ in Eq. (4.2), the state $|a\ 1001\rangle$ evolves into a superposition

$$|\Psi(t)\rangle \mapsto c_1(t)|c\ 0101\rangle + c_2(t)|b\ 0001\rangle + c_3(t)|a\ 1001\rangle + c_4(t)|d\ 1000\rangle + c_5(t)|c\ 1010\rangle \quad (4.34)$$

It is clear from $|\Psi(t)\rangle$ in 4.34 that basis states link to no more than a couple of the nearest states and there is no loop, such conditions for a system described by a RWA tridiagonal Hamiltonian [51]. The spin-J model (see Sec. 3.2), thus, can be applied and the proper values for the sequence of effective couplings can be determined by $g^{(n)} = g_0\sqrt{n(N-n)}$. The RWA Hamiltonian for this system in the interaction picture $\hat{H}'$, therefore, can be expressed in the tridiagonal form. In the basis $\{|c\ 0101\rangle, |b\ 0001\rangle, |a\ 1001\rangle, |d\ 1000\rangle, |c\ 1010\rangle\}$,

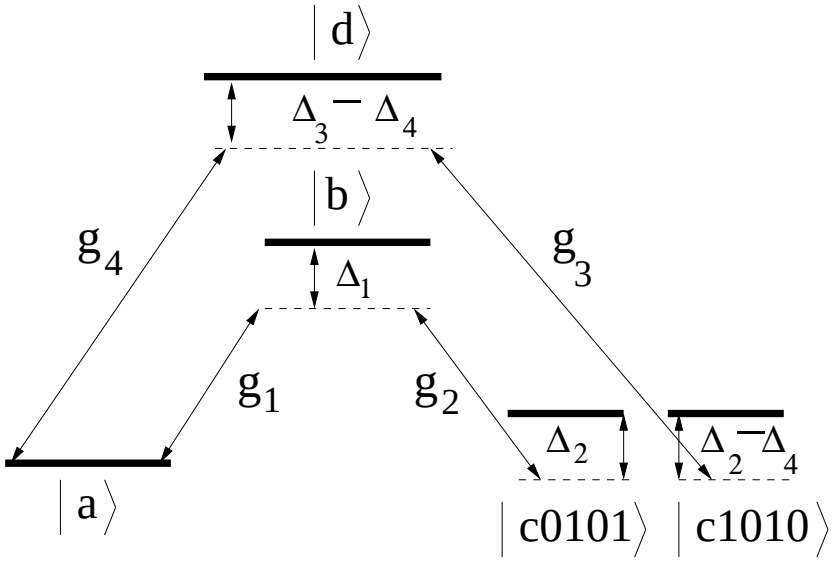

Figure 4.12: A possible schematics showing the time evolution of the qubit state $|a\ 11\rangle$.

the Hamiltonian $\hat{H}'$, by setting $|a\ 1001\rangle$ to be the zero point of energy, can be written as

$$\hat{H}' = \begin{bmatrix} \Delta_2 & g_2 & 0 & 0 & 0 \\ g_2 & \Delta_1 & g_1 & 0 & 0 \\ 0 & g_1 & 0 & g_4 & 0 \\ 0 & 0 & g_4 & \Delta_3 - \Delta_4 & g_3 \\ 0 & 0 & 0 & g_3 & \Delta_2 - \Delta_4 \end{bmatrix}, \tag{4.35}$$

where Δ_i (with $i = 1, 2, 3, 4$) can be defined by Eq. (4.5). Considering the configurations interchanging the qubit states $|a\ 10\rangle$ and $|a\ 01\rangle$, we check in the subsequent sections whether the system in 4.34 remains or returns to $|a\ 11\rangle$ at t_{int} given by Eq. (3.16).

4.8.1 Model (10001)

In Sec. 4.3, the detunings Δ_1, Δ_2, and Δ_3 are large and the sharp Δ_4 is predicted by Eq. (4.8). Considering these values of detunings in the system in the Hamiltonian (4.35), all states other than $|a\ 1001\rangle$ are set to be spanned by $\mathbb{Q}$ projector. So it is not surprising to observe that the system is sufficiently confined in the state $|a\ 1001\rangle$ (see Fig. 4.13). This implies that this configuration can realize the iSWAP gate.

4.8.2 Models: (10011), (11001), (10101)

Considering the model (11001) in Sec. 4.4.2, in this model $\Delta_{2,3} >> \Delta_{1,4},\ g_k$ (where $k = 1, 2, 3, 4$). Applying parameters of this model (see Eqs. (4.17, 4.18)) to the system in (4.35) eliminates adiabatically the basis states $|d\ 1000\rangle$, $|c\ 0101\rangle$ and $|c\ 1010\rangle$. At the

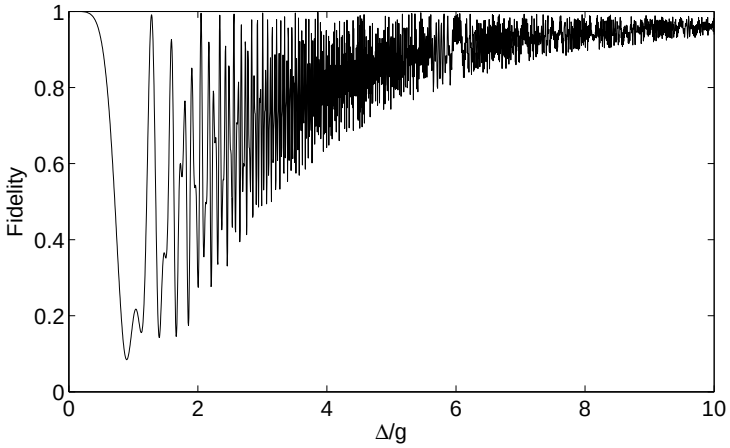

(a)

Figure 4.13: Fidelity of the system in (4.35) to be confined in $|a11\rangle$. Parameters as in Fig. 4.3.

interaction time $|g^{(n)}\ t_{\rm int}| = \sqrt{n(N-n)}\ \pi/2$ (with $N = 3$ and $n = 1, 2$) the system in (4.34) can be largely confined in the state $|a\ 1001\rangle$, as demonstrated by Fig. 4.14. A similar story can be said to the case of the model (10011). The models (10011) and (11001) are, therefore, able to realize the iSWAP gate.

Moving now to the model (10101) (see Sec. 4.4.1), this model requires both Δ_1 and Δ_3 to be larger than $\Delta_{2,4}$ and g_k ($k = 1, 2, 3, 4$). Substituting the parameters in the model (10101) into the Hamiltonian $\hat{H}$ (4.35) shows that, unfortunately, the model (10101) is unable to form the iSWAP gate, as illustrated by Fig. 4.15.

To give more explanations, the corresponding (10101) for the system (4.35) yields the resultant operators

$$\hat{H}_0 = \begin{bmatrix} \Delta_2 & 0 & 0 \\ 0 & 0 & 0 \\ 0 & 0 & \Delta_2 - \Delta_4 \end{bmatrix}, \quad \hat{A} = \begin{bmatrix} \Delta_1 & 0 \\ 0 & \Delta_3 - \Delta_4 \end{bmatrix}, \quad \hat{B} = \begin{bmatrix} g_2 & 0 \\ g_1 & g_4 \\ 0 & g_3 \end{bmatrix}. \tag{4.36}$$

Then the effective couplings can be given by

$$g^{(1)} = -g_1 g_2/\Delta_1\ , \quad g^{(2)} = -g_3 g_4/(\Delta_3 - \Delta_4)\ , \tag{4.37}$$

and the resonance conditions can be defined as

$$\begin{aligned} \Delta^{(1)} &= \Delta_2 - \frac{g_2^2}{\Delta_1} + \frac{g_1^2}{\Delta_1} + \frac{g_4^2}{\Delta_3 - \Delta_4}\ , \\ \Delta^{(2)} &= \Delta_2 - \Delta_4 - \frac{g_3^2}{\Delta_3 - \Delta_4} + \frac{g_1^2}{\Delta_1} + \frac{g_4^2}{\Delta_3 - \Delta_4}\ . \end{aligned} \tag{4.38}$$

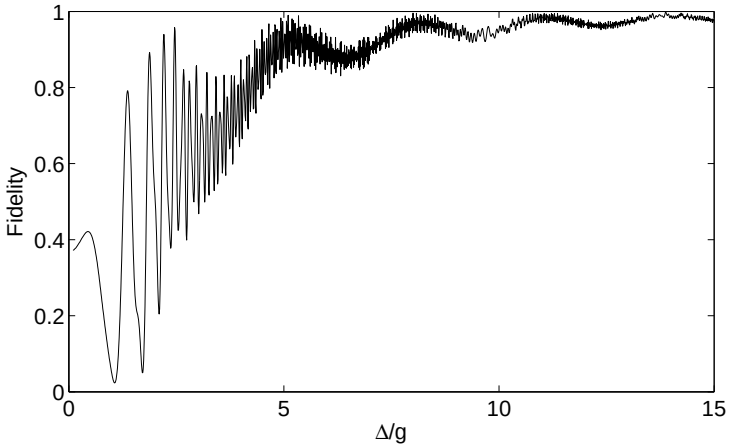

Figure 4.14: Fidelity of the system (4.35) to be in the qubit state $|a\ 1001\rangle$ when considering the model (11001). Parameters are the same as Fig. 4.5.

By setting the effective couplings $\Delta^{(1)}$ and $\Delta^{(2)}$ to zero (i.e. $\Delta^{(1)} = \Delta^{(2)} = 0$), the resonance conditions are

$$\begin{aligned} \Delta_2 &\approx \frac{g_2^2}{\Delta_1} - \frac{g_1^2}{\Delta_1} - \frac{g_4^2}{\Delta_3}\ , \\ \Delta_4 &\approx \frac{g_2^2}{\Delta_1} - \frac{g_3^2}{\Delta_3}\ . \end{aligned} \tag{4.39}$$

The qubit state $|a\ 1001\rangle$ can be completely repopulated at $|g^{(1)}t'| = |g^{(2)}t'| = \pi/\sqrt{2}$ which is equivalent to the interaction time needed to exchange the qubit states $|a\ 1010\rangle$ and $|a\ 0101\rangle$. Values of Δ_2 and Δ_4 determined by the resonance conditions in (4.39) do not match with those ones predicted by the resonance conditions in model (10101) (see Eqs. (4.14, 4.15)). It is observable that when exact parameters of $g_{1,2,3,4}$, $\Delta_{1,3}$, and t_{int} have been considered for both systems, the changes in the resonance conditions (4.39) (either in the amplitude or even in the sign) can destroy the system fidelity, reflecting how effective systems are strongly sensitive to the resonance conditions.

4.8.3 Models: (10111), (11101), (11011)

Setting Δ_2 in the Hamiltonian $\hat{H}$ to be large (as in the model (11011) in Sec. 4.5.1), the population of the system can be confined between the states $|a\ 1001\rangle$, $|b\ 0001\rangle$, and $|d\ 1000\rangle$, producing a three-level configuration. Fig. 4.16 represents the fidelity of the system in (4.34) to be completely in the qubit state $|a\ 1001\rangle$ at the interaction time t_{int} given by Eq. (3.16) (with $N = 4$), where the parameters defined by Eqs. (4.23, 4.24) are considered. It can be shown that the model (11011) is unable to return to the qubit state $|a\ 1001\rangle$ at t_{int} above. The model (11011), thus, is no longer a candidate for realizing the

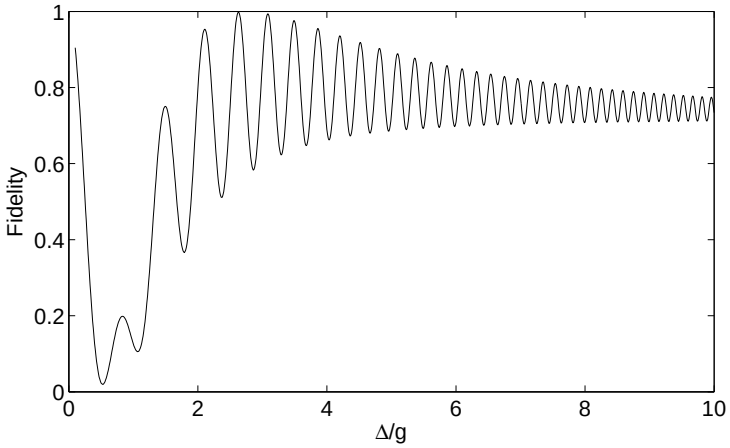

Figure 4.15: Fidelity of the qubit state $|a\ 1001\rangle$ to remain or return to its initial state when applying the model (10101) in Sec. 4.4.1. Parameters can be found in Fig. 4.4.

iSWAP gate.

With Δ_2 being larger than any parameters in H (4.35) and following the effective Hamiltonian theory [46], the behaviour of this system can be addressed as follows. The corresponding operators $\hat{H}_0$, $\hat{A}$, and $\hat{B}$ can be written as

$$\hat{H}_0 = \begin{bmatrix} 0 & g_1 & g_4 \\ g_1 & \Delta_1 & 0 \\ g_4 & 0 & \Delta_3 - \Delta_4 \end{bmatrix}, \quad \hat{A} = \begin{bmatrix} \Delta_2 & 0 \\ 0 & \Delta_2 - \Delta_4 \end{bmatrix}, \quad \hat{B} = \begin{bmatrix} 0 & 0 \\ g_2 & 0 \\ 0 & g_3 \end{bmatrix}. \tag{4.40}$$

The effective detunings then, can be determined by

$$\begin{aligned} \Delta^{(1)} &= \Delta_1 - \frac{g_2^2}{\Delta_2} \\ \Delta^{(2)} &= \Delta_3 - \Delta_4 - \frac{g_3^2}{(\Delta_2 - \Delta_4)} \\ &\approx \Delta_3 - \Delta_4 - \frac{g_3^2}{(\Delta_2)}\ , \end{aligned} \tag{4.41}$$

and the effective couplings read

$$g^{(1)} = g_1 \quad g^{(2)} = g_4\ . \tag{4.42}$$

Even if it is possible to set all parameters in this system (i.e. parameters of coupling constants and detunings in Eqs. (4.41, 4.42)) to be completely equal to those parameters in the model (11011), the interaction time in these systems can be still different. That is, by using Eq. (3.16) the interaction time t'_{int} for the system [4.41] can be obtained by setting $N = 3$, whereas in the model (11011) we use $N = 4$ to find the corresponding t_{int}. Then, one finds that $t' = \sqrt{\frac{2}{3}}\ t$.

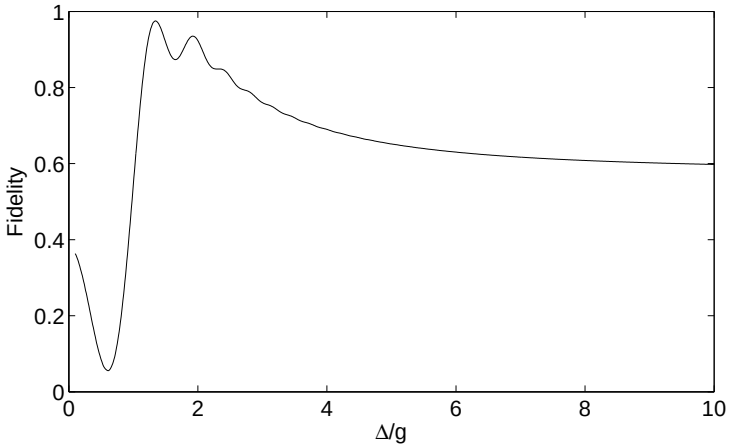

Figure 4.16: Fidelity of the system to be in $|a\ 1001\rangle$ when using the parameters in the model (11011). Values of different g and Δ in Fig. 4.6.

We now move to check whether or not the models (10111) and (11101) can keep the system (4.34) in the state $|a\ 1001\rangle$ at t_{int} (with $N = 4$). As the same argument can be made for these models, more details have been provided for the model (11101) alone. In this model, we choose Δ_3 to be large. Substituting the parameters for this model into the Hamiltonian H (4.35) produces a four-level behaviour. In Fig. 4.17, we observe that for different values of the detunings Δ the system is not confined in the state $|a\ 1001\rangle$ at t_{int}. In order to define the effective couplings and detunings in the effective system (when Δ_3 is large), one recalls the effective two-level Hamiltonian theory [46]. The operators in the expression $\hat{H}_{\text{eff}} = \hat{H}_0 - \hat{B}\ \hat{A}^{-1}\ \hat{B}^{\dagger}$, therefore, can be given by

$$\hat{H}_0 = \begin{bmatrix} 0 & g_1 & 0 & 0 \\ g_1 & \Delta_1 & g_2 & 0 \\ 0 & g_2 & \Delta_2 & 0 \\ 0 & 0 & 0 & \Delta_2 - \Delta_4 \end{bmatrix} , \quad \hat{A} = \Delta_3 - \Delta_4 , \quad \hat{B} = \begin{bmatrix} g_4 \\ 0 \\ 0 \\ g_3 \end{bmatrix} . \tag{4.43}$$

The effective detunings can be expressed as

$$\begin{aligned} \Delta^{(1)} &= \Delta_1 + \frac{g_4^2}{(\Delta_3 - \Delta_4)} , \\ \Delta^{(2)} &= \Delta_2 + \frac{g_4^2}{(\Delta_3 - \Delta_4)} , \\ \Delta^{(3)} &= \Delta_2 - \Delta_4 - \frac{g_3^2}{(\Delta_3 - \Delta_4)} + \frac{g_4^2}{(\Delta_3 - \Delta_4)} , \end{aligned} \tag{4.44}$$

and the effective couplings can be defined as

$$g^{(1)} = g_2 , \quad g^{(2)} = g_1 , \quad g^{(3)} = -\frac{g_3 g_4}{\Delta_3 - \Delta_4} . \tag{4.45}$$

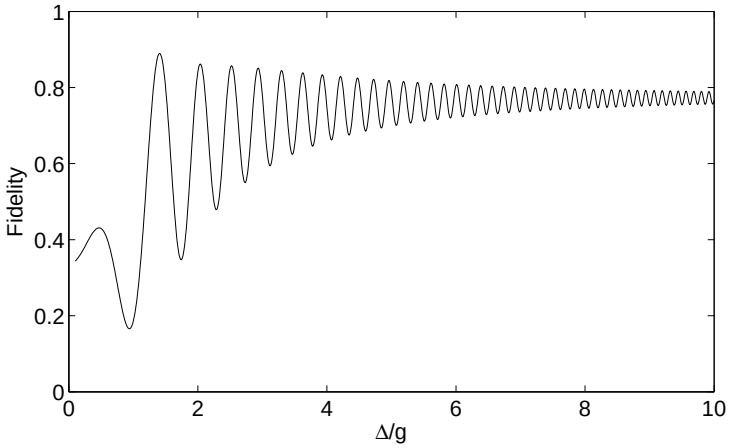

Figure 4.17: Fidelity showing the probability to set all populations in $|a\rangle$ at the same interaction time in the model (11101). Parameters for the coupling constants and detunings can be found in Fig. 4.7

The resonance conditions for this system (with $\Delta^{(1)} = \Delta^{(2)} = \Delta^{(3)} = 0$) can be given as

$$\begin{aligned} \Delta_1 = \Delta_2 &\approx -\frac{g_4^2}{\Delta_3} \ , \\ \Delta_4 &\approx -\frac{g_3^2}{\Delta_3} \ . \end{aligned} \tag{4.46}$$

The previous resonance conditions show that we deal with a four-level system. These conditions, on the other hand, may not completely give the same $\Delta_{1,2,4}$ provided by Eq. (4.27). Additionally, the differences between the effective couplings $g_{1,2}$ in both systems may result in different interaction times.

4.8.4 Five-level model (11111)

The final model tested in this section is the five-level model (11111) in (4.6). All detunings in the Hamiltonian (4.35) are set to zero, so a five-level approximation can be formed. The resultant effective couplings can be written as

$$g^{(1)} = g_2 \quad g^{(2)} = g_1 \quad g^{(3)} = g_4 \quad g^{(4)} = g_3 \ . \tag{4.47}$$

This system completely returns to $|a\ 11\rangle$ if the coupling constants satisfy $g_2 = \sqrt{\frac{2}{3}} g_1$, $g_3 = g_2$, and $g_4 = g_1$. These values, in contrast, do not match with coupling constants in the model (11111), so the system returns to $|a\ 1001\rangle$ at different t'_{int} (see Fig. 4.18).

At the end of this section, regarding the different configurations in Secs. 4.2-4.6, only three models, namely the models (10001), (11001), and (10011), have been successfully enforced

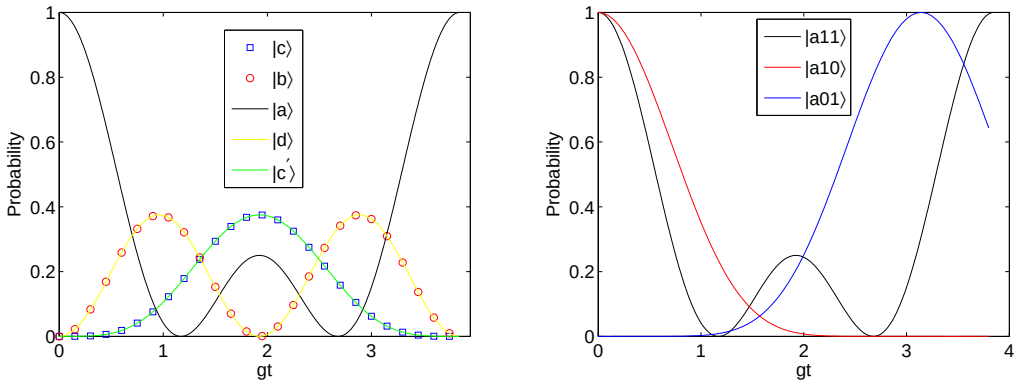

(a) (b)

Figure 4.18: (a) The five-level model of the system (4.35) when setting all detunings to zero. The coupling constant g_1 is set to g, and the remaining coupling strengths can be determined by Eq. (4.47). (b) When considering the model (11111) and with $|a\ 10\rangle$ being the initial state, it interchanges the qubit states $|a\ 10\rangle$ and $|a\ 01\rangle$ at $|g_1 t| = \pi$ (see Sec. 4.6), and (when $|a\ 11\rangle$ is the initial state) it returns the qubit $|a\ 11\rangle$ to its initial state at $|g_1 t'| = \sqrt{\frac{3}{2}}\,\pi$. The qubit state $|a\ 00\rangle$ remains unchanged. So it is clear that this model is not able to realize the iSWAP gate.

$|\Psi\rangle$ in (4.34) to be in $|a\ 1001\rangle$ at the appropriate t_{int}. It is observable that these models help the system in (4.35) to be confined in the initial state $|a\ 1001\rangle$ by allowing large detunings for all states other than $|a\ 1001\rangle$, as shown by the model (10001). Moreover, by reducing the value of the coupling constant linked to one of the most upper states $|b\rangle$ or $|d\rangle$ and allowing large detunings to the remaining states (as demonstrated by the models (11001) and (10011)), we can realize the iSWAP gate.

The iSWAP gate given by the models (11001) and (10011), in contrast, are faster than the iSWAP gate realized by (10001); the iSWAP gate with the models (11001) and (10011) are simpler than (as yet undiscussed) the three-qubit Fredkin gate in Sec. 5.8. Fig. 4.19 illustrates the truth table of the iSWAP gate by the models (10001) and (11001).

4.9 Summary

Based on multi-photon resonance theory and dual-rail qubits encoded in cavities, the universal iSWAP gate has been realized. The use of effective N-level Hamiltonians (with $N = 2, 3, 4$, and 5) generates various configurations that transform the qubit state $|a\ 10\rangle$ to $|a\ 01\rangle$. Applying parameters of these configurations to the system of $|a\ 11\rangle$ yields the iSWAP gate by three models, namely (10001), (11001), and (10011). The last two models

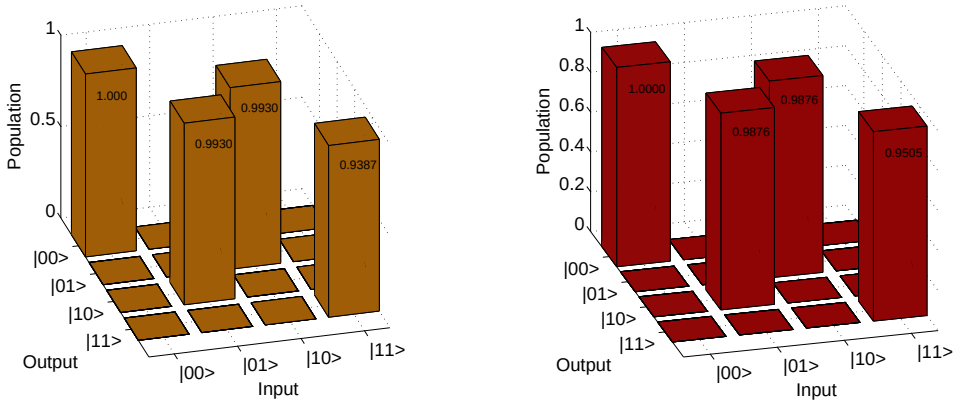

(a) (b)

Figure 4.19: Truth table of the numerically simulated iSWAP gate with $\Delta = 10\ g$ in the absence of decoherence processes. (a) in the configuration (10001). (b) in the model (11001). Parameters for (a) can be found in Fig. 4.3 and for (b) in Fig. 4.5.

own a practical operation time for cavity-QED QIP applications.

We now discuss in brief the experimental feasibility of implementing this scheme. Our scheme requires that the atom-cavity coupling strength g to be larger than the coupling of the system by the surrounding environment. In other words, the interactions of the atom-cavity must be in the strong coupling regime where the condition $g >> \Gamma,\ \kappa$ is satisfied, with Γ^{-1} and κ^{-1} are the radiative lifetime and the photon lifetime, respectively. Various modern cavities with a high Q factor meet these conditions (see for example [2, 6, 73]). In a micromaser [2], a two-level ^{85}Rb Rydberg atom (with atomic decay rate $\Gamma/2\pi = 500$ Hz) interacts with a high-Q superconducting cavity ($Q = 8\times10^8$). The photonic relaxation rate is about $\kappa/2\pi = 0.4$ Hz and the coupling constant is $g_0/2\pi = 7$ kHz. The interaction time τ_{int} for the iSWAP gate in the model (11001) and with the choice $\Delta_2 = \Delta_3 = \Delta = 5g$ is on the order $\pi\Delta^2/(\sqrt{2}g^3) \sim 1 \times 10^{-3}$ s which is much shorter than κ^{-1}. This scheme, consequently, can be realized by the recent cavity QED techniques.

At present, the strong interaction between a multi-level atom with a multi-mode field (such an interaction proposed in our scheme) remains an experimental challenge. In fact, with the remarkable progress in nanotechnology, this kind of interaction might be possible in the near future [69]. It is reported in [74] that a transfer of energy between two individual nanoparticles strongly coupled to high-Q whispering-gallery modes in a microsphere resonator is experimentally achieved. This achievement gives great hope for finding experiments that proceed an interaction between a single multi-mode cavity interacting with a multi-level atom in the limit of strong coupling.

Chapter 5

The Fredkin gate

In chapter 4, we have seen that a universal double-qubit gate is realizable in the scheme based on multi-photon resonances and dual-rail qubits encoded in cavities. In this chapter, on the other hand, we apply the multi-photon resonance theory in chapter 3 in order to perform the three-qubit Fredkin gate for dual-rail CQED QIP. This gate has been proposed by [56] since the iSWAP gate in a two-level configuration has been demonstrated to be slow for QIP applications. However, we have seen in the previous chapter that a fast iSWAP gate in a three-level model could be theoretically achieved. So, we aim in this chapter to confirm whether or not a Fredkin gate in a different N-level approximation can be realized. Indeed, this gate requires deeper understanding of the multi-photon resonance theory in chapter 3 and more challenges in forming different configurations.

The Fredkin gate [75] is a universal gate owning important properties which sets up the general principles of logic gates and circuits in both classical and quantum computing [26]. As demonstrated in Fig. 5.1, this gate swaps the second and the third qubits if the first qubit is $|1\rangle$, otherwise, all qubits remain unchanged. Two examples of quantum circuits generating this gate have been provided in Fig. 5.1. In this figure, it is observable that the Fredkin gate can be generated by the controlled SWAP gate. Moreover, since the SWAP gate is equivalent to three CNOT gates, we can see that the Fredkin gate is a combination of the Toffoli gate together with two CNOT gates [25].

In the following section, we give a description for the general model of the atom+field system. In Secs. 5.2, 5.6 we discuss different configurations that transform the qubit state $|a\ 101\rangle$ to $|a\ 110\rangle$. The gate fidelity has been studied for variations in the system parameters in Sec. 5.7. In the subsequent section time evolution of the rest qubits in the Fredkin truth table has been investigated. Finally, we conclude in Sec. 5.9.

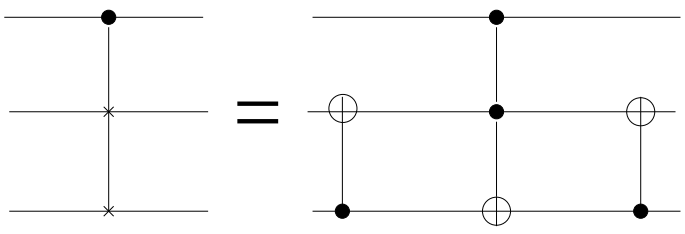

:≡

Input	Output
$\|000\rangle$	$\|000\rangle$
$\|001\rangle$	$\|001\rangle$
$\|010\rangle$	$\|010\rangle$
$\|011\rangle$	$\|011\rangle$
$\|100\rangle$	$\|100\rangle$
$\|110\rangle$	$\|101\rangle$
$\|101\rangle$	$\|110\rangle$
$\|111\rangle$	$\|111\rangle$

Figure 5.1: Quantum circuits generating the Fredkin gate [25] plus the logic and the truth table for the gate [26].

5.1 The model

As demonstrated in Fig. 5.1, the Fredkin gate can be simulated by the controlled-SWAP quantum circuit [25, 26]. It is possible, then, to employ the iSWAP model in chapter 4 in order to perform the Fredkin gate. This is exactly what has been proposed by [56]. There are a number of different schemes based on cavity-QED that have been proposed to realize the Fredkin or the controlled-SWAP gate (see e.g. [76] and [77]). Apart from our scheme, neither of the existing cavity QED-based proposals for the Fredkin gate use the advantageous dual-rail approach. Following the same proposal in [56], two further atomic states $|e\rangle$ and $|f\rangle$ and a single mode, which is used twice during the system transitions, have been added to the iSWAP model in Sec. 4.1. Moreover, the energies of the new levels satisfy $E_d, E_f > E_e$ and $E_e > E_a$ (see Figs. 4.2, 5.2), introducing another lambda configuration (so the extension of the definitions for parameters such as detunings can be made easily). The iSWAP model is linked to the new states via the mode n_4; therefore, this mode alongside the first mode n_1 can be chosen to form the control qubit C$\equiv |n_1\ n_4\rangle$ in this system [56] in order that the controlled-SWAP (or the Fredkin) gate can be generated. On the other hand, the remaining modes paired as$|n_2\ n_3\rangle$ and $|n_5\ n_6\rangle$ can be considered as the target qubits. Note that all these qubits can be represented by the dual-rail qubits (see Sec. 4.1), where each of them contains two modes and a single photon. The control qubit C can be encoded as $|1\rangle$ if there is a photon in n_1 alone, and then the swap operation can be performed on the target qubits. In the case of $C \equiv |0\rangle$ (i.e. the presence of the photon is in n_4) the target qubits remain unchanged.

Following the argument in Sec. 4.1 and considering the energy-level configuration in [5.2],

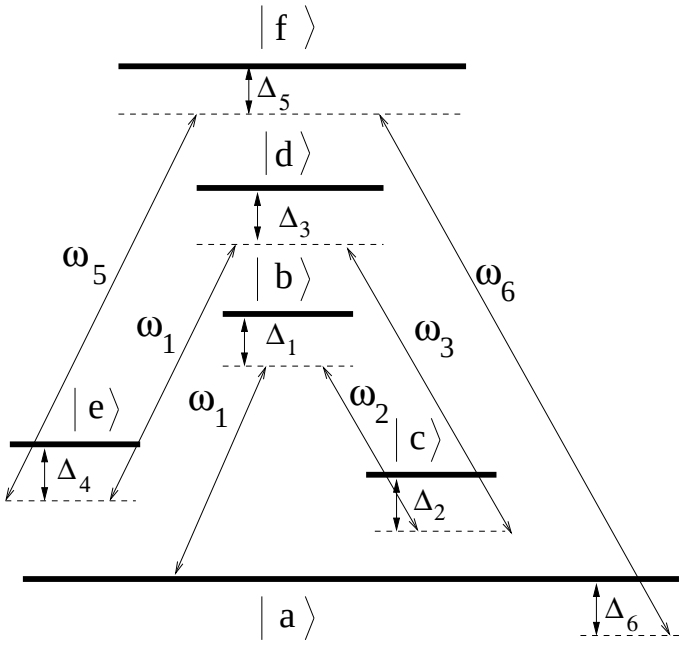

Figure 5.2: A possible schematics for the Fredkin gate. More details can be found within the context.

the general Hamiltonian $\hat{H}$ can be constructed as

$$\hat{H} = \underbrace{\hbar \sum_i \omega_i \, \hat{\sigma}_{ii} + \hbar \sum_j \omega_j \, \hat{a}_j^\dagger \hat{a}_j}_{\hat{H}_0} \overbrace{-\hat{\mu} \cdot \hat{E}(z,t)}^{\hat{H}_{int}} \, , \tag{5.1}$$

with $i = a, b, c, d, e, f$ and $j = 1, 2, 3, 5, 6$. The Hamiltonian $\hat{H}_0$ is a combination of the free atom and the free field Hamiltonians, and $\hat{H}_{int}$ is the interaction Hamiltonian. In our case, $\hat{H}_{int}$ can be expressed as

$$\begin{aligned} \hat{H}_{int} = \; & - \; \mu_{ab}(\hat{\sigma}_{ab} + \hat{\sigma}_{ba}) \cdot \hat{E}_1(z,t) - \mu_{bc}(\hat{\sigma}_{bc} + \hat{\sigma}_{cb}) \cdot \hat{E}_2(z,t) \\ & - \; \mu_{cd}(\hat{\sigma}_{cd} + \hat{\sigma}_{dc}) \cdot \hat{E}_3(z,t) - \mu_{de}(\hat{\sigma}_{de} + \hat{\sigma}_{ed}) \cdot \hat{E}_1(z,t) \\ & - \; \mu_{ef}(\hat{\sigma}_{ef} + \hat{\sigma}_{fe}) \cdot \hat{E}_5(z,t) - \mu_{fa}(\hat{\sigma}_{fa} + \hat{\sigma}_{af}) \cdot \hat{E}_6(z,t) \; , \end{aligned}$$

where, once again, we assume that $\mu_{\alpha\beta}$ is real, and at the atomic position z the electric field is given by $\hat{E}_m(z,t) = \epsilon_{\omega_m} \left[\hat{a}_m^\dagger(t) + \hat{a}_m(t)\right] \sin(k_m z)$ with $\epsilon_\omega = \sqrt{\frac{\hbar\omega}{\epsilon_0 V}}$. Defining the atom-field coupling strength $g_m = -\mu_{\alpha\beta} \, \epsilon_{\omega_m} \sin(k_m z)/\hbar$, one then can rewrite the Hamiltonian $\hat{H}_{int}$ in RWA as

$$\hat{H}_{int} = \hbar[g_1 \, \hat{a}_1 \, \hat{\sigma}_{ba} + g_2 \, \hat{\sigma}_{cb} \, \hat{a}_2^\dagger + g_3 \, \hat{a}_3 \, \hat{\sigma}_{dc} + g_1 \, \hat{\sigma}_{ed} \, \hat{a}_1^\dagger + g_5 \, \hat{a}_5 \, \hat{\sigma}_{fa} + g_6 \, \hat{\sigma}_{af} \, \hat{a}_6^\dagger + \text{h.c.}] \; .$$

The total Hamiltonian $\hat{H}$, thus, becomes

$$\begin{aligned}\hat{H} = \hbar\sum_i \omega_i\hat{\sigma}_{ii} + \hbar\sum_j \omega_j\hat{a}_j^\dagger\hat{a}_j \quad &+ \quad \hbar[g_1\ \hat{\sigma}_{ba}\ \hat{a}_1 + g_2\ \hat{\sigma}_{cb}\ \hat{a}_2^\dagger + g_3\ \hat{\sigma}_{dc}\ \hat{a}_3 \\ &+ \quad g_1\ \hat{\sigma}_{ed}\ \hat{a}_1^\dagger + g_5\ \hat{\sigma}_{fe}\ \hat{a}_5 + g_6\hat{\sigma}_{af}\ \hat{a}_6^\dagger + \text{h.c.}]\ , \quad (5.2)\end{aligned}$$

where $(i = a, b, c, d, e, f)$ and $(j = 1, 2, 3, 5, 6)$.

Given that an atom in the ground state $|a\rangle$ interacts with six modes (one of them is repeated), one then can represent the initial atom-field state as $|a\ n_1n_4, n_2n_3, n_5n_6\rangle$. Encoding the atomic state $|a\rangle$ with the photonic qubits in the Fredkin truth table in 5.1 shows that the initial state of the atom-field system can be either $|a\ 000\rangle$, $|a\ 001\rangle$, $|a\ 010\rangle$, $|a\ 011\rangle$, $|a\ 100\rangle$, $|a\ 110\rangle$, $|a\ 101\rangle$, or $|a\ 111\rangle$.

5.2 Time evolution of the qubit states $|a\ 110\rangle$ and $|a\ 101\rangle$

In order to meet the Fredkin truth table 5.1, we aim to carry out the transformation of the qubit states $|a\ 101\rangle \leftrightarrow |a\ 110\rangle$, and keep the remaining qubits unchanged. Beginning with the initial state of the atom-field system $|\Psi(0)\rangle = |a\ 10, 01, 10\rangle \equiv |a\ 101\rangle$ and following the same argument in Secs. 4.2, 4.8, the time evolution of $|\Psi(0)\rangle$ can be a superposition

$$\begin{aligned}|\Psi(t)\rangle \quad &= \quad c_1(t)\ |a\ 10, 01, 10\rangle + c_2(t)\ |b\ 00, 01, 10\rangle + c_3(t)\ |c\ 00, 11, 10\rangle \\ &+ \quad c_4(t)\ |d\ 00, 10, 10\rangle + c_5(t)\ |e\ 10, 10, 10\rangle + c_6(t)\ |f\ 10, 10, 00\rangle \\ &+ \quad c_7(t)\ |a\ 10, 10, 01\rangle + c_8(t)\ |b\ 00, 10, 01\rangle + c_9(t)\ |c\ 00, 20, 01\rangle\ . \quad (5.3)\end{aligned}$$

In the basis states of the previous wavevector, i.e. $\{|a\ 10, 01, 10\rangle, |b\ 00, 01, 10\rangle, |c\ 00, 11, 10\rangle, |d\ 00, 10, 10\rangle, |e\ 10, 10, 10\rangle, |f\ 10, 10, 00\rangle, |b\ 00, 10, 01\rangle, |c\ 00, 20, 01\rangle, |a\ 10, 10, 01\rangle\}$, one can represent the Hamiltonian $\hat{H}$ in the interaction picture as $(\hbar = 1)$

$$\hat{H}' = \begin{bmatrix} 0 & g_1 & 0 & 0 & 0 & 0 & 0 & 0 & 0 \\ g_1 & \Delta_1 & g_2 & 0 & 0 & 0 & 0 & 0 & 0 \\ 0 & g_2 & \Delta_2 & g_3 & 0 & 0 & 0 & 0 & 0 \\ 0 & 0 & g_3 & \Delta_3 & g_1 & 0 & 0 & 0 & 0 \\ 0 & 0 & 0 & g_1 & \Delta_4 & g_5 & 0 & 0 & 0 \\ 0 & 0 & 0 & 0 & g_5 & \Delta_5 & 0 & 0 & g_6 \\ 0 & 0 & 0 & 0 & 0 & 0 & \Delta_6 + \Delta_1 & g_2\sqrt{2} & g_1 \\ 0 & 0 & 0 & 0 & 0 & 0 & g_2\sqrt{2} & \Delta_6 + \Delta_2 & 0 \\ 0 & 0 & 0 & 0 & 0 & g_6 & g_1 & 0 & \Delta_6 \end{bmatrix}\ . \quad (5.4)$$

N-level system	On-resonance state(s)	Label
2-level	Nil	(1000001)
3-level	$\|d\ 00,10,10\rangle$	(1001001)
	$\|e\ 10,10,10\rangle$	(1000101)
	$\|f\ 10,10,00\rangle$	(1000011)
4-level	$\|d\ 0010,10\rangle$ & $\|e\ 10,10,10\rangle$	(1001101)
	$\|e\ 10,10,10\rangle$ & $\|f\ 10,10,00\rangle$	(1000111)
	$\|d\ 00,10,10\rangle$ & $\|f\ 10,10,00\rangle$	(1001011)
5-level	$\|d\ 00,10,10\rangle$ & $\|e\ 10,10,10\rangle$ & $\|f\ 10,10,00\rangle$	(1001111)

Table 5.1: The models that proceed the transformation $|a\ 101\rangle \leftrightarrow |a\ 110\rangle$. Note that the states $|a\ 101\rangle$ and $|a\ 110\rangle$ are always assumed to be on- or near-resonance. The over-shot states $|b\ 00,10,01\rangle$ and $|c\ 00,20,01\rangle$ are not considered in our label.

The definition of the detunings Δ_i (with $i = 1,2,...,6$) can be straightforwardly obtained by adding one more lambda configuration to the double lambda system in chapter 4 and by considering the energy-level system in (5.2). That is,

$$\begin{aligned}
\Delta_1 &= (\omega_{ba} - \omega_1)\ , \\
\Delta_2 &= (\omega_{ba} - \omega_1) - (\omega_{bc} - \omega_2)\ , \\
\Delta_3 &= (\omega_{ba} - \omega_1) - (\omega_{bc} - \omega_2) + (\omega_{dc} - \omega_3)\ , \\
\Delta_4 &= (\omega_{ba} - \omega_1) - (\omega_{bc} - \omega_2) + (\omega_{dc} - \omega_3) - (\omega_{de} - \omega_1)\ , \\
\Delta_5 &= (\omega_{ba} - \omega_1) - (\omega_{bc} - \omega_2) + (\omega_{dc} - \omega_3) - (\omega_{de} - \omega_1) + (\omega_{fe} - \omega_5)\ , \\
\Delta_6 &= (\omega_{ba} - \omega_1) - (\omega_{bc} - \omega_2) + (\omega_{dc} - \omega_3) - (\omega_{de} - \omega_1) + (\omega_{fe} - \omega_5) - (\omega_{fa} - \omega_6)\ .
\end{aligned} \tag{5.5}$$

To proceed the transformation $|a\ 101\rangle \leftrightarrow |a\ 110\rangle$, several configurations can be figured out. From the Hamiltonian 5.4, it is observable that the system (when either the initial state is $|a\ 101\rangle$ or $|a\ 110\rangle$) makes the "unwanted" transitions to the states $|b,00,10,01\rangle$, and $|c,00,20,01\rangle$. Since we always want the atom to be in the ground state $|a\rangle$ in and out the cavity, we can effectively avoid these further transitions by allowing large detunings for the states $|b,00,10,01\rangle$, and $|c,00,20,01\rangle$. Throughout this thesis, we will name the states $|b,00,10,01\rangle$, and $|c,00,20,01\rangle$ as over-shot or far-shot states. Similar to the iSWAP case, we label the different configurations as shown in table 5.1. Note that for convenience the

over-shot states $|b, 00, 10, 01\rangle$, and $|c, 00, 20, 01\rangle$ have been ignored.

At first glance, it may appear from the wavefunction $|\Psi\rangle$ (5.3) that we can produce N-level configurations (with $N = 2, 3, ..., 9$). However, the presence of the far-shot states above reduces the number of allowed states to be resonant. That is, we want the system in $|\Psi\rangle$ to move between the states $|a10, 01, 10\rangle$ and $|a10, 10, 01\rangle$ and no further. This is possible by keeping the detunings in the states $|b, 00, 10, 01\rangle$ and $|c, 00, 20, 01\rangle$ to be always far-resonance, and as a result the detunings in the states $|b\ 00, 01, 10\rangle$ and $|c\ 00, 11, 10\rangle$ must be large, too. Consequently, the number of states N in the $\mathbb{P}$ space can not exceed five states. Furthermore, we will see in the subsequent sections that the presence of the repeated coupling constant g_1 adds another limitation to the possible configurations.

5.3 Effective two-state behaviour: the model (1000001)

Assuming the space of the projection operator $\mathbb{P}$ contains the states $|a\ 101\rangle$ and $|a\ 110\rangle$ and the remaining states in Eq. (5.3) reside in the space of $\mathbb{Q} = I - \mathbb{P}$, the operators $\hat{H}_0 = \mathbb{P}\hat{H}\mathbb{P}$, $\hat{B} = \mathbb{P}\hat{H}\mathbb{Q}$, and $\hat{A} = \mathbb{Q}\hat{H}\mathbb{Q}$ (where $\hat{H}$ is given by Eq. (5.4)), can be written as

$$\hat{H}_0 = \begin{bmatrix} 0 & 0 \\ 0 & \Delta_6 \end{bmatrix}, \hat{B} = \begin{bmatrix} g_1 & 0 & 0 & 0 & 0 & 0 & 0 \\ 0 & 0 & 0 & 0 & g_6 & g_1 & 0 \end{bmatrix}, \tag{5.6}$$

$$\hat{A} = \begin{bmatrix} \Delta_1 & g_2 & 0 & 0 & 0 & 0 & 0 \\ g_2 & \Delta_2 & g_3 & 0 & 0 & 0 & 0 \\ 0 & g_3 & \Delta_3 & g_1 & 0 & 0 & 0 \\ 0 & 0 & g_1 & \Delta_4 & g_5 & 0 & 0 \\ 0 & 0 & 0 & g_5 & \Delta_5 & 0 & 0 \\ 0 & 0 & 0 & 0 & 0 & \Delta_6 + \Delta_1 & g_2\sqrt{2} \\ 0 & 0 & 0 & 0 & 0 & g_2\sqrt{2} & \Delta_6 + \Delta_2 \end{bmatrix}. \tag{5.7}$$

The effective Hamiltonian describing this system can be calculated by $\hat{H}_{\text{eff}} = \hat{H}_0 - \hat{B}\ \hat{A}^{-1}\ \hat{B}^{\dagger}$[46]. Note that the calculations of $\hat{A}^{-1}$ can be significantly simplified by realizing that $\hat{A}^{-1}$ is Hermitian and by carrying out $\hat{B}\ \hat{A}^{-1}\ \hat{B}^{\dagger}$ before calculating $\hat{A}^{-1}$.

The resonance condition, therefore, is

$$\begin{aligned}\Delta_{\rm eff} = \Delta_6 \;&-\; \frac{g_6^2[(\Delta_1\Delta_2 - g_2^2)(\Delta_3\Delta_4 - g_1^2) - \Delta_1\Delta_4\; g_3^2]}{[(\Delta_1\Delta_2 - g_2^2)(\Delta_3\Delta_4\Delta_5 - \Delta_3\; g_5^2 - \Delta_5\; g_1^2) - \Delta_1\; g_3^2(\Delta_4\Delta_5 - g_5^2)]} \\ &-\; \frac{g_1^2(\Delta_2 + \Delta_6)}{[(\Delta_1 + \Delta_6)(\Delta_2 + \Delta_6) - 2g_2^2]} \qquad (5.8) \\ &+\; \frac{g_1^2[(\Delta_2\Delta_3 - g_3^2)(\Delta_4\Delta_5 - g_5^2) - \Delta_2\Delta_5\; g_1^2]}{[(\Delta_1\Delta_2 - g_2^2)(\Delta_3\Delta_4\Delta_5 - \Delta_3\; g_5^2 - \Delta_5\; g_1^2) - \Delta_1\; g_3^2(\Delta_4\Delta_5 - g_5^2)]}\;, \\ &\approx\; \Delta_6 - \frac{g_6^2}{\Delta_5}\;, \qquad (5.9)\end{aligned}$$

and the effective coupling can be given by

$$\begin{aligned} g_{\rm eff} \;&=\; -\frac{g_1^2 g_2 g_3 g_5 g_6}{[(\Delta_1\Delta_2 - g_2^2)(\Delta_3\Delta_4\Delta_5 - \Delta_3\; g_5^2 - \Delta_5\; g_1^2) - \Delta_1\; g_3^2(\Delta_4\Delta_5 - g_5^2)]} \\ &\approx\; -\frac{g_1^2 g_2 g_3 g_5 g_6}{\Delta_1\Delta_2\Delta_3\Delta_4\Delta_5}\;. \qquad (5.10)\end{aligned}$$

Recalling Eq. (4.9), the time evolution of the initial state, say $|a\ 101\rangle$, can be expressed as

$$\begin{aligned} |a,101\rangle \;&\rightarrow\; \cos(g_{\rm eff}\ t)|a,101\rangle - {\rm i}\ \sin(g_{\rm eff}\ t)|a,110\rangle\;, \\ |a,110\rangle \;&\rightarrow\; \cos(g_{\rm eff}\ t)|a,110\rangle - {\rm i}\ \sin(g_{\rm eff}\ t)|a,101\rangle\;. \qquad (5.11)\end{aligned}$$

By setting $|g_{\rm eff}t| = \pi/2$, a complete population inversion takes place. Note that a global phase can be considered in order that $|a\ 101\rangle \mapsto |a\ 110\rangle$. Clearly, under the condition $\Delta >> g$ this gate requires a very long interaction time. So for QIP applications there is a need to improve its performance.

5.4 Three-level approximation

In the previous section, a two-level system has been employed to realize $|a\ 101\rangle \mapsto |a\ 110\rangle$. In order to increase the speed of this transformation, the transitions to either the level $|d\rangle$, $|e\rangle$, or $|f\rangle$ have been allowed. As we have previously mentioned, the states $|b, 00, 01, 10\rangle$ and $|c, 00, 11, 10\rangle$ must be always highly detuned, otherwise the over-shot states $|b, 00, 10, 01\rangle$ and $|c, 00, 20, 01\rangle$ can be populated.

The following effective three-state systems can be described by the general theory already discussed in Sec. 4.4. Therefore, the effective three-level Hamiltonian can be expressed as

$$\hat{H}_{\rm eff} = \begin{bmatrix} 0 & g^{(1)} & 0 \\ g^{(1)} & \Delta^{(1)} & g^{(2)} \\ 0 & g^{(2)} & \Delta^{(2)} \end{bmatrix}\;,$$

with the basis $\{|a\ 101\rangle, |\Phi\rangle, |a\ 110\rangle\}$. The state $|\Phi\rangle$ works as an auxiliary state, and the system moves back and forth between the qubit states $|a\ 101\rangle$ and $|a\ 110\rangle$. Given

the system initially in the state $|a, 101\rangle$ this state, at subsequent times, evolves into the superposition

$$|a\ 101\rangle \mapsto c_1(t)|a\ 101\rangle + c_2(t)|\Phi\rangle + c_3(t)|a\ 110\rangle\ . \tag{5.12}$$

In the case of resonance, i.e. $\Delta^{(1)} = \Delta^{(2)} = 0$, the time-dependent amplitudes $c_1(t)$, $c_2(t)$, and $c_3(t)$ can be determined by Eq. (4.11) as

$$\begin{aligned} c_1(t) &= \frac{1}{\bar{g}^2}[g_{(2)}^2 + g_{(1)}^2\ \cos(\bar{g}t)]\ , \\ c_2(t) &= i\frac{g_{(1)}}{\bar{g}}\ \sin(\bar{g}t)\ , \\ c_3(t) &= \frac{g_{(1)}g_{(2)}}{\bar{g}^2}[\cos(\bar{g}t) - 1]\ e^{i\eta t}\ , \end{aligned}$$

where $\bar{g} = \sqrt{g_{(1)}^2 + g_{(2)}^2}$. Clearly, under the condition $g^{(1)} = g^{(2)}$, a complete population inversion can take place at $|\bar{g}t| = \pi$. Setting the phase $\eta t = \pi$ leads to $|a\ 101\rangle \mapsto |a\ 110\rangle$.

5.4.1 The model (1001001)

An effective three-level behaviour can be analysed by allowing the $\mathbb{P}$-space to include the states $|a, 101\rangle$, $|d\rangle$, and $|a, 110\rangle$. The states $|b, 00, 01, 10\rangle, |c, 00, 11, 10\rangle, |e, 10, 10, 10\rangle$, $|f, 10, 10, 00\rangle, |b, 00, 10, 01\rangle$, and $|c, 00, 20, 01\rangle$ must be off-resonant so that they remain unpopulated. The required operators for the effective Hamiltonian (3.6) can be expressed as

$$\hat{H}_0 = \begin{bmatrix} 0 & 0 & 0 \\ 0 & \Delta_3 & 0 \\ 0 & 0 & \Delta_6 \end{bmatrix}\ ,\ \hat{B} = \begin{bmatrix} g_1 & 0 & 0 & 0 & 0 & 0 \\ 0 & g_3 & g_1 & 0 & 0 & 0 \\ 0 & 0 & 0 & g_6 & g_1 & 0 \end{bmatrix}\ , \tag{5.13}$$

$$\hat{A} = \begin{bmatrix} \Delta_1 & g_2 & 0 & 0 & 0 & 0 \\ g_2 & \Delta_2 & 0 & 0 & 0 & 0 \\ 0 & 0 & \Delta_4 & g_5 & 0 & 0 \\ 0 & 0 & g_5 & \Delta_5 & 0 & 0 \\ 0 & 0 & 0 & 0 & (\Delta_1 + \Delta_6) & \sqrt{2}g_2 \\ 0 & 0 & 0 & 0 & \sqrt{2}g_2 & (\Delta_2 + \Delta_6) \end{bmatrix}\ . \tag{5.14}$$

Under the assumption $\Delta >> g$, the effective couplings $g^{(1)}$ and $g^{(2)}$ can be given by

$$g^{(1)} = \frac{g_1 g_2 g_3}{\Delta_1\Delta_2 - g_2^2} \approx \frac{g_1 g_2 g_3}{\Delta_1\Delta_2}\ ,\quad g^{(2)} = \frac{g_1 g_5 g_6}{\Delta_4\Delta_5 - g_5^2} \approx \frac{g_1 g_5 g_6}{\Delta_4\Delta_5}\ . \tag{5.15}$$

The coupling constant $g^{(1)}$ is the linkage between the states $|a\ 101\rangle$ and $|d\rangle$, and $g^{(2)}$ is the coupling between the states $|d\rangle$ and $|a\ 110\rangle$. The effective detunings, by setting the initial state to be the zero-point energy, are

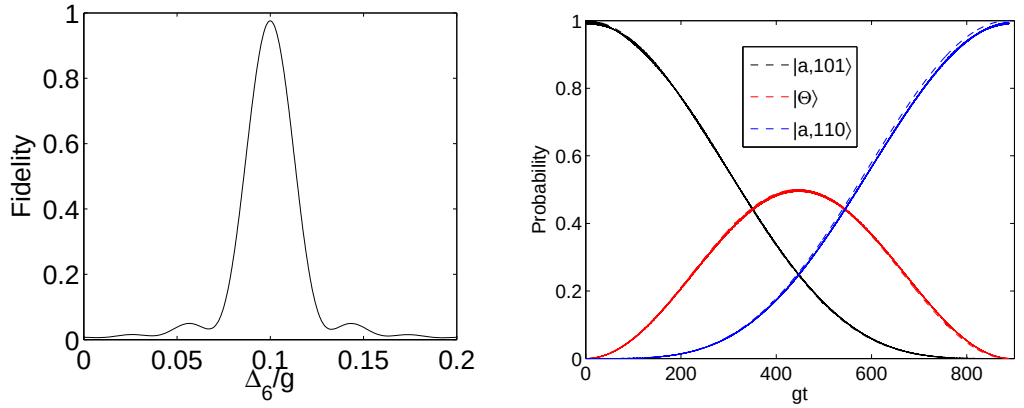

(a) (b)

Figure 5.3: (a) The fidelity of the effective three-level system with $|d\rangle$ is on-resonance. The coupling constants g_i $(i = 1, 2, 3, 5, 6)$ are set to g, and the detunings Δ_j $(j = 1, 2, 4, 5)$ are set to $\Delta = 10g$. Time has been frozen at $|g^{(n)}t| = \frac{\pi}{\sqrt{2}}$ with $n = 1$ or $n = 2$. The resonance condition by Eq. (5.16) determines the detuning Δ_3. As observed by this figure, the maximum fidelity occurs at a value of Δ_6 agreed completely with Eq. (5.17). (b) The populations of the three states $|a, 10, 01, 10\rangle$, $|d00, 10, 10\rangle \equiv |\Theta\rangle$, and $|a, 10, 10, 01\rangle$ in the effective three-level system in (a), with $\Delta = 20g$. The detuning Δ_6 is given by Eq. (5.17).

$$\begin{aligned}
\Delta^{(1)} &= \Delta_3 - \frac{g_1^2\Delta_5}{(\Delta_4\Delta_5 - g_5^2)} - \frac{g_3^2\Delta_1}{(\Delta_1\Delta_2 - g_2^2)} + \frac{g_1^2\Delta_2}{(\Delta_1\Delta_2 - g_2^2)} \,, \\
&\approx \Delta_3 - \frac{g_1^2}{\Delta_4} - \frac{g_3^2}{\Delta_2} + \frac{g_1^2}{\Delta_1} \,, \qquad (5.16) \\
\Delta^{(2)} &= \Delta_6 - \frac{g_6^2\Delta_4}{(\Delta_4\Delta_5 - g_5^2)} - \frac{g_1^2(\Delta_2 + \Delta_6)}{[(\Delta_1 + \Delta_6)(\Delta_2 + \Delta_6) - 2g_2^2]} + \frac{g_1^2\Delta_2}{(\Delta_1\Delta_2 - g_2^2)}, \\
&\approx \Delta_6 - \frac{g_6^2}{\Delta_5} \,. \qquad (5.17)
\end{aligned}$$

Note that, under the condition $\Delta_1 >> \Delta_6$, the term $\frac{g_1^2}{(\Delta_1+\Delta_6)}$ can be adequately approximated by the first-order Taylor expansion, i.e. it can be reduced to g_1^2/Δ_1.

Following the spin-J model [47], the sequence of Rabi frequencies can be given by $g = g_0\sqrt{n(N-n)}$, where N represents the number of the effective system levels (in our case $N = 3$). Then, the complete population transfer for a three-level behaviour happens at $|g^{(1)}t| = |g^{(2)}t| = \pi/\sqrt{2}$ (for N-level system $|g_0 t| = \pi/2$).

Numerical simulations of the full Hamiltonian (5.4) can be carried out to show how this system behaves for $t > 0$ (see Fig. 5.3). It is demonstrated that numerical integration of the full Hamiltonian and solutions by the theory (5.4) show a sufficient agreement.

5.4.2 The model (1000101)

In the case when the projection operator $\mathbb{P}$ comprises the states $|a\ 101\rangle$, $|e\rangle$, and $|a\ 110\rangle$, one can find that the operators $\hat{H}_0 = \mathbb{P}\hat{H}\mathbb{P}$, $\hat{B} = \mathbb{P}\hat{H}\mathbb{Q}$, and $\hat{A} = \mathbb{Q}\hat{H}\mathbb{Q}$ can be defined as

$$\begin{aligned}\hat{H}_0 &= \begin{bmatrix} 0 & 0 & 0 \\ 0 & \Delta_4 & 0 \\ 0 & 0 & \Delta_6 \end{bmatrix}, \hat{B} = \begin{bmatrix} g_1 & 0 & 0 & 0 & 0 & 0 \\ 0 & 0 & g_1 & g_5 & 0 & 0 \\ 0 & 0 & 0 & g_6 & g_1 & 0 \end{bmatrix}, \\ \hat{A} &= \begin{bmatrix} \Delta_1 & g_2 & 0 & 0 & 0 & 0 \\ g_2 & \Delta_2 & g_3 & 0 & 0 & 0 \\ 0 & g_3 & \Delta_3 & 0 & 0 & 0 \\ 0 & 0 & 0 & \Delta_5 & 0 & 0 \\ 0 & 0 & 0 & 0 & (\Delta_1+\Delta_6) & \sqrt{2}g_2 \\ 0 & 0 & 0 & 0 & \sqrt{2}g_2 & (\Delta_2+\Delta_6) \end{bmatrix}.\end{aligned} \tag{5.18}$$

With $\Delta >> g$, the effective couplings are

$$\begin{aligned} g^{(1)} &= -\frac{g_1^2 g_2 g_3}{(\Delta_1\Delta_2\Delta_3 - \Delta_1 g_3^2 - \Delta_3 g_2^2)} \approx -\frac{g_1^2 g_2 g_3}{\Delta_1\Delta_2\Delta_3}, \\ g^{(2)} &= -\frac{g_5 g_6}{\Delta_5}, \end{aligned} \tag{5.19}$$

and the effective detunings are

$$\begin{aligned} \Delta^{(1)} &= \Delta_4 - \frac{g_5^2}{\Delta_5} - \frac{g_1^2(\Delta_1\Delta_2 - g_2^2)}{(\Delta_1\Delta_2\Delta_3 - \Delta_1 g_3^2 - \Delta_3 g_2^2)} + \frac{g_1^2(\Delta_2\Delta_3 - g_3^2)}{(\Delta_1\Delta_2\Delta_3 - \Delta_1 g_3^2 - \Delta_3 g_2^2)} \\ &\approx \Delta_4 - \frac{g_5^2}{\Delta_5} - \frac{g_1^2}{\Delta_3} + \frac{g_1^2}{\Delta_1}, \end{aligned} \tag{5.20}$$

$$\begin{aligned} \Delta^{(2)} &= \Delta_6 - \frac{g_6^2}{\Delta_5} - \frac{g_1^2(\Delta_2+\Delta_6)}{[(\Delta_1+\Delta_6)(\Delta_2+\Delta_6) - 2g_2^2]} + \frac{g_1^2(\Delta_2\Delta_3 - g_3^2)}{(\Delta_1\Delta_2\Delta_3 - \Delta_1 g_3^2 - \Delta_3 g_2^2)} \\ &\approx \Delta_6 - \frac{g_6^2}{\Delta_5} - \frac{g_1^2}{(\Delta_1+\Delta_6)} + \frac{g_1^2(\Delta_2\Delta_3 - g_3^2)}{(\Delta_1\Delta_2\Delta_3 - \Delta_1 g_3^2 - \Delta_3 g_2^2)}. \end{aligned} \tag{5.21}$$

The study for the fidelity in this system (an example is illustrated by Fig. 5.4 a) shows that higher-order corrections in $\Delta^{(2)}$ must be considered, so that the proper resonance condition for $|a\ 110\rangle$ can be obtained. Mathematically, we follow two different approaches in order to find the appropriate formula for Δ_6. The first method is by approximating the last term in $\Delta^{(2)}$ to its second-degree Taylor expansion. This leads to

$$\Delta_6 \approx \frac{g_6^2}{\Delta_5} - \frac{g_1^2 g_2^2}{\Delta_1^2\Delta_2}. \tag{5.22}$$

Alternatively, we can replace $(z\hat{I} - \hat{A})^{-1}$ in Eq. (3.6) by $(-\hat{A}^{-1} - z\hat{I}\ \hat{A}^{-2})$. As a result, the effective Hamiltonian can be rewritten as

$$\hat{H}_{\text{eff}} = \hat{H}_0 - \hat{B}\frac{1}{\hat{A}}\hat{B}^\dagger - z\ \hat{B}\frac{1}{\hat{A}^2}\hat{B}^\dagger\ , \tag{5.23}$$

where z represents a typical eigenfrequency of $\hat{H}_{\text{eff}}$. After a few lines of algebra, one finds that

$$\Delta_6 \approx \frac{g_6^2}{\Delta_5} + z\left[\frac{g_6^2}{\Delta_5^2} + \frac{g_1^2 g_2^2}{\Delta_1^2 \Delta_2^2}\right]\ . \tag{5.24}$$

The value of Δ_6 determined by either Eq. (5.22) or Eq. (5.24) represents the proper value of this detuning to achieve the maximum value for the model fidelity, as shown by Fig. 5.4(a). Furthermore, the swapping plot in this model can only take place at this value of Δ_6 (see Fig. 5.4(b)). The population of the states $|a\ 101\rangle$, $|e\rangle$, and $|a\ 110\rangle$ is depicted in Fig. 5.4(b), showing that $|a\ 101\rangle \mapsto |a\ 110\rangle$ at $|g^{(1)}\ t| = |g^{(2)}\ t| = \pi/\sqrt{2}$. Clearly, the interaction time in this model is much longer, compared to the previous model.

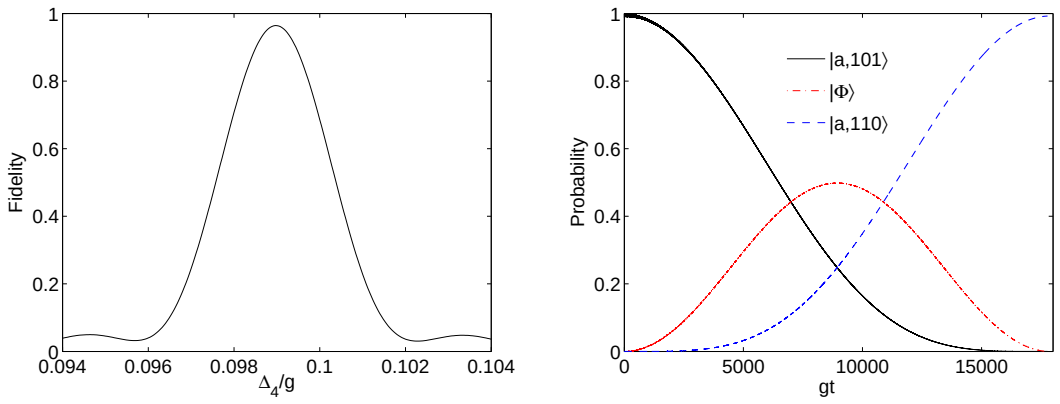

(a) (b)

Figure 5.4: (a) The fidelity of the three-level behaviour with the state $|e\rangle$ is set to resonance, in addition to the terminal states $|a\ 101\rangle$ and $|a\ 110\rangle$. The coupling constants g_1, g_2, g_3, and g_6 are all set to g. The detunings Δ_1, Δ_2, Δ_3, and Δ_5 are set to $\Delta = 10g$. The coupling strength g_5 is given by $g_5 = (\frac{g_1^2 g_2 g_3}{g_6})(\frac{\Delta_5}{\Delta_1\Delta_2\Delta_3})$ so that $g^{(1)} = g_2^{(2)}$, and the detuning Δ_4 is determined by the resonance condition (5.20). (b) The probability of the same system in (a), with $\Delta = 20g$. The detuning Δ_6 can be determined by either Eq. (5.22) or Eq. (5.24).

5.4.3 The model (1000011)

Considering the states $|a\ 101\rangle$, $|f\rangle$, and $|a\ 110\rangle$ to be on-resonance, the effective three-level Hamiltonian $\hat{H}_{\text{eff}}$ can be constructed with the help of the operators

$$\hat{H}_0 = \begin{bmatrix} 0 & 0 & 0 \\ 0 & \Delta_5 & g_6 \\ 0 & g_6 & \Delta_6 \end{bmatrix}, \ \hat{B} = \begin{bmatrix} g_1 & 0 & 0 & 0 & 0 & 0 \\ 0 & 0 & 0 & g_5 & 0 & 0 \\ 0 & 0 & 0 & 0 & g_1 & 0 \end{bmatrix}, \tag{5.25}$$

$$\hat{A} = \begin{bmatrix} \Delta_1 & g_2 & 0 & 0 & 0 & 0 \\ g_2 & \Delta_2 & g_3 & 0 & 0 & 0 \\ 0 & g_3 & \Delta_3 & g_1 & 0 & 0 \\ 0 & 0 & g_1 & \Delta_4 & 0 & 0 \\ 0 & 0 & 0 & 0 & (\Delta_1+\Delta_6) & \sqrt{2}g_2 \\ 0 & 0 & 0 & 0 & \sqrt{2}g_2 & (\Delta_2+\Delta_6) \end{bmatrix}. \tag{5.26}$$

With $\Delta >> g$, the effective couplings are

$$g^{(1)} = \frac{g_1^2 g_2 g_3 g_5}{[(\Delta_1\Delta_2 - g_2^2)(\Delta_3\Delta_4 - g_1^2) - \Delta_1\Delta_4 g_3^2]} \approx \frac{g_1^2 g_2 g_3 g_5}{\Delta_1\Delta_2\Delta_3\Delta_4}, \tag{5.27}$$

$$g^{(2)} = g_6, \tag{5.28}$$

and the effective detunings are

$$\begin{aligned} \Delta^{(1)} &= \Delta_5 - \frac{g_5^2(\Delta_1\Delta_2\Delta_3 - \Delta_1 g_3^2 - \Delta_3 g_2^2)}{[(\Delta_1\Delta_2 - g_2^2)(\Delta_3\Delta_4 - g_1^2) - \Delta_1\Delta_4 g_3^2]} + \frac{g_1^2(\Delta_2\Delta_3\Delta_4 - \Delta_2 g_1^2 - \Delta_4 g_3^2)}{[(\Delta_1\Delta_2 - g_2^2)(\Delta_3\Delta_4 - g_1^2) - \Delta_1\Delta_4 g_3^2]} \\ &\approx \Delta_5 - \frac{g_5^2}{\Delta_4} + \frac{g_1^2}{\Delta_1}, \end{aligned} \tag{5.29}$$

$$\begin{aligned} \Delta^{(2)} &= \Delta_6 - \frac{g_1^2(\Delta_2+\Delta_6)}{[(\Delta_1+\Delta_6)(\Delta_2+\Delta_6) - 2g_2^2]} + \frac{g_1^2(\Delta_2\Delta_3\Delta_4 - \Delta_2 g_1^2 - \Delta_4 g_3^2)}{[(\Delta_1\Delta_2 - g_2^2)(\Delta_3\Delta_4 - g_1^2) - \Delta_1\Delta_4 g_3^2]} \\ &\approx \Delta_6 + \frac{g_1^2 g_2^2}{\Delta_1^2\Delta_2}. \end{aligned} \tag{5.30}$$

Note that we follow the same argument in the last model in order that Δ_6 has been described by the formula (5.30). Fig. 5.5 demonstrates the probability of all states in this model. Amongst the models behaving as a three-level system, it is shown that this model is the slowest one.

At the end of this section, it is clear that the transformation $|a\ 101\rangle \leftrightarrow |a\ 110\rangle$ by the model (1001001) achieves the shortest interaction time. This is similar to the case in Sec. 4.4. That is, the effective couplings in all these models show that (under the conditions $g^{(1)} = g^{(2)}$ and $\Delta >> g$) the effective couplings in the model (1001001) are always stronger, and then it has the shortest interaction time. Indeed, we will see later that this model is the only one which can realize the Fredkin gate.

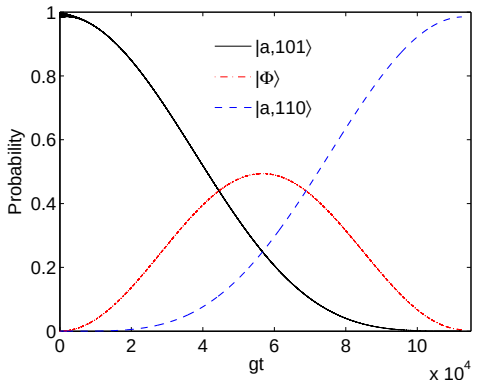

Figure 5.5: The populations in the effective three-state system of Eqs. (5.29, 5.30). The coupling constants g_1, g_2, g_3 and g_5 are set to g and Δ_1, Δ_2, Δ_3 and Δ_4 are set to $\Delta = 15$g. The detunings Δ_5 and Δ_6 are determined by the resonance conditions in Eqs. (5.29, 5.30), and the coupling constant g_6 are given by $g_6 = \frac{g_1^2 g_2 g_3 g_5}{\Delta_1 \Delta_2 \Delta_3 \Delta_4}$ so that $g^{(1)} = g^{(2)}$. This figure describes the populations of the terminal states $|a, 101\rangle$ and $|a, 110\rangle$ besides the auxiliary state $|\Phi\rangle \equiv |f, 10, 10, 00\rangle$.

5.5 Four-level system

The next logical step beyond the effective three-level system is the effective four-level system. The states $|d\rangle$, $|e\rangle$, and $|f\rangle$ are the only states which are allowed to be resonant. This means, we can choose any two states of them, in addition to the qubit states in the atomic state $|a\rangle$, to perform a four-level system. in this case, the space of $\mathbb{P}$ contains four states, i.e. $N = 4$, and three different four-level configurations can be addressed.

By using the multi-photon resonance theory, we firstly analyse the resonance conditions for each of the possible models so that a four-level behaviour can be recognized. Then, the time evolution of the system is numerically simulated, where the full Hamiltonian of the system is numerically integrated. The results, finally, are compared with the theory, where the effective Hamiltonians from Shore's method are considered.

The effective four-level configurations, generally speaking, can be theoretically described as follows. The general effective Hamiltonian can be written as (once again we set the state $|a\ 101\rangle$ to be the initial state and the energy reference point)

$$\hat{H}_{\text{eff}} = \begin{bmatrix} 0 & g^{(1)} & 0 & 0 \\ g^{(1)} & \Delta^{(1)} & g^{(2)} & 0 \\ 0 & g^{(2)} & \Delta^{(2)} & g^{(3)} \\ 0 & 0 & g^{(3)} & \Delta^{(3)} \end{bmatrix} . \tag{5.31}$$

Recalling Eq. (4.21) the state $|a\ 101\rangle$, in the case of resonance, evolves as

$$
\begin{aligned}
|a\ 101\rangle \longrightarrow \quad & [\frac{(g_{(1)}^2 - g_-^2)}{(g_+^2 - g_-^2)}\ \cos(g_+ t) - \frac{(g_{(1)}^2 - g_+^2)}{(g_+^2 - g_-^2)}\ \cos(g_- t)]\ |a, 101\rangle \\
+ \quad & \mathrm{i}[\frac{g_+(g_{(1)}^2 - g_-^2)}{g_{(1)}(g_+^2 - g_-^2)}\ \sin(g_+ t) - \frac{g_-(g_{(1)}^2 - g_+^2)}{g_{(1)}(g_+^2 - g_-^2)}\ \sin(g_- t)]\ |\Phi\rangle \\
- \quad & [\frac{(g_{(1)}^2 - g_+^2)(g_{(1)}^2 - g_-^2)}{g_{(1)}g_{(2)}(g_+^2 - g_-^2)}\ \cos(g_+ t) + \frac{(g_{(1)}^2 - g_-^2)(g_{(1)}^2 - g_+^2)}{g_{(1)}g_{(2)}(g_+^2 - g_-^2)}\ \cos(g_- t)]\ |\Theta\rangle \\
+ \quad & \mathrm{i}[\frac{g_+(g_+^2 - g_{(1)}^2 - g_{(2)}^2)(g_{(1)}^2 - g_-^2)}{g_{(1)}g_{(2)}g_{(3)}(g_+^2 - g_-^2)}\ \sin(g_+ t) \\
- \quad & \frac{g_-(g_-^2 - g_{(1)}^2 - g_{(2)}^2)(g_{(1)}^2 - g_+^2)}{g_{(1)}g_{(2)}g_{(3)}(g_+^2 - g_-^2)}\ \sin(g_- t)]\ e^{i\eta t}|a\ 110\rangle\ ,
\end{aligned}
\tag{5.32}
$$

where $g_\pm = \sqrt{(g/2) \pm \sqrt{(g/2)^2 - \tilde{g}^2}}$ (with $g = g_{(1)}^2 + g_{(2)}^2 + g_{(3)}^2$ and $\tilde{g} = g_{(1)}g_{(3)}$). By setting $\eta = \pi/2$ and $|g_{(2)}t| = \pi$ (note that $g^{(1)} = g^{(3)} = \frac{\sqrt{3}}{2}g^{(2)}$), one finds easily that $|a\ 101\rangle \mapsto |a\ 110\rangle$.

5.5.1 The model (1001011)

With the states of interest $|a\ 101\rangle$, $|d\rangle$, $|e\rangle$, and $|a\ 110\rangle$ to be on-resonance, the operators needed to build the effective Hamiltonian $\hat{H}_{\text{eff}} = \hat{H}_0 - \hat{B}\ \hat{A}^{-1}\ \hat{B}^\dagger$ can be written as

$$
\hat{H}_0 = \begin{bmatrix} 0 & 0 & 0 & 0 \\ 0 & \Delta_3 & 0 & 0 \\ 0 & 0 & \Delta_5 & g_6 \\ 0 & 0 & g_6 & \Delta_6 \end{bmatrix}\ ,\ \hat{B} = \begin{bmatrix} g_1 & 0 & 0 & 0 & 0 \\ 0 & g_3 & g_1 & 0 & 0 \\ 0 & 0 & g_5 & 0 & 0 \\ 0 & 0 & 0 & g_1 & 0 \end{bmatrix}\ ,
$$

$$
\hat{A} = \begin{bmatrix} \Delta_1 & g_2 & 0 & 0 & 0 \\ g_2 & \Delta_2 & 0 & 0 & 0 \\ 0 & 0 & \Delta_4 & 0 & 0 \\ 0 & 0 & 0 & (\Delta_1 + \Delta_6) & \sqrt{2}g_2 \\ 0 & 0 & 0 & \sqrt{2}g_2 & (\Delta_2 + \Delta_6) \end{bmatrix}\ . \tag{5.33}
$$

Assuming the state $|a\ 101\rangle$ is linked to $|d\rangle$ by $g^{(1)}$, the states $|d\rangle$ and $|e\rangle$ are coupled to each other by $g^{(2)}$, and $g^{(3)}$ is the coupling strength between $|e\rangle$ and $|a\ 110\rangle$, these effective couplings (under the condition $\Delta >> g$) can be expressed as

$$
g^{(1)} = \frac{g_1 g_2 g_3}{(\Delta_1\Delta_2 - g_2^2)} \approx \frac{g_1 g_2 g_3}{\Delta_1\Delta_2}\ ,\quad g^{(2)} = -\frac{g_1 g_5}{\Delta_4}\ ,\quad g^{(3)} = g_6\ . \tag{5.34}
$$

The effective detunings are

$$\begin{aligned}
\Delta^{(1)} &= \Delta_3 - \frac{g_1^2}{\Delta_4} - \frac{g_3^2\Delta_1}{(\Delta_1\Delta_2 - g_2^2)} + \frac{g_1^2\Delta_2}{(\Delta_1\Delta_2 - g_2^2)} \\
&\approx \Delta_3 - \frac{g_1^2}{\Delta_4} - \frac{g_3^2}{\Delta_2} + \frac{g_1^2}{\Delta_1} \ , \qquad (5.35) \\
\Delta^{(2)} &= \Delta_5 - \frac{g_5^2}{\Delta_4} + \frac{g_1^2\Delta_2}{(\Delta_1\Delta_2 - g_2^2)} \\
&\approx \Delta_5 - \frac{g_5^2}{\Delta_4} + \frac{g_1^2}{\Delta_1} \ , \qquad (5.36) \\
\Delta^{(3)} &= \Delta_6 - \frac{g_1^2(\Delta_2 + \Delta_6)}{[(\Delta_1 + \Delta_6)(\Delta_2 + \Delta_6) - 2g_2^2]} + \frac{g_1^2\Delta_2}{(\Delta_1\Delta_2 - g_2^2)} \\
&\approx \Delta_6 \ . \qquad (5.37)
\end{aligned}$$

The strength of the couplings g_5 and g_6 can be set as

$$g_5 = -\frac{2}{\sqrt{3}}\frac{g_2 g_3 \Delta_4}{\Delta_1\Delta_2} \ , \quad g_6 = \frac{g_1 g_2 g_3}{\Delta_1\Delta_2} \ , \qquad (5.38)$$

so that $g^{(1)} = g^{(3)} = \frac{\sqrt{3}}{2}g^{(2)}$. The interaction time of this system can be determined by $|g_0 t| = \pi/2$, with $g_0 = \frac{1}{\sqrt{3}}g^{(1)} = \frac{1}{\sqrt{3}}g^{(3)} = \frac{1}{2}g^{(2)}$. With $|a\ 101\rangle$ being the initial state and at the interaction time of the system, the interchange $|a\ 101\rangle \mapsto |a\ 110\rangle$ has been numerically and theoretically demonstrated by Fig. 5.6. The operation time in this model is close in value to the interaction time in the three-level (1001001).

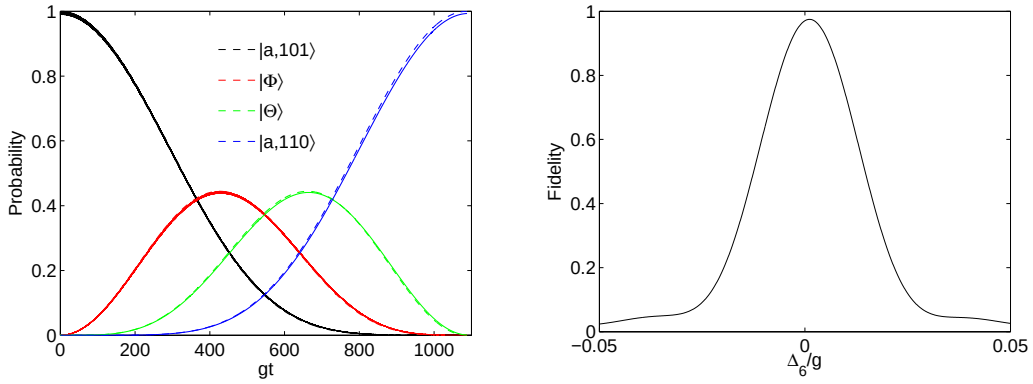

(a) (b)

Figure 5.6: (a) The probability of the four-level behaviour in the basis $\{|a10, 01, 10\rangle$ $, |d, 00, 10, 10\rangle, |f, 10, 10, 00\rangle, |a, 10, 10, 01\rangle\}$. The coupling constants g_1, g_2, and g_3 are set to g, and the coupling constants g_5 and g_6 are given by Eq. (5.38) so that $g^{(1)} = g^{(3)} = \frac{\sqrt{3}}{2}g^{(2)}$. The detunings Δ_1, Δ_2, and Δ_4 are set to $\Delta = 20$g, and the detunings Δ_3, Δ_5, and Δ_6 are given by the resonance conditions [5.35,5.36,5.37]. This system has two auxiliary states $|d, 00, 10, 10\rangle \equiv |\Phi\rangle$ and $|f, 10, 10, 00\rangle \equiv |\Theta\rangle$. (b) The fidelity of this model (1001011), demonstrating the value for Δ_6 (with $\Delta_1 = \Delta_2 = \Delta_4 = \Delta = 10g$).

5.5.2 The model (1000111)

With the states $|a\ 101\rangle$, $|e\rangle$, $|f\rangle$, and $|a\ 110\rangle$ to be resonant, a further effective four-level Hamiltonian can be built with the resultant operators

$$\hat{H}_0 = \begin{bmatrix} 0 & 0 & 0 & 0 \\ 0 & \Delta_4 & g_5 & 0 \\ 0 & g_5 & \Delta_5 & g_6 \\ 0 & 0 & g_6 & \Delta_6 \end{bmatrix}, \ \hat{B} = \begin{bmatrix} g_1 & 0 & 0 & 0 & 0 \\ 0 & 0 & g_1 & 0 & 0 \\ 0 & 0 & 0 & 0 & 0 \\ 0 & 0 & 0 & g_1 & 0 \end{bmatrix},$$

$$\hat{A} = \begin{bmatrix} \Delta_1 & g_2 & 0 & 0 & 0 \\ g_2 & \Delta_2 & g_3 & 0 & 0 \\ 0 & g_3 & \Delta_3 & 0 & 0 \\ 0 & 0 & 0 & (\Delta_1+\Delta_6) & \sqrt{2}g_2 \\ 0 & 0 & 0 & \sqrt{2}g_2 & (\Delta_2+\Delta_6) \end{bmatrix}. \tag{5.39}$$

Under $\Delta >> g$ the effective four-photon couplings are

$$g^{(1)} = -\frac{g_1^2 g_2 g_3}{(\Delta_1\Delta_2\Delta_3 - g_2^2\Delta_3 - g_3^2\Delta_1)} \approx -\frac{g_1^2 g_2 g_3}{\Delta_1\Delta_2\Delta_3}, \quad g^{(2)} = g_5, \quad g^{(3)} = g_6, \tag{5.40}$$

and the four-photon detunings are

$$\begin{aligned} \Delta^{(1)} &= \Delta_4 - \frac{g_1^2(\Delta_1\Delta_2 - g_2^2)}{(\Delta_1\Delta_2\Delta_3 - g_2^2\Delta_3 - g_3^2\Delta_1)} + \frac{g_1^2(\Delta_2\Delta_3 - g_3^2)}{(\Delta_1\Delta_2\Delta_3 - g_2^2\Delta_3 - g_3^2\Delta_1)} \\ &\approx \Delta_4 - \frac{g_1^2}{\Delta_3} + \frac{g_1^2}{\Delta_1}, \end{aligned} \tag{5.41}$$

$$\begin{aligned} \Delta^{(2)} &= \Delta_5 + \frac{g_1^2(\Delta_2\Delta_3 - g_3^2)}{(\Delta_1\Delta_2\Delta_3 - g_2^2\Delta_3 - g_3^2\Delta_1)} \\ &\approx \Delta_5 + \frac{g_1^2}{\Delta_1}, \end{aligned} \tag{5.42}$$

$$\begin{aligned} \Delta^{(3)} &= \Delta_6 - \frac{g_1^2(\Delta_2+\Delta_6)}{[(\Delta_1+\Delta_6)(\Delta_2+\Delta_6) - 2g_2^2]} + \frac{g_1^2(\Delta_2\Delta_3 - g_3^2)}{(\Delta_1\Delta_2\Delta_3 - g_2^2\Delta_3 - g_3^2\Delta_1)} \\ &\approx \Delta_6 + \frac{g_1^2 g_2^2}{(\Delta_1^2\Delta_2)}. \end{aligned} \tag{5.43}$$

The strength of the couplings g_5 and g_6 can be defined by

$$g_5 = -\frac{2}{\sqrt{3}}\frac{g_1^2 g_2 g_3}{\Delta_1\Delta_2\Delta_3}, \quad g_6 = -\frac{g_1^2 g_2 g_3}{\Delta_1\Delta_2\Delta_3}, \tag{5.44}$$

so that $g^{(1)} = g^{(3)} = \frac{\sqrt{3}}{2}g^{(2)}$. This system, in contrast, is fairly slower than the last model (see Fig. 5.7). This is due to the quite weak effective coupling $g^{(1)}$ linking the state $|a, 101\rangle$ with the auxiliary state $|e\rangle$. This effective coupling is weak, compared to the couplings in the previous model, as it requires three largely detuned states (see Eq. (5.40).

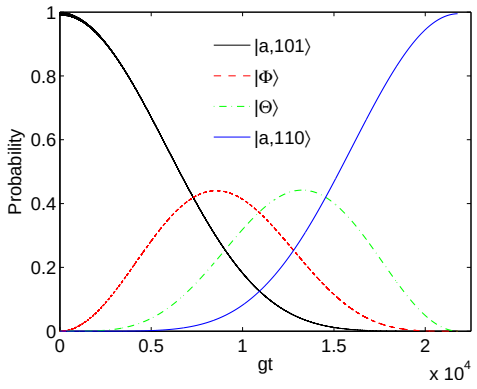

Figure 5.7: The probability of the states $|a10, 01, 10\rangle, |e, 10, 10, 10\rangle, |f, 10, 10, 00\rangle$, and $|a, 10, 10, 01\rangle$ using the four-level approximation of Eqs. (5.41, 5.42, 5.43). The coupling constants g_1, g_2, and g_3 are all set to g and the coupling constants g_5 and g_6 are given by Eq. (5.44). The detunings Δ_1, Δ_2, and Δ_3 are set to 20g, and the detunings Δ_4, Δ_5, and Δ_6 are set by the resonance conditions. Note that the states $|e, 10, 10, 10\rangle \equiv |\Phi\rangle$ and $|f, 10, 10, 00\rangle \equiv |\Theta\rangle$ work as auxiliary states in this configuration.

5.5.3 The model (1001101)

The last four-state approximation we discuss in this section is the model with the states of interest $|a\ 101\rangle$, $|d\rangle$, $|e\rangle$, and $|a\ 110\rangle$. As shown in previous sections, the theory of multi-photon resonance provides a useful tool to determine the resonance conditions and the proper values for the coupling constants so that the probabilities of the system can be greatly confined between the states of interest. Recalling Shore's method, the effective Hamiltonian $\hat{H}_{\text{eff}}$ can be constructed with the help of the following operators

$$\hat{H}_0 = \begin{bmatrix} 0 & 0 & 0 & 0 \\ 0 & \Delta_3 & g_1 & 0 \\ 0 & g_1 & \Delta_4 & 0 \\ 0 & 0 & 0 & \Delta_6 \end{bmatrix}, \ \hat{B} = \begin{bmatrix} g_1 & 0 & 0 & 0 & 0 \\ 0 & g_3 & 0 & 0 & 0 \\ 0 & 0 & g_5 & 0 & 0 \\ 0 & 0 & g_6 & g_1 & 0 \end{bmatrix},$$

$$\hat{A} = \begin{bmatrix} \Delta_1 & g_2 & 0 & 0 & 0 \\ g_2 & \Delta_2 & 0 & 0 & 0 \\ 0 & 0 & \Delta_5 & 0 & 0 \\ 0 & 0 & 0 & (\Delta_1 + \Delta_6) & \sqrt{2}g_2 \\ 0 & 0 & 0 & \sqrt{2}g_2 & (\Delta_2 + \Delta_6) \end{bmatrix}. \tag{5.45}$$

The resonance conditions, under $\Delta >> g$, can be determined by

$$\begin{aligned}
\Delta^{(1)} &= \Delta_3 - \frac{g_3^2\Delta_1}{(\Delta_1\Delta_2 - g_2^2)} + \frac{g_1^2\Delta_2}{(\Delta_1\Delta_2 - g_2^2)} \\
&\approx \Delta_3 - \frac{g_3^2}{\Delta_2} + \frac{g_1^2}{\Delta_1} \ , \qquad (5.46) \\
\Delta^{(2)} &= \Delta_4 - \frac{g_5^2}{\Delta_5} + \frac{g_1^2\Delta_2}{(\Delta_1\Delta_2 - g_2^2)} \\
&\approx \Delta_4 - \frac{g_5^2}{\Delta_5} + \frac{g_1^2}{\Delta_1} \ , \qquad (5.47) \\
\Delta^{(3)} &= \Delta_6 - \frac{g_6^2}{\Delta_5} - \frac{g_1^2(\Delta_2 + \Delta_6)}{[(\Delta_1 + \Delta_6)(\Delta_2 + \Delta_6) - 2g_2^2]} + \frac{g_1^2\Delta_2}{(\Delta_1\Delta_2 - g_2^2)} \\
&\approx \Delta_6 - \frac{g_6^2}{\Delta_5} \ , \qquad (5.48)
\end{aligned}$$

and the effective couplings are

$$g^{(1)} \approx \frac{g_1 g_2 g_3}{\Delta_1\Delta_2} \ , \quad g^{(2)} = g_1 \ , \quad g^{(3)} = -\frac{g_5 g_6}{\Delta_5} \ . \qquad (5.49)$$

Although we have succeeded in finding the resonance conditions for this model, the presence of the repeated coupling g_1 as a linkage between the auxiliary states $|d\rangle$ and $|e\rangle$ causes a failure to meet simultaneously the conditions $\Delta >> g$ and $g^{(1)} = g^{(3)} = \frac{\sqrt{3}}{2}g^{(2)}$. We can conclude that this model, with the procedure followed here, can not perform the Fredkin gate.

In this section, a couple of models behaving as a four-level system have been developed, so that $|a\ 101\rangle$ maps to $|a\ 110\rangle$. However, the speed of these operations could not exceed the speed of the three-level model (1001001). Since the four-level model (1000111) requires a very long interaction time, this model is unlikely appropriate candidate for applications in cavity-QED. In the following sections, therefore, we only consider the model (1001011) as a possible four-level configuration for the Fredkin gate.

5.6 An effective five-level five-photon model

Alongside the states $|a\ 101\rangle$ and $|a\ 110\rangle$, the states $|d, 00, 10, 10\rangle$, $|e, 10, 10, 10\rangle$ and $|f, 10, 10, 00\rangle$ can be set to be resonant; hence, an effective five-state behaviour can be analysed. To

create the five-level Hamiltonian $\hat{H}_{\rm eff}$, we can use the following operators

$$\begin{aligned}
\hat{H}_0 &= \begin{bmatrix} 0 & 0 & 0 & 0 & 0 \\ 0 & \Delta_3 & g_1 & 0 & 0 \\ 0 & g_1 & \Delta_4 & g_5 & 0 \\ 0 & 0 & g_5 & \Delta_5 & g_6 \\ 0 & 0 & 0 & g_6 & \Delta_6 \end{bmatrix}, \ \hat{B} = \begin{bmatrix} g_1 & 0 & 0 & 0 \\ 0 & g_3 & 0 & 0 \\ 0 & 0 & 0 & 0 \\ 0 & 0 & 0 & 0 \\ 0 & 0 & g_1 & 0 \end{bmatrix}, \\
\hat{A} &= \begin{bmatrix} \Delta_1 & g_2 & 0 & 0 \\ g_2 & \Delta_2 & 0 & 0 \\ 0 & 0 & (\Delta_1+\Delta_6) & \sqrt{2}g_2 \\ 0 & 0 & \sqrt{2}g_2 & (\Delta_2+\Delta_6) \end{bmatrix}. \qquad (5.50)
\end{aligned}$$

The effective Hamiltonian calculated by $\hat{H}_{\rm eff} = \hat{H}_0 - \hat{B}\hat{A}^{-1}\hat{B}^{\dagger}$ can be expressed by

$$\hat{H}_{\rm eff} = \begin{bmatrix} 0 & g^{(1)} & 0 & 0 & 0 \\ g^{(1)} & \Delta^{(1)} & g^{(2)} & 0 & 0 \\ 0 & g^{(2)} & \Delta^{(2)} & g^{(3)} & 0 \\ 0 & 0 & g^{(3)} & \Delta^{(3)} & g^{(4)} \\ 0 & 0 & 0 & g^{(4)} & \Delta^{(4)} \end{bmatrix},$$

where (with $\Delta >> g$) the effective five-state five-photon couplings are

$$g^{(1)} = -\frac{g_1 g_2 g_3}{(\Delta_1\Delta_2 - g_2^2)} \approx -\frac{g_1 g_2 g_3}{\Delta_1\Delta_2}, \quad g^{(2)} = g_1, \quad g^{(3)} = g_5, \quad g^{(4)} = g_6. \qquad (5.51)$$

The effective detunings are

$$\begin{aligned}
\Delta^{(1)} &= \Delta_3 - \frac{g_3^2\Delta_1}{(\Delta_1\Delta_2 - g_2^2)} + \frac{g_1^2\Delta_2}{(\Delta_1\Delta_2 - g_2^2)} \approx \Delta_3 - \frac{g_3^2}{\Delta_2} + \frac{g_1^2}{\Delta_1}, \\
\Delta^{(2)} &= \Delta_4 + \frac{g_1^2\Delta_2}{(\Delta_1\Delta_2 - g_2^2)} \approx \Delta_4 + \frac{g_1^2}{\Delta_1}, \\
\Delta^{(3)} &= \Delta_5 + \frac{g_1^2\Delta_2}{(\Delta_1\Delta_2 - g_2^2)} \approx \Delta_5 + \frac{g_1^2}{\Delta_1}, \qquad (5.52) \\
\Delta^{(4)} &= \Delta_6 - \frac{g_1^2(\Delta_2+\Delta_6)}{[(\Delta_1+\Delta_6)(\Delta_2+\Delta_6) - 2g_2^2]} + \frac{g_1^2\Delta_2}{(\Delta_1\Delta_2 - g_2^2)} \approx \Delta_6 - \frac{g_1^2}{(\Delta_1+\Delta_6)} + \frac{g_1^2}{\Delta_1}.
\end{aligned}$$

To ensure a complete population inversion has been taken place, the previous effective couplings can be related to each other by the formula $g^{(n)} = g_0\sqrt{n(N-n)}$. In our case (with $N = 5$ and $n = 1, 2, 3, 4$), it is easy to find that $g^{(1)} = g^{(4)}$, $g^{(2)} = g^{(3)}$, and $g^{(2)} = \sqrt{\frac{3}{2}}g^{(1)}$.

Since the state $|a\ 101\rangle$ is linked to the auxiliary state $|d\rangle$ by the effective coupling $g^{(2)} = g_1$, it is not difficult to prove mathematically that the condition $\Delta >> g$ can not be met in

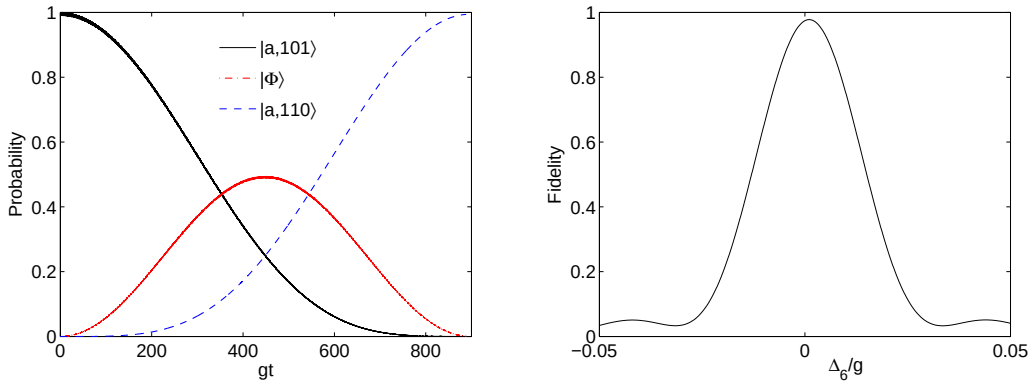

(a) (b)

Figure 5.8: (a) The probability in the three-level system of Eq. (5.52). The coupling constants g_1, g_2, and g_3 all are set to g and $g_5 = 10g^{(2)}$. The detunings Δ_1, and Δ_2 are set to 20g. The detunings Δ_3, Δ_4, Δ_5 and Δ_6 are determined by the resonance conditions. The coupling constant g_6 is given by $g_6 = -\frac{g_2 g_3 g_5}{\Delta_1 \Delta_2}$ so that $G^{(1)} = G^{(2)}$. The three-level behaviour can be realized at $|G^{(1)}t| = |G^{(2)}t| = \pi/\sqrt{2}$. (b) This figure shows the proper value for Δ_6 so that the fidelity of the three-level system (which is generated by five-level (1001111)) is in the maximum value. Note that $\Delta_1 = \Delta_2 = \Delta = 10g$.

this case. This means that our procedure fails to generate the Fredkin gate by using a five-level system.

The previous five-level model; however, can be employed to construct an effective three-level behaviour. In the five-level system, by allowing the effective coupling $g^{(3)}$ to be large compared to the couplings $g^{(2)}$ and $g^{(4)}$, i.e. $g^{(3)} >> g^{(2)}, g^{(4)}$, this system can be reduced to a three-level approximation [47] with the following new effective couplings

$$\mathrm{G}^{(1)} = g^{(1)} \ , \quad \mathrm{G}^{(2)} = \frac{g^{(2)} g^{(4)}}{g^{(3)}} \ . \tag{5.53}$$

This model comprises the states $|a\ 101\rangle$, $|d\rangle$, and $|a\ 110\rangle$. Unlike the previous three-state system (1001001), this model requires at least two additional resonance conditions (see Eq. (5.52)). In contrast, Fig. 5.8 demonstrates that this model is as fast as the three-level system (1001001).

For a certain large system, the three-level system generated from the model (1001111) shows that applying the two methods in Shore's theory, namely by large detunings and large coupling strengths, can give better results than by using one method alone. That is, in our case we have reduced a nine-level system into an effective five-level behaviour by applying the adiabatic elimination method. Then, this effective system has been further truncated into a three-level system by the second Shore's method, where certain couplings

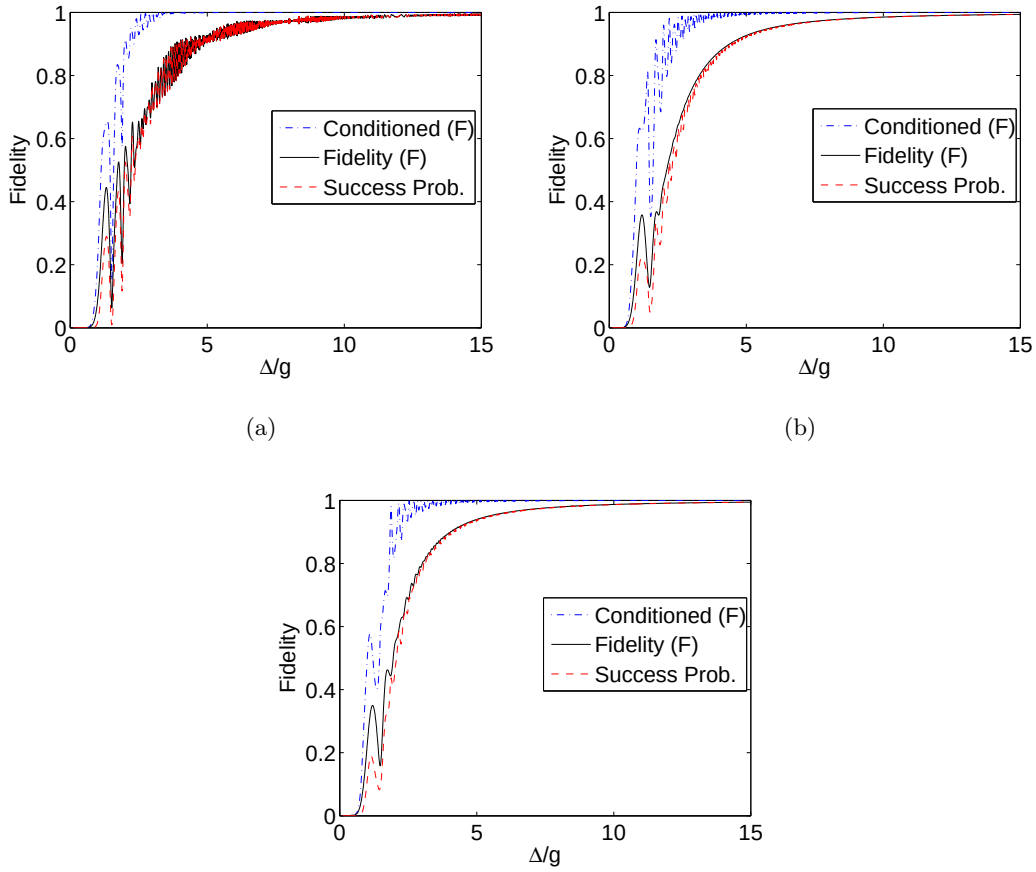

Figure 5.9: Fidelity (black solid line), the conditional measurement (blue dotted-dashed line), and the success probability (red dashed line) in the configurations (a) (1001001) (b) (1001011), and (c) (1001111). Parameters of the coupling constants and the resonance conditions can be found in Figs. 5.3, 5.6, 5.8. Note that the product of the fidelity and the conditioned fidelity gives the success probability.

are allowed to be very large, resulting in a faster three-level approximation than the three-level models (1000101) and (100011).

5.7 The robustness of the gate

So far, based on the models, namely the spin-J model and the effective two-level Hamiltonian, we have analysed several configurations which are all able to transform the qubit state $|a\ 101\rangle$ to $|a\ 110\rangle$. We have seen that amongst these configurations the models (1001001), (1001011), and (1001111) are faster than other models. Considering only these three models, similarly to the case in the iSWAP gate in this section, we provide more details about the effect of variations in the values of the coupling constant g and the

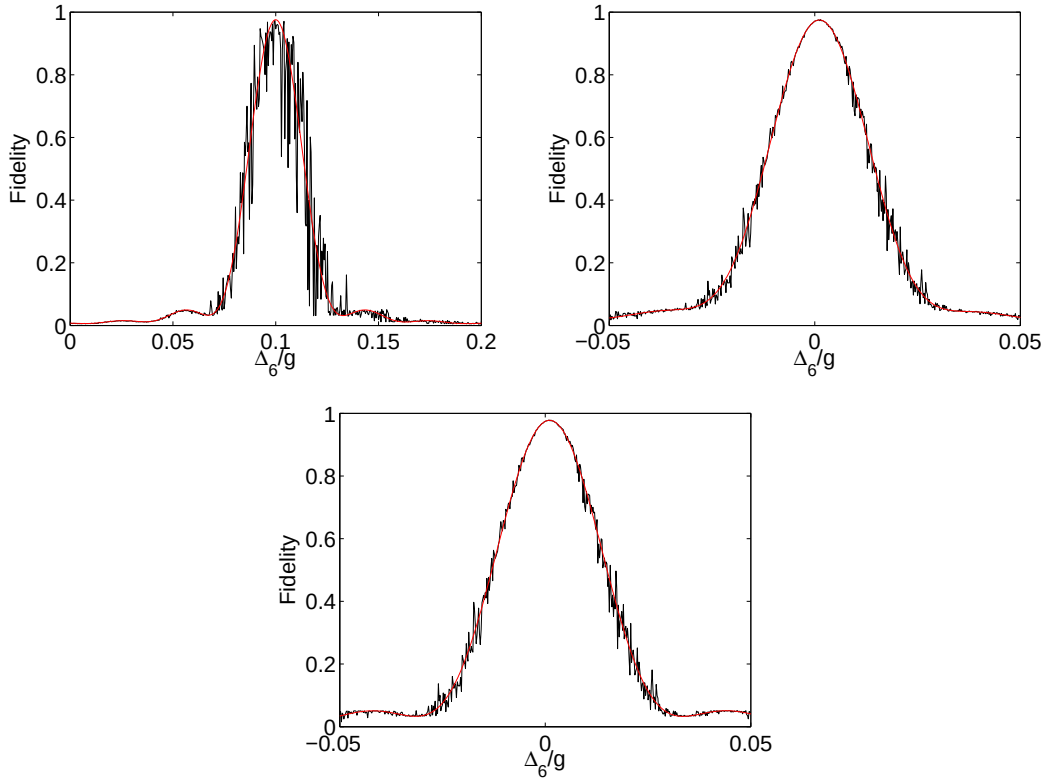

Figure 5.10: Fidelity of the configurations (a) (1001001), (b) (1001011), and (c) (1001111) with $g = g_0$ (red line) and g described by the norm distribution in Fig. 4.10*a*. Parameters can be found in Figs. 5.3, 5.6, 5.8.

detunings Δ and Δ_6 on the model fidelity.

5.7.1 Fidelity and the conditional measurement

Following the arguments in Sec. 4.7.1, one can find that the fidelity of the configurations of interest is nothing but the probability of the system to be in the state $|a\ 110\rangle$, (note that all systems have been assumed to be initially in the state $|a\ 101\rangle$). Fig. 5.9 illustrates the fidelity for these models. The blue dashed lines in this figure demonstrate that the conditional measurement (more details can be found in Sec. 4.7.1) can notably enhance the fidelity of the system.

5.7.2 Sensitivity to the changes in the coupling and detuning

In Fig. 5.10 we can check the sensitivity of the models (1001001), (1001011), and (1001111) to the variations in Δ_6 (red lines) around its proper values (the resonance conditions for each model can be found in Secs. 5.4.1, 5.5.1, 5.6). Numerically, the width of curves can be given by FWHM=(28.7, 27.6, 28.5)$\times 10^{-3}$, respectively. It is observable that these models

show almost the same response. This is reasonable as there is no considerable difference in the values of the effective couplings for these models (see Eqs. (5.15, 5.34, 5.53).

Given the value of the coupling constant g to be described by the normal distribution in Fig. 4.10, at the proper value of Δ_6 the fidelity of the configurations in Fig. 5.10 has approached the maximum value predicted by the theoretical g_0. This confirms that these models can accept the uncertainty in the atom-field coupling strength measured in the laboratory.

To outline this section, we have investigated the effect of allowing variations in values of characteristic parameters around their theoretical estimations. We have found that the configurations (1001001), (1001011), and (1001111) are not fragile. That is, they show that high fidelity can be achieved after introducing some uncertainty into values of parameters such as Δ_6 and g_0.

5.8 Time evolution of the qubit state $|a\ 100\rangle$

In previous sections, based on the effective Hamiltonian theory several configurations have been developed in order to transform the qubit state $|a\ 101\rangle$ to $|a\ 110\rangle$. On the other hand, the remaining qubits in the truth table 5.1 must stay in their initial states so that the Fredkin gate can be performed.

Recalling the Hamiltonian 5.2, it is found that the qubit states $|a\ 001\rangle$ and $|a\ 011\rangle$ do not show any response to this Hamiltonian action, i.e. $\hat{H}|a\ 001\rangle = \hat{H}|a\ 011\rangle = 0$. It is clear that these two qubit states will have the same population loss due to the atomic and photonic decays, as will be shown in chapter 6. Furthermore, the qubit state $|a\ 010\rangle$ evolves as

$$|a\ 01,10,01\rangle \mapsto c_a(t)|a\ 01,10,01\rangle + c_f(t)|f\ 01,10,00\rangle + c_e(t)|e\ 01,10,10\rangle\ . \tag{5.54}$$

This system can be described by the Hamiltonian $\hat{H}'$ in the interaction picture and in the basis $\{|a\ 01,10,01\rangle, |f\ 01,10,00\rangle, |e\ 01,10,10\rangle\}$ as

$$\hat{H}' = \begin{bmatrix} 0 & 0 & g_6 \\ 0 & (\Delta_4 - \Delta_6) & g_5 \\ g_6 & g_5 & (\Delta_5 - \Delta_6) \end{bmatrix}\ . \tag{5.55}$$

The qubit state $|a\ 010\rangle$ remains unchanged when $\Delta_{4,5} >> g$. Likewise, the time evolution of the state $|a\ 000\rangle$ can be given by

$$|a\ 01,01,01\rangle \mapsto c_a(t)|a\ 01,01,01\rangle + c_f(t)|f\ 01,01,00\rangle + c_e(t)|e\ 01,01,10\rangle\ . \tag{5.56}$$

Considering the basis $\{|a\ 01,01,01\rangle, |f\ 01,01,00\rangle, |e\ 01,01,10\rangle\}$, the Hamiltonian in (5.55) can be used to describe the state above in the interaction picture. Once again, with $\Delta_{4,5} >> g$ the qubit state $|a\ 000\rangle$ can stay in its initial state. Once again, the qubit states $|a\ 010\rangle$ and $|a\ 000\rangle$ will show the same sensitivity to the decoherence processes as given in chapter 6. Moving now to the qubit state $|a\ 111\rangle$, one finds that

$$|a\ 10,10,10\rangle \mapsto c_a(t)|a\ 10,10,10\rangle + c_b(t)|b\ 00,10,10\rangle + c_c(t)|c\ 00,20,10\rangle\ , \tag{5.57}$$

and the Hamiltonian of the system in the interaction picture can be

$$\hat{H}' = \begin{bmatrix} 0 & 0 & g_1 \\ 0 & \Delta_2 & \sqrt{2}g_2 \\ g_1 & \sqrt{2}g_2 & \Delta_1 \end{bmatrix}\ . \tag{5.58}$$

By setting $\Delta_{1,2} >> g$, we adiabatically eliminate the states other than $|a\ 111\rangle$, and then the system stays unchanged. This implies that the model (1001001) in Sec. 5.4.1 is probably the only remaining configuration that can be used to perform the Fredkin gate (note that we completely ignore the model (1000001) as it is a very slow model).
Lastly, considering now the qubit state $|a\ 10,01,01\rangle$, this initial state evolves as

$$\begin{aligned} |\Psi(t)\rangle &= c_1(t)|e\ 10,10,01\rangle + c_2(t)|d\ 00,10,01\rangle + c_3(t)|c\ 00,11,01\rangle \\ &+ c_4(t)|b\ 00,01,01\rangle + c_5(t)|a\ 10,01,01\rangle + c_6(t)|f\ 10,01,00\rangle \\ &+ c_7(t)|e\ 10,01,10\rangle + c_8(t)|d\ 00,01,10\rangle + c_9(t)|c\ 00,02,10\rangle\ . \end{aligned} \tag{5.59}$$

In the basis $\{|e\ 10,10,01\rangle, |d\ 00,10,01\rangle$
$, |c\,00,11,01\rangle, |b\,00,01,01\rangle, |a\ 10,01,01\rangle, |f\ 10,01,00\rangle, |e\ 10,01,10\rangle, |d\,00,01,10\rangle, |c\,00,02,10\rangle\}$, the tridiagonal Hamiltonian of this system in the interaction picture can be written as

$$\hat{H}' = \begin{bmatrix} \Delta_4 & g_1 & 0 & 0 & 0 & 0 & 0 & 0 & 0 \\ g_1 & \Delta_3 & g_3 & 0 & 0 & 0 & 0 & 0 & 0 \\ 0 & g_3 & \Delta_2 & g_2 & 0 & 0 & 0 & 0 & 0 \\ 0 & 0 & g_2 & \Delta_1 & g_1 & 0 & 0 & 0 & 0 \\ 0 & 0 & 0 & g_1 & 0 & g_6 & 0 & 0 & 0 \\ 0 & 0 & 0 & 0 & g_6 & (\Delta_5 - \Delta_6) & g_5 & 0 & 0 \\ 0 & 0 & 0 & 0 & 0 & g_5 & (\Delta_4 - \Delta_6) & g_1 & 0 \\ 0 & 0 & 0 & 0 & 0 & 0 & g_1 & (\Delta_3 - \Delta_6) & \sqrt{2}g_3 \\ 0 & 0 & 0 & 0 & 0 & 0 & 0 & \sqrt{2}g_3 & (\Delta_2 - \Delta_6) \end{bmatrix} \tag{5.60}$$

where Δ_i $(i = 1, 2, ..., 6)$ has the same definition in Eq. (5.5). Applying the model (1001001) is equivalent to set the transitions to the basis states $|d\ 00,10,01\rangle$, $|a\ 10,01,01\rangle$,

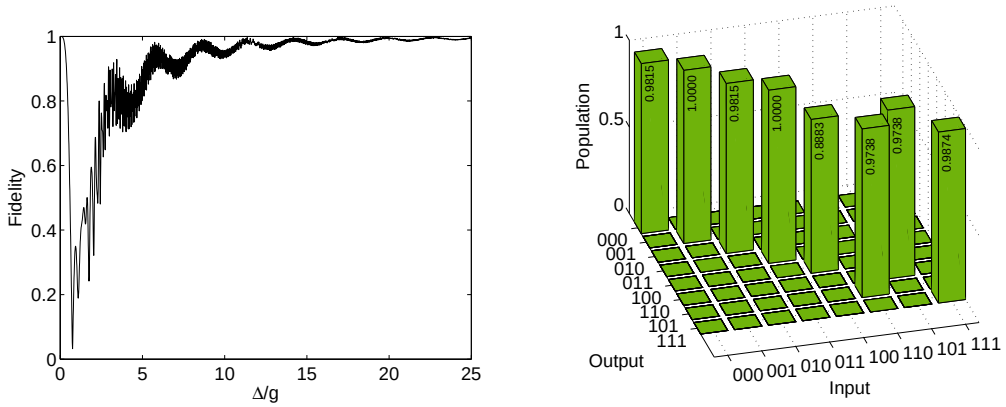

(a) (b)

Figure 5.11: (a) The system in (5.60) is largely confined in the qubit state $|a\ 100\rangle$ when considering the resonance conditions (5.16, 5.17). Parameters are the same as Fig. 5.3b. (b) Simulation of all qubits in the truth table (5.1) with the same parameters in (a) where $\Delta_{1,2,4,5} = 10\ g$.

and $|d\ 00, 01, 10\rangle$ to be resonant. That is, we use the effective two-level Hamiltonian theory to reduce the system (5.60) to a three-level behaviour. One then defines the corresponding operators $\hat{H}_0$, $\hat{A}$, and $\hat{B}$ as

$$\hat{H}_0 = \begin{bmatrix} \Delta_3 & 0 & 0 \\ 0 & 0 & 0 \\ 0 & 0 & \Delta_3 - \Delta_6 \end{bmatrix}, \hat{B} = \begin{bmatrix} g_1 & g_3 & 0 & 0 & 0 & 0 \\ 0 & 0 & g_1 & g_6 & 0 & 0 \\ 0 & 0 & 0 & 0 & g_1 & \sqrt{2}g_3 \end{bmatrix}, \tag{5.61}$$

$$\hat{A} = \begin{bmatrix} \Delta_4 & 0 & 0 & 0 & 0 & 0 \\ 0 & \Delta_2 & g_2 & 0 & 0 & 0 \\ 0 & g_2 & \Delta_1 & 0 & 0 & 0 \\ 0 & 0 & 0 & \Delta_5 - \Delta_6 & g_5 & 0 \\ 0 & 0 & 0 & g_5 & \Delta_4 - \Delta_6 & 0 \\ 0 & 0 & 0 & 0 & 0 & \Delta_2 - \Delta_6 \end{bmatrix}. \tag{5.62}$$

With ($\Delta_{1,2,4,5} >> \ g_i$ with $i = 1, 2, 3, 5, 6$), the effective couplings read

$$g^{(1)} \approx \frac{g_1 g_2 g_3}{\Delta_1 \Delta_2}\ , \quad g^{(2)} \approx \frac{g_1 g_5 g_6}{\Delta_4 \Delta_5}\ , \tag{5.63}$$

and the effective detunings can be given as

$$\begin{aligned} \Delta^{(1)} &\approx \Delta_3 - \frac{g_1^2}{\Delta_4} - \frac{g_3^2}{\Delta_2} + \frac{g_1^2}{\Delta_1} + \frac{g_6^2}{\Delta_5}\ , \\ \Delta^{(2)} &\approx \Delta_3 - \Delta_6 - \frac{g_1^2}{\Delta_4} - \frac{2g_3^2}{\Delta_2} + \frac{g_1^2}{\Delta_1} + \frac{g_6^2}{\Delta_5}\ . \end{aligned} \tag{5.64}$$

When setting $\Delta^{(1)}$ and $\Delta^{(2)}$ to zero, the resonance conditions are

$$\Delta_3 \approx \frac{g_1^2}{\Delta_4} + \frac{g_3^2}{\Delta_2} - \frac{g_1^2}{\Delta_1} - \frac{g_6^2}{\Delta_5} \ , \quad \Delta_6 \approx -\frac{g_3^2}{\Delta_2} \ . \tag{5.65}$$

A three-level approximation can be formed by the resonance conditions (5.65). Replacing these resonance conditions by those ones in the model (1001001) (see Eqs. (5.16, 5.17)) destroys the previous three-level system in (5.65), but, fortunately, confines sufficiently this system in the level $|a\rangle$, as demonstrated by Fig. 5.11 a. As a result, the model (1001001) is an appropriate configuration to realize the Fredkin gate (see Fig. 5.11).

5.9 Summary

In conclusion, several N-level approximations (with $N = 2, 3, 4, 5$) have been employed in order to interchange the qubit states $|a\ 101\rangle$ and $|a\ 110\rangle$. The locations of sharp resonances are predicted by the effective two-level Hamiltonian and the coupling constants are properly scaled by the spin-J model.

In the effective three-level model (1001001), we set all detunings excluding Δ_3 and Δ_6 to be much larger in magnitude than any parameter in the system. As a result, all qubits other than $|a\ 101\rangle$ and $|a\ 110\rangle$ in the truth table of the Fredkin gate, fortunately, stay sufficiently in their initial states (see Sec. 5.8), meaning that this configuration is suited for the realization of the Fredkin gate.

With the same microwave cavity considered in Sec. 4.9, the operation time for the Fredkin gate by the model (1001001), with the choice $\Delta_1 = \Delta_2 = \Delta_4 = \Delta_5 = 5g$, is much shorter than the decoherence times (for the interaction time τ_{int} and the photon lifetime in cavity τ_{ph}, $\tau_{int}/\tau_{ph} \sim 2.5$ms). This means that this gate can be acceptable for the applications in the quantum information process.

Part III

Decoherence process in quantum gates with multi-mode cavities

Chapter 6

Atomic and photonic relaxations

So far, a set of universal gates for dual-rail CQED QIP has been theoretically investigated. In our treatment, we have assumed a completely controlled interaction between the photonic qubits in those logic gates. In real systems, however, this is not the case. Since quantum computers always require an interaction between the quantum operations and the outside world [15, 26], practical quantum gates have suffered from the decoherence process.

In what follows, we discuss the influence of decoherence processes on the quantum operations already performed in chapters 4, 5. In Sec. 6.2, an introduction for the master equation and the wave-function approaches, as two different methods used to describe decoherence mechanisms, is given with applications to a simple Jaynes-Cummings model. Then, we apply these approaches to some quantum systems in the iSWAP and Fredkin gates (in Secs. 6.3, 6.4). Considering all qubit states in these operations, we (in Sec. 6.5) use the master equation to address the population loss in these qubit states. Finally, we conclude in Sec. 6.6.

6.1 Loss mechanisms in the recent cavity QED techniques

Since the birth of quantum computing, it was realized that decoherence will be one of the difficulties to build quantum computers [78]. In the process of decoherence, qubits of the computation couple the environment to a greater or lesser extent, which then leads to loss of the quantum information stored in qubits. Therefore, one of the main criteria for physical implementation of a quantum computer is that qubit decoherence times must be much longer than the operation time [57].

The phase fluctuations of the classical field, collisions between particles in gases, random-

ness caused by the excited vibrations in solid, and the relaxation decay rates carried out by the excited states into the lower states are examples of decoherence sources [15, 79]. The last decoherence channel itself may include the spontaneous emission Γ by atoms into modes other than the cavity mode of interest or photonic decays κ by fields into a reservoir. The rates of this decoherence resource can be determined by the radiative lifetime of the atomic levels τ_{rad} and by the photon lifetime τ_{cav}.

Recently, significant improvements introduced in modern cavities have reduced the impact of previous dampings. Experiments of the semiconductor quantum dots in nanocavities, for example, show that (at low temperatures) decoherence processes other than relaxation decay rates can be neglected (e.g. the radiative lifetime $\tau \sim 2$ ns and other dissipative processes ~ 30 ns)[36, 80]. Moreover, it is reported that only the atomic and photonic relaxation rates have been considered as sources of the incoherence process in the interaction between highly-excited Rydberg atoms and high-Q cavity in either microwave or optical regimes [9, 39, 81]. These experimental schemes and other setups show that relaxations can be the only dominant loss mechanism in the present cavity-QED techniques.

With high control for decays due to Γ and κ, the strong coupling regime (where $g >> \kappa, \Gamma$) has been achieved. Examples may include semiconductor quantum dots in optical nanocavities, such devices possess a very small-volume V (so very large g and very small Γ) and high quality factor Q (i.e. very small κ), resulting in a strong coupling regime [82, 83]. Furthermore, the strong coupling interaction can be generated by the interaction of the relatively long excited-state lifetime in Rydberg atoms with high-Q superconducting cavity. This system has been widely utilized in applications of the fields of quantum information processing (see e.g. [84, 85]).

Subsequently, decays due to Γ and κ where atoms interacting with cavities in the strong coupling domain have been considered, and any other sources of decoherence processes have been completely ignored.

6.2 The dissipative processes in the JCM

In order to study the influence of decoherence on the logic gates in part II, we start our discussion here by introducing two possible treatments, namely the master equation and the wave-function approaches. Although the former approach is valid for all quantum systems in the iSWAP and the Fredkin gates (see chapters 4, 5), we observe that analytical solutions can be obtained by following the wave-function approach. Therefore, analytical and numerical solutions for the impact of the dissipation processes in the qubit state $|a\ 10\rangle$

in the iSWAP gate and the qubit state $|a\ 101\rangle$ in the Fredkin gate will be undertaken. Then, for the remaining qubit states in either the iSWAP or the Fredkin gate we will consider Liouville's equation alone.

Indeed, this section will be the starting point for the following sections, and then we will try to give more details for the main principles in both approaches with a simple application to the Jaynes-Cummings model.

6.2.1 The general master equation

As a starting point in this chapter, we here introduce the formal derivation for the master equation. Assuming a small system S interacting with a large system (well-known as the reservoir) R, the total Hamiltonian is then $\hat{H} = \hat{H}^{\mathrm{S}} + \hat{H}^{\mathrm{R}} + \hat{H}_{int} = \hat{H}_0 + \hat{H}_{int}$. As we have seen in chapter 1, in the interaction picture $\hat{H}'_{int} \mapsto e^{\mathrm{i}\hat{H}_0 t}\ \hat{H}_{int}\ e^{-\mathrm{i}\hat{H}_0 t}$. As an example, the system S can be either a two-level atom or a harmonic oscillator coupled to the system R containing many infinitely harmonic oscillators. Furthermore, we assume at time $t = 0$ the states of S and R to be described as $\rho(0)^{\mathrm{S}}$ and $\rho(0)^{\mathrm{R}}$, respectively, and the initial state for the compound system $\rho(0) = \rho^{\mathrm{S}}(0) \otimes \rho^{\mathrm{R}}(0)$, implying that S and R to be initially decorrelated. The time evolution of the compound system $(S + R)$ can be given by

$$\frac{d}{dt}\tilde{\rho}(t) = -\frac{\mathrm{i}}{\hbar}[\hat{H}'_{int}(t), \tilde{\rho}(t)]\ , \tag{6.1}$$

where $\tilde{\rho}(t)$ to be the density operator of the compound system in the interaction picture. The large system R is assumed not to be affected by the interaction (i.e. $\rho^{\mathrm{R}}(t) \mapsto \rho^{\mathrm{R}}(0)$ for all time t). This is the Born approximation, which assumes that the environment (the bath) is essentially unaltered by the weak interaction. The main aim now is to find the equation of motion for the S alone (i.e. the so-called master equation). Therefore, it is possible to express the density matrix of the compound system as

$$\tilde{\rho}(t) = \rho^{\mathrm{R}}(0) \otimes \tilde{\rho}^{\mathrm{S}}(t)\ . \tag{6.2}$$

Tracing of $\tilde{\rho}(t)$ over the degrees of freedom of the reservoir results in the density matrix of S alone. That is, $\tilde{\rho}^{\mathrm{S}}(t) = \mathrm{Tr}_R(\tilde{\rho}(t)) = \tilde{\rho}^{\mathrm{S}}(t)\mathrm{Tr}_R(\rho^{\mathrm{R}}(0))$. By applying the previous partial trace to Eq. (6.1) with considering Eq. (6.2), one finds the following master equation

$$\frac{d}{dt}\tilde{\rho}^{\mathrm{S}}(t) = -\frac{\mathrm{i}}{\hbar}\ \mathrm{Tr}_R[\hat{H}'_{int}(t), \rho^{\mathrm{R}}(0) \otimes \tilde{\rho}^{S}(t)]\ . \tag{6.3}$$

The right-hand side of this equation vanishes since the reservoir R is considered to be in thermal equilibrium, which means $\rho^{\mathrm{R}}(0)$ is diagonal in the energy representation [15]. The

formal integrating of Eq. (6.1) yields

$$\tilde{\rho}(t) = \tilde{\rho}(0) - \frac{\mathrm{i}}{\hbar}\int_0^t [\hat{H}'_{int}(t'), \tilde{\rho}(t')]dt' \ , \tag{6.4}$$

where $t' \leq t$. By substituting this equation into Eq. (6.1) and taking the trace over R with the help of Eq. (6.2), one then obtains

$$\frac{d}{dt}\tilde{\rho}^{\mathrm{S}}(t) = -\frac{\mathrm{i}}{\hbar}\,\mathrm{Tr}_R[\hat{H}'_{int}(t), \tilde{\rho}(0)] - \frac{1}{\hbar^2}\int_0^t \mathrm{Tr}_R[\hat{H}'_{int}(t), [\hat{H}'_{int}(t'), \rho(0)^{\mathrm{R}}\ \tilde{\rho}^{\mathrm{S}}(t')]]dt' \ . \tag{6.5}$$

Once again, the first term is zero since it is assumed that R in thermal equilibrium and the density operator of R at $t = 0$ to be diagonal in the energy representation. We now introduce another important approximation into the last equation, namely the Markov approximation. In this approximation, $\tilde{\rho}^{\mathrm{S}}(t')$ is replaced by $\tilde{\rho}^{\mathrm{S}}(t)$. To this end, it is assumed that the reservoir correlation functions vanish rapidly compared to the time scale on which $\tilde{\rho}^{\mathrm{S}}(t')$ changes [15]. This means that the changes in the reservoir can be ignored in the limit of time needed for $\tilde{\rho}^{\mathrm{S}}(t')$ to change. As a result of the Markov approximation, any dependence on the initial state of the system at $t = 0$ can be eliminated by making a change of variable. That is, the limit of the integration above is extended $t \mapsto \infty$ and $t' \mapsto t - t'$ is considered so that

$$\frac{d}{dt}\tilde{\rho}^{\mathrm{S}}(t) = -\frac{1}{\hbar^2}\int_0^\infty \mathrm{Tr}_R[\hat{H}'_{int}(t), [\hat{H}'_{int}(t-t'), \rho(0)^{\mathrm{R}}\ \tilde{\rho}^{\mathrm{S}}(t)]]dt' \ . \tag{6.6}$$

This is a Born-Markov master equation. Under the previous approximations, this general formula for the master equation can be used to address the time evolution of specific systems such as a two-level atom coupled to a reservoir of many harmonic oscillators or a single-mode cavity field damped into modes outside the field modes of interest. In these cases, we expand the commutators in the previous master equation and insert $H'_{int}(t-t')$ and $H'_{int}(t)$ expressed through system and reservoir operators (see [15, 16]).

At very low temperature (i.e. $k_BT << \hbar\omega$ and then thermal photon number $\bar{n} \mapsto 0$), the master equation for the two-level atom is

$$\frac{d}{dt}\tilde{\rho}^A(t) = \frac{1}{2}\Gamma(2\hat{\sigma}_-\tilde{\rho}^A\hat{\sigma}_+ - \hat{\sigma}_+\hat{\sigma}_-\tilde{\rho}^A - \tilde{\rho}^A\hat{\sigma}_+\hat{\sigma}_-) \ . \tag{6.7}$$

where Γ is the atomic decay rate. In the case of a single-mode damping into the empty cavity under the condition $\bar{n} \mapsto 0$

$$\frac{d}{dt}\tilde{\rho}^F(t) = \frac{1}{2}\kappa(2\hat{a}\tilde{\rho}^F\hat{a}^\dagger - \hat{a}^\dagger\hat{a}\tilde{\rho}^F - \tilde{\rho}^F\hat{a}^\dagger\hat{a}) \ . \tag{6.8}$$

where κ is the cavity field decay.

6.2.2 The damped JCM by the master equation approach

The quantum systems describing the logic gates in the previous chapters consist of a multi-level "atom" interacting with multi-mode cavities in a strong coupling regime. At a very low temperature (i.e. the average number of thermal photons $\bar{n} \mapsto 0$), the time evolution of the system (atom+field) can be governed by Liouville's equation (see previous section (6.2.1))

$$\frac{d}{dt}\,\rho = -\mathrm{i}\left[\hat{H},\ \rho\right] + \hat{\mathcal{L}}\,\rho\ , \tag{6.9}$$

where ρ is the density operator of the atom-field system. The first term in this formula and the so-called Liouvillian operator $\hat{\mathcal{L}}\rho$ (the second term on the right-hand side) together give a master equation that describes the atom-field dynamics in which there are strong couplings in addition to the weak interaction with the environment. Obviously, at the absence of any decoherence process the previous equation returns back to Schrödinger equation in terms of ρ.

Generally, in the previous chapters we deal with quantum systems where each couple of atomic states interacts with a single mode. Then, the general Lindblad form of the Liouvillian operator $\hat{\mathcal{L}}\rho$ can be expressed as [15, 86]

$$\hat{\mathcal{L}}\,\rho \ \ = \ \ \sum_i \frac{\eta_{(i)}}{2}\,([\hat{L}_{(i)}\ \rho\ ,\ \hat{L}^{\dagger}_{(i)}] + [\hat{L}_{(i)}\ ,\ \rho\ \hat{L}^{\dagger}_{(i)}])\ , \tag{6.10}$$

where η represents the loss of population. In our case η may refer to the spontaneous emission Γ or to the cavity field rate κ. The operators $\hat{L}$ and $\hat{L}^{\dagger}$ are the corresponding system operators. More precisely, in the case of atomic decays $\hat{L}$ and $\hat{L}^{\dagger}$ represent the corresponding atomic operators $\hat{\sigma}_-$ and $\hat{\sigma}_+$ (see Eq. (6.7)); likewise, in the case of field decays they have been replaced by the annihilation and creation operators, $\hat{a}$ and $\hat{a}^{\dagger}$ (as in Eq. (6.8)).

On the one hand, the atomic relaxation rate Γ in free space can be defined as [14, 15, 79]

$$\Gamma = \frac{1}{\tau_R} = \frac{\omega_{12}^3 \mu_{12}^2}{3\pi\epsilon_0\hbar c^3}\ , \tag{6.11}$$

where τ_R is the radiative lifetime, ω_{12} represents the atomic transition frequency, and μ_{12} is the dipole matrix element. Inside a cavity the atomic emission rate in free space Γ is modified, such an effect known as the Purcell effect [79] and experimentally observed by Haroche et al.(1983) [87]. Physically, this is explained as a result of the change in the free-space modes which in this case subjects to the cavity geometry [15]. That is, the spontaneous emission in a high-Q cavity can be enhanced as

$$\Gamma_c = \Gamma Q\ (\frac{6\pi c^3}{V\omega^3})\ . \tag{6.12}$$

The photonic decay rate κ, on the other hand, can be represented as [79]

$$\kappa = \frac{1}{\tau_{cav}} = \frac{\omega}{Q} \ , \tag{6.13}$$

where τ_{cav} is the photon lifetime. The atomic and photonic decay rates defined in Eqs. (6.12, 6.13) in addition to the coupling strength g can be considered as the characteristic parameters for a cavity.

For convenience, Liouville's operator in Eq. (6.10) can be written as a sum of two terms, the term represented by the so-called jump superoperator $\hat{J}$ and the anticommutator term given by the superoperator $\hat{S}$ [15, 16],

$$\hat{\mathcal{L}}\ \rho = \sum_i \eta_{(i)}\ \ \hat{L}_{(i)}\ \rho\ \hat{L}^{\dagger}_{(i)} + \sum_i -\frac{\eta_{(i)}}{2}\ \{\hat{L}^{\dagger}_{(i)}\ \hat{L}_{(i)}, \rho\} \equiv (\hat{J} + \hat{S})\ \rho\ . \tag{6.14}$$

The Liouvillian operator expressed in this formula would give us further details for the population decays from the excited states and the quantum jumps events in the damped systems. Subsequently, according to information provided by the superoperators $\hat{J}$ and $\hat{S}$ we are able (in some cases) to find solvable expressions describing the dissipative processes for some quantum systems of interest.

As a simple application for the previous master equation, we discuss in brief the dynamics of the Jaynes-Cummings model in Sec. 1.3.1 under the presence of the atomic and photonic relaxations (a similar discussion can be found in many textbooks, see for example [15, 16]). From Sec. 1.3.1, the wavevector for the JCM with a cavity initially in the number state $|1\rangle$ is

$$|\Psi(t)\rangle = c_1(t)\ |a,1\rangle + c_2(t)\ |b,0\rangle\ . \tag{6.15}$$

The density matrix for this system $\rho = \sum_i P_i |\psi_i\rangle\langle\psi_i|$ can be expressed as

$$\rho = |c_1|^2\ |a,1\rangle\langle a,1| + c_1 c_2^*\ |a,1\rangle\langle b,0| + c_2 c_1^*\ |b,0\rangle\langle a,1\rangle + |c_2|^2\ |b,0\rangle\langle b,0|\ . \tag{6.16}$$

In order to calculate the Liouvillian operator $\hat{\mathcal{L}}\rho$, we can write the superoperator $\hat{J}$ and $\hat{S}$ as

$$\hat{J}^A\rho = \Gamma\hat{\sigma}_{ab}\rho\hat{\sigma}_{ba}\ , \quad \hat{J}^C\rho = \kappa\hat{a}\rho\hat{a}^{\dagger}\ , \quad \begin{aligned} \hat{S}^A\rho &= -\frac{\Gamma}{2}(\hat{\sigma}_{ba}\hat{\sigma}_{ab}\rho + \rho\hat{\sigma}_{ba}\hat{\sigma}_{ab})\ , \\ \hat{S}^C\rho &= -\frac{\kappa}{2}(\hat{a}^{\dagger}\hat{a}\rho + \rho\hat{a}^{\dagger}\hat{a})\ , \end{aligned} \tag{6.17}$$

where $\hat{J}^A$ and $\hat{S}^A$ can be considered as the atomic parts in these identities, and $\hat{J}^C$ and $\hat{S}^C$ represent the field parts. It is easy now to find that

$$\hat{J}\rho = (\Gamma|c_2|^2 + \kappa|c_1|^2)\ |a,0\rangle\langle a,0|\ , \tag{6.18}$$

and for the superoperator $\hat{S}$

$$\begin{aligned}\hat{S}\rho = \; & - \; \Gamma|c_2|^2 \; |b,0\rangle\langle b,0| - \kappa|c_1|^2 \; |a,1\rangle\langle a,1| \\ & - \; \frac{1}{2}(\Gamma+\kappa)(c_1 c_2^* \; |a,1\rangle\langle b,0| + c_2 c_1^* \; |b,0\rangle\langle a,1|).\end{aligned} \tag{6.19}$$

These operators construct the Liouvillian operator $\hat{\mathcal{L}}\rho$. By adding Eqs. (6.18, 6.19) to the strong coupling term $-\mathrm{i}[\hat{H},\rho]$, we can describe the dynamics of the damped system. Further details will be provided after discussing the following section.

6.2.3 Wave-function approach

In general, the master equation in (6.9) provides a very useful way of simulating the density matrix for quantum systems. Nevertheless, a direct solution for the density matrix of large systems would be extremely complicated and impractical. An alternative method to the master equation approach has been introduced in this section in order to yield solvable expressions. Instead of describing the dissipative mechanisms in a system by the time evolution of the density matrix, an alternative treatment based on the wavefunction of the system developed by [88, 89] can be used. This method, on the one hand, gives a powerful tool for generating numerical solutions based on wavefunctions [3, 15, 90]. In brief, when considering only the dissipation of population, this method assumes that the quantum jumps in a system occur at random times. As a starting point in this approach, for the time interval $[0,\ t_1]$ the time evolution of the system is governed by the effective Hamiltonian

$$\hat{H}' = \hat{H} - \frac{\mathrm{i}}{2}\sum_i \; \eta_{(i)} \; \hat{L}^\dagger_{(i)}\hat{L}_{(i)} \; , \tag{6.20}$$

where $\hat{H}$ is the original Hamiltonian of the system in the absence of any decay, and once again $\hat{L}^\dagger$ and $\hat{L}$ represent the corresponding system operators. Once a quantum jump (either via the atomic or the photonic decay) takes place at t_1, the wavefunction is renormalized to unity. Then the propagation of the new wavefunction continues till the next quantum jump at t_2, and again the resulted wavefunction is renormalized. This procedure is repeated till t_{end}, and the so-called quantum trajectory is created. By repeating the same procedure, many quantum trajectories can be formed, and the average of all trajectories yield an approximate density matrix of the system [15]. The Hamiltonian in Eq. (6.20) can be easily analysed from the original Liouville equation (6.9). That is, in terms of this Hamiltonian, one can rewrite the master equation of the system as (see appendix C.2)

$$\frac{d}{dt}\;\rho = -\mathrm{i}\left(\hat{H}'\rho - \; \rho\;\hat{H}'^\dagger\right) + \hat{J}\;\rho \; , \tag{6.21}$$

where $\hat{J}$ is the quantum-jump superoperator given by Eq. (6.14). Further details, examples, and applications for the quantum-jump approach to a number of problems in quantum optics can be found in [91].

In the case when all decoherence channels result in an irreversible loss of population (i.e. the atomic and photonic relaxations take the system outside of $\hat{H}$ space), it is possible to propagate the statevector of the system $|\Psi(t)\rangle$ with Schrödinger equation using the non-Hermitian Hamiltonian in Eq. (6.20). This means that the previously discussed Monte-Carlo wave-function method, on the other hand, is not only useful for numerical simulations, but also can provide theoretical methods to describe the dissipative quantum systems (further examples of using the wave-function approach to investigate the quantum dynamics of a system can be found in [92] and [93]). We will see later on that details provided by the Liouvillian operator $\hat{\mathcal{L}}\ \rho$ will show that all decay channels, either in the iSWAP or the Fredkin gate, produce an irreversible loss of population from the basis states of the corresponding Hamiltonians, and all of these decays are outside the space of interest.

We now employ the wave-function treatment to describe the damped JCM in the previous section. In Eqs. (6.18, 6.19) it is noticeable that the state $|g,1\rangle$ decays via κ, and the damping in the state $|b,0\rangle$ is due to Γ. Both states decay to the uncoupled state $|a,0\rangle$. One then observes that quantum jump events in the damped system take place outside the space of the Hamiltonian (1.21). More precisely, both decays due to κ and Γ take the system outside of space $\hat{H}$ (in our case the space of $\hat{H}$ is $\mathbb{H} \equiv \{|a,1\rangle, |b,0\rangle\}$, and $|a,0\rangle \notin \mathbb{H}$). Applying the wave-function method modifies this Hamiltonian into the non-Hermitian Hamiltonian $\hat{H}'$

$$\hat{H}' = \hat{H} - \frac{\mathrm{i}\hbar}{2}\Gamma\hat{\sigma}_{ba}\hat{\sigma}_{ab} - \frac{\mathrm{i}\hbar}{2}\kappa\hat{a}^{\dagger}\hat{a}\ . \tag{6.22}$$

Under the initial conditions $c_{a,1}(0) = 1$ and $c_{b,0}(0) = 0$ and in the strong coupling regime, the time evolution of the resonant system in the presence of the atomic and photonic decays is

$$|\Psi(t)\rangle \mapsto e^{-\frac{1}{4}(\Gamma+\kappa)t}\Big[\cos(gt)\ |a,1\rangle - \mathrm{i}\sin(gt)\ |b,0\rangle\Big]\ . \tag{6.23}$$

In Fig. 6.1, it is observed that, in the situation we consider here, we can use either the master equation or the wave-function approach to study the damped JCM. In other words, these two methods, under certain conditions, are in good agreement.

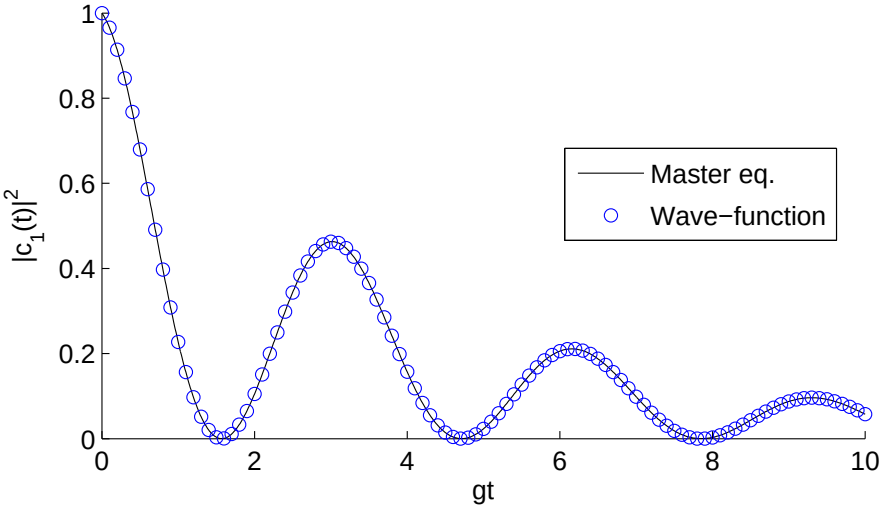

Figure 6.1: The probability of the ground state in the damped JCM in (1.3.1). Parameters: the coupling constant g, the atomic decay Γ, and the cavity field decay κ are given as $g = 4\Gamma$ and $\kappa = \Gamma$. The system is said to be in the resonance case (i.e. $\Delta = 0$).

6.3 Damping processes for the qubit states $|a\ 10\rangle$ and $|a\ 01\rangle$

We seek now to study the effect of the atomic and photonic decay rates on the qubit states $|a\ 10\rangle$ and $|a\ 01\rangle$, such qubit states in the iSWAP gate. We apply the previous approaches to obtain analytical and numerical solutions so that we are able to have a general understanding of the influence of decoherence on the iSWAP gate. The dissipation processes in the remaining qubit states, namely the qubit states $|a\ 11\rangle$ and $|a\ 00\rangle$, have been left to the last section in this chapter, where we use the master equation method alone.

6.3.1 Liouville's equation approach

Considering the iSWAP gate in chapter 4 we have found that for the initial state (either $|a\ 1010\rangle$ or $|a\ 0101\rangle$) the Hamiltonian $\hat{H}$ (4.4) acts in the space

$$\mathbb{H} \equiv \{|a\ 1010\rangle, |b\ 0010\rangle, |c\ 0110\rangle, |d\ 0100\rangle, |a\ 0101\rangle\}.$$

In the limit of $\bar{n} \mapsto 0$ and for the system in Fig. 4.2, the decay channel due to the atomic relaxation rate can be given by the actions of $\hat{J}^A$ and $\hat{S}^A$ as

$$\hat{J}^A\ \rho = \Gamma_{_{ba}}\ (\hat{\sigma}_{ab}\ \rho\ \hat{\sigma}_{ba}) + \Gamma_{_{bc}}\ (\hat{\sigma}_{cb}\ \rho\ \hat{\sigma}_{bc}) + \Gamma_{_{dc}}\ (\hat{\sigma}_{cd}\ \rho\ \hat{\sigma}_{dc}) + \Gamma_{_{da}}\ (\hat{\sigma}_{ad}\ \rho\ \hat{\sigma}_{da})\ , \quad (6.24)$$

and

$$\begin{aligned}\hat{S}^A\ \rho = \ &- \ [\frac{\Gamma_{ba}}{2}\ (\hat{\sigma}_{ba}\ \hat{\sigma}_{ab}\ \rho + \rho\ \hat{\sigma}_{ba}\ \hat{\sigma}_{ab}) + \frac{\Gamma_{bc}}{2}\ (\hat{\sigma}_{bc}\ \hat{\sigma}_{cb}\ \rho + \rho\ \hat{\sigma}_{bc}\ \hat{\sigma}_{cb}) \\ &+ \ \frac{\Gamma_{dc}}{2}\ (\hat{\sigma}_{dc}\ \hat{\sigma}_{cd}\ \rho + \rho\ \hat{\sigma}_{dc}\ \hat{\sigma}_{cd}) + \frac{\Gamma_{da}}{2}\ (\hat{\sigma}_{da}\ \hat{\sigma}_{ad}\ \rho + \rho\ \hat{\sigma}_{da}\ \hat{\sigma}_{ad})]\ ,\end{aligned} \tag{6.25}$$

where the atomic operators for our system can be defined as $\hat{\sigma}_{mn} \mapsto |m\rangle\langle n|$. Similarly, the photonic decay channels for the same system can be described by

$$\hat{J}^C\ \rho\ \ = \ \ \sum_{i=1}^{4}\ \kappa_i\ \ \hat{a}_i\ \rho\ \hat{a}_i^\dagger\ , \tag{6.26}$$

and

$$\hat{S}^C\ \rho = -\sum_{i=1}^{4}\frac{\kappa_i}{2}\ (\hat{a}_i^\dagger\ \hat{a}_i\ \rho + \rho\ \hat{a}_i^\dagger\ \hat{a}_i)\ , \tag{6.27}$$

with $a_{\rm i} \mapsto |0\rangle\langle 1|$ represents the annihilation operator for the mode i.
Now and after a few lines of algebra, the action of the superoperator $\hat{S}$ yields

$$\begin{aligned}(\hat{S}^A + \hat{S}^C)\ \rho = \ &- \ (\kappa_1 + \kappa_3)\ |c_1|^2\ |a\ 1010\rangle\langle a\ 1010| \\ &- \ (\Gamma_{ba} + \Gamma_{bc} + \kappa_3)\ |c_2|^2\ |b\ 0010\rangle\langle b\ 0010| \\ &- \ (\kappa_2 + \kappa_3)\ |c_3|^2\ |c\ 0110\rangle\langle c\ 0110| \\ &- \ (\Gamma_{dc} + \Gamma_{da} + \kappa_2)\ |c_4|^2\ |d\ 0100\rangle\langle d\ 0100| \\ &- \ (\kappa_2 + \kappa_4)\ |c_5|^2\ |a\ 0101\rangle\langle a\ 0101| \\ &- \ \ \ldots\ .\end{aligned} \tag{6.28}$$

These terms show the influence of the decay channels (either via Γ or κ) on the populations of the states in $\mathbb{H}$-space. Note that off-diagonal terms have not been listed in Eq. (6.28), but we must consider them so that the density matrix of the Liouville space can be numerically integrated.

The effect of the jump superoperator $\hat{J}$, on the other hand, shows that

$$\begin{aligned}(\hat{J}^A \ + \ \hat{J}^C)\ \rho = \ &+ \ (\ \Gamma_{ba}\ |a\ 0010\rangle\langle a\ 0010| + \Gamma_{bc}\ |c\ 0010\rangle\langle c\ 0010|\ )\ |c_2|^2 \\ &+ \ (\ \Gamma_{dc}\ |c\ 0100\rangle\langle c\ 0100| + \Gamma_{da}\ |a\ 0100\rangle\langle a\ 0100|\ )\ |c_4|^2 \\ &+ \ \kappa_1\ |c_1|^2\ |a\ 0010\rangle\langle a\ 0010| \\ &+ \ \kappa_2\ (\ |c_3|^2\ |c\ 0010\rangle\langle c\ 0010| + |c_4|^2\ |d\ 0000\rangle\langle d\ 0000| + |c_5|^2\ |a\ 0001\rangle\langle a\ 0001|\ ) \\ &+ \ \kappa_3\ (\ |c_1|^2\ |a\ 1000\rangle\langle a\ 1000| + |c_2|^2\ |b\ 0000\rangle\langle b\ 0000| + |c_3|^2\ |c\ 0100\rangle\langle c\ 0100|\ ) \\ &+ \ \kappa_4\ |c_5|^2\ |a\ 0100\rangle\langle a\ 0100| \\ &+ \ \ldots\ .\end{aligned} \tag{6.29}$$

Clearly, these terms inform us that the atomic and the photonic relaxations from the basis states decay outside the space $\mathbb{H}$; the quantum jump events in the system occur in a space outside of $\mathbb{H}$. These results are the starting point in order to analyse analytical solutions as will be seen soon.

Before moving to the second approach, we introduce below a formal derivation for the effective Hamiltonian $\hat{H}_{\text{eff}}$ in Shore's method where incoherence processes are now taken into account.

6.3.2 Decoherence treated with Shore's method

So far, in the preceding chapters the effective two-level Hamiltonian theory [46] has been employed to form the iSWAP and the Fredkin gates. At the absence of any dissipation process, the treatment was completely based on Hermitian Hamiltonians. In what follows, we reapply this theory, but in the case where the non-Hermitian Hamiltonian in Eq. (6.20) is to be considered. In Chapter 3, we have deduced the effective Hamiltonian $\hat{H}_{\text{eff}}$ for time-independent Hermitian Hamiltonians. Indeed, this theoretical method can be extended to include non-Hermitian Hamiltonians such as the Hamiltonian $\hat{H}'$. The main change is that the eigenvalues for the effective Hamiltonian $\hat{H}_{\text{eff}}$ in (3.6) are no longer real.

In [54], Shore hinted that the assumption of Hermitian Hamiltonians in his method is not essential, and that method can be used even with non-Hermitian Hamiltonians. In this section and for the rest of this chapter, I confirm that Shore's method is valid for both the Hermitian and non-Hermitian Hamiltonians. To this end, I combine the Hamiltonians describing the undamped systems in chapters 4, 5 with the non-Hermitian Hamiltonian (6.20) in the wave-function approach, and then investigate the time evolution for the effective N-level systems in the presence of atomic and photonic relaxations.

Now considering the time-independent Hamiltonian $\hat{H}'$ in (6.20), we have seen that the system spanned by the projector $\mathbb{P}$ evolves as

$$\mathbb{P}|\Psi(t)\rangle \;=\; \frac{1}{2\pi i}\int dz\; e^{-izt}\;\mathbb{P}\;\hat{G}(z)\;|\Psi(0)\rangle\;. \tag{6.30}$$

Following the traditional operator algebra in appendix C, $\mathbb{P}\;\hat{G}(z)$ can be given as

$$\mathbb{P}\;\hat{G}(z)=\mathbb{P}(z\hat{I}-\hat{H}')^{-1}=\mathbb{P}\{z\hat{I}-\mathbb{P}\hat{H}'\mathbb{P}-\mathbb{P}\hat{H}'\mathbb{Q}[z\hat{I}-\mathbb{Q}\hat{H}'\mathbb{Q}]^{-1}\mathbb{Q}\hat{H}'\mathbb{P}\}^{-1}\;, \tag{6.31}$$

where

$$\mathbb{P}\hat{H}'\mathbb{P} \mapsto \hat{H}_0 - \frac{\mathrm{i}}{2}\sum \eta\ \mathbb{P}L^\dagger L\mathbb{P}\ , \tag{6.32a}$$

$$\mathbb{P}\hat{H}'\mathbb{Q} \mapsto \hat{B}\ , \tag{6.32b}$$

$$\mathbb{Q}\hat{H}'\mathbb{Q} \mapsto \hat{A} - \frac{\mathrm{i}}{2}\sum \eta\ \mathbb{Q}L^\dagger L\mathbb{Q}\ , \tag{6.32c}$$

with $\hat{H}_0 = \mathbb{P}\hat{H}\mathbb{P}$, $\hat{B} = \mathbb{P}\hat{H}\mathbb{Q}$, and $\hat{A} = \mathbb{Q}\hat{H}\mathbb{Q}$. We are interested in the case when populations of the basis states in P- and Q-space decay irreversibly, and no reappearance of probabilities in these states occurs. In other words, no quantum jump events take place in the basis states of the spaces $\mathbb{P}$ and $\mathbb{Q}$. This is the case already demonstrated by the master equation approach in the previous section for the quantum system of the qubit states $|a\ 10\rangle$ and $|a\ 01\rangle$ (indeed this is the situation for all qubit states in the iSWAP and Fredkin gates). Since we set all highly detuned states to be spanned by $\mathbb{Q}$ and only study the dynamics of the systems spanned by $\mathbb{P}$, we do not expect $\mathbb{P}$ space to be affected by the dissipation processes in $\mathbb{Q}$. Consequently, the second term in Eq. (6.32c) can be safely omitted. Then in the presence of the dissipation processes in the space of P, one can redefine the effective Hamiltonian for the truncated system as

$$\hat{H}'_{\text{eff}} = \hat{H}_{\text{eff}} - \frac{\mathrm{i}}{2}\sum \eta\ \mathbb{P}\hat{L}^\dagger\hat{L}\mathbb{P}\ , \tag{6.33}$$

where $\hat{H}_{\text{eff}} = \hat{H}_0 - \hat{B}\ \hat{A}^{-1}\ \hat{B}^\dagger$. Therefore, the time evolution of the damped system $\mathbb{P}|\Psi(t)\rangle$ can be given by

$$\mathbb{P}|\Psi(t)\rangle = \ \exp\{-\frac{1}{2}\sum \eta\ \mathbb{P}\hat{L}^\dagger\hat{L}\mathbb{P}\ t\}\ \exp\{-\mathrm{i}\hat{H}_{\text{eff}}t\}\ |\Psi(0)\rangle\ . \tag{6.34}$$

6.3.3 Wave-function approach

We are now in the position to apply the wave-function treatment on the quantum system describing the qubit states $|a\ 10\rangle$ and $|a\ 01\rangle$. We have seen that the Hamiltonian $\hat{H}$ (4.4) describing these states acts in the basis $\{|a\ 1010\rangle, |b\ 0010\rangle, |c\ 0110\rangle, |d\ 0100\rangle, |a\ 0101\rangle\}$. By recalling the Hamiltonian (6.20), then the "effective" Hamiltonian $\hat{H}'$ of the damped system in this basis can be written, in the matrix form, as

$$\hat{H}' = \begin{pmatrix} -\mathrm{i}\kappa & g_1 & 0 & 0 & 0 \\ g_1 & \Delta_1 - \mathrm{i}(\frac{2\Gamma+\kappa}{2}) & g_2 & 0 & 0 \\ 0 & g_2 & \Delta_2 - \mathrm{i}\kappa & g_3 & 0 \\ 0 & 0 & g_3 & \Delta_3 - \mathrm{i}(\frac{2\Gamma+\kappa}{2}) & g_4 \\ 0 & 0 & 0 & g_4 & \Delta_4 - \mathrm{i}\kappa \end{pmatrix}\ . \tag{6.35}$$

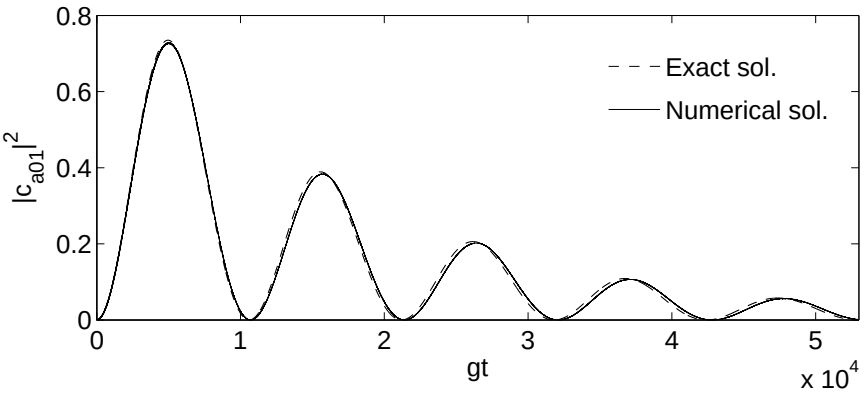

Figure 6.2: The probability $|c_{a\ 01}|^2$ of the state $|a\ 01\rangle$ in the model (10001) as a function of time. We compare the exact result in Eq. (6.37) with the simulation of Liouville equation (6.9). Parameters: all coupling strengths g_i $(i = 1, 2, 3, 4)$ are set to g, and all detunings Δ_j $(j = 1, 2, 3)$ are set to $\Delta = 15g$. The detuning Δ_4 is given by the resonance condition (4.8). The relaxation rate κ is given as $\kappa = 0.1\ g_{\rm eff}$.

Note that for simplicity we assume that all spontaneous decay rates $\Gamma_{ba}, \Gamma_{bc}, \Gamma_{dc}$ and Γ_{da} are set to Γ, and similarly the photonic field rates $\kappa_1, \kappa_2, \kappa_3$ and κ_4 all are set to κ. Since the iSWAP gate has been realized by the models (10001) and (11001), in the subsequent sections we check the sensitivity of these models to the decoherence process.

6.3.4 The model (10001)

We seek now to study the effect of the atomic and photonic relaxations in a specific model such as the model (10001). Recalling the effective Hamiltonian $\hat{H}'_{\rm eff} = \hat{H}_{\rm eff} - \frac{\rm i}{2} \sum \eta\ \mathbb{P} L^\dagger L \mathbb{P}$, the first term $\hat{H}_{\rm eff}$ represents the effective Hamiltonian for the two-level behaviour discussed early in Sec. 4.3. The second term, on the other hand, addresses the decay of the energy in $\mathbb{P}$ space, where $\mathbb{P}$-space includes the states $|a\ 1010\rangle$ and $|a\ 0101\rangle$. Consequently, it is straightforward to write the effective Hamiltonian $\hat{H}'_{\rm eff}$ for the damped model (10001) as

$$\hat{H}'_{\rm eff} = \begin{pmatrix} -{\rm i}\kappa & g_{\rm eff} \\ g_{\rm eff} & \Delta_{\rm eff} - {\rm i}\kappa \end{pmatrix} , \tag{6.36}$$

where $g_{\rm eff}$ and $\Delta_{\rm eff}$ can be given by Eqs. (4.7, 4.8). The equations of motion describing the time evolution for the state $|\Psi(t)\rangle = c_{a10}(t)|a\ 10\rangle + c_{a01}(t)|a\ 01\rangle$ can be simply given by applying Schrödinger's amplitude equation. For the initial conditions $c_{a10}(0) = 1$ and $c_{a01}(0) = 0$ and in the limit $g_{\rm eff} >> \kappa$, one finds

$$c_{a01} \quad = \quad -{\rm i}\frac{g_{\rm eff}}{\tilde{g}}\ \ e^{-\kappa t}\ \sin(\tilde{g}t)\ e^{-{\rm i}\Delta_{\rm eff}t/2}\ , \tag{6.37}$$

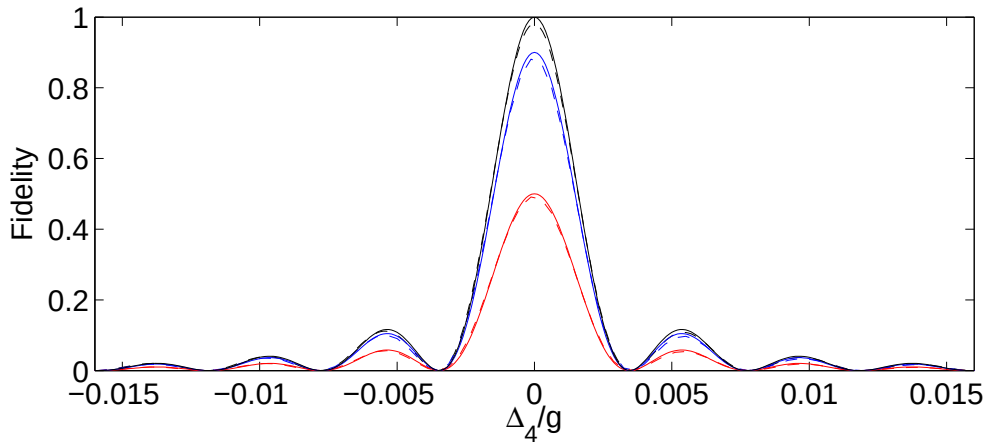

Figure 6.3: Fidelity of the damped configuration (10001). Solid and dashed lines represent the theoretical and numerical solutions, respectively. Parameters are same as those ones in Fig. 6.2, except $\Delta = 10g$. The black, blue, and red lines respectively show the system fidelity $F \sim (1, 0.9, 0.5)F_0$ (where the numerically maximum fidelity $F_0 \sim 0.9812$). The three curves corresponding to the values of photonic decays $\kappa \sim (0, 0.033, 0.24)g_{\text{eff}}$ (when no atomic decay rate has been considered).

where $\tilde{g} = \sqrt{g_{\text{eff}}^2 + (\Delta_{\text{eff}}/2)^2}$. The norm of the system shows that it decays with the rate (2κ).

Figure 6.2 illustrates good agreement between the simulation solutions provided by the master equation approach and the analytical solutions predicted by the theory of the effectively damped Hamiltonian. In this figure, the numerical solutions consider all possible cavity field relaxations in the corresponding Liouville's space. In the exact solution, in contrast, we only take into account the cavity decays by the states spanned by the projector $\mathbb{P}$, which include the cavity field rates $\kappa_{1,3}$ by the state $|a\ 1010\rangle$ and $\kappa_{2,4}$ by the state $|a\ 0101\rangle$.

The (10001) sensitivity to the atomic decay Γ and to the cavity field rate κ can be further investigated. In Fig. 6.3, the theoretical and numerical solutions have been used to measure the fidelity with different values of the cavity decay rates. The corresponding Γ values (i.e. for $F \sim (1, 0.9, 0.5)F_0$) are $\Gamma \sim (0, 3, 23)g_{\text{eff}}$ (where $\kappa = 0$). Note that to find the previous values of Γ we need to work in the weak coupling regime (i.e. $\Gamma > g_{\text{eff}}$), therefore, we use the master equation to determine them. As expected, one then can observe that the model (10001) is much more sensitive to the photonic relaxations.

6.3.5 The model (11001)

The iSWAP gate can be performed by the model (11001), too. We now, thus, study the influence of Γ and κ on $|a\ 10\rangle$ and $|a\ 01\rangle$ by considering this model. Following the arguments in the previous model (10001), we can easily analyse the equations of motion for this model. That is, by introducing the effective Hamiltonian $\hat{H}'_{\rm eff}$ for the damped model (11001) in Schrödinger's amplitudes equation, one finds (at the resonance case i.e. the effective detunings in Eq. (4.18) $\Delta^{(1)} = \Delta^{(2)} = 0$) that

$$\frac{d}{dt}\begin{pmatrix} c_{a1010} \\ c_{b0010} \\ c_{a0101} \end{pmatrix} = \text{-i}\begin{pmatrix} -\text{i}\kappa & g^{(1)} & 0 \\ g^{(1)} & -\text{i}(\frac{2\Gamma+\kappa}{2}) & g^{(2)} \\ 0 & g^{(2)} & -\text{i}\kappa \end{pmatrix}\begin{pmatrix} c_{a1010} \\ c_{b0010} \\ c_{a0101} \end{pmatrix} . \tag{6.38}$$

The eigenvalues for this effective Hamiltonian can be determined, under the condition $4\bar{g} \geq (\kappa - 2\Gamma)$, as

$$\lambda_1 = -\kappa\ , \quad \lambda_{2,3} = -(\frac{3\kappa + 2\Gamma}{4}) \pm \text{i}\ \lambda\ , \tag{6.39}$$

where $\lambda = \{\bar{g}^2 - \frac{1}{16}(\kappa - 2\Gamma)^2\}^{1/2}$, $\bar{g} = \sqrt{(g^2_{(1)} + g^2_{(2)})}$, and $g_{(1)}$ and $g_{(2)}$ are the effective couplings given by Eq. (4.17). For the initial conditions $c_{a10}(0) = 1$, $c_{b0010}(0) = 0$, and $c_{a01}(0) = 0$, the time evolution of the state $|a\ 01\rangle$ can be expressed as

$$c_{a01} = \frac{g^{(1)}g^{(2)}}{\bar{g}^2}\ \exp(-\kappa\ t)\ \{-1 + \left[\cos(\lambda t) - (\frac{\kappa - 2\Gamma}{4\lambda})\ \sin(\lambda t)\right]\ \exp(\frac{\kappa - 2\Gamma}{4}\ t)\}\ . \tag{6.40}$$

The agreement between this expression and the numerical integration of the full system density matrix has been illustrated by Fig. 6.4.

Figure 6.5 demonstrates the effect of the atomic and cavity field decays on the fidelity of the system. The sensitivity of the model (11001) is higher to the photonic decay rates than to Γ. Due to the presence of the upper state $|b\ 0010\rangle$ in the model (11001) and unlike the model (10001), the model (11001) becomes more sensitive to the atomic relaxations Γ. We have seen that the speed of the iSWAP gate has been significantly improved when applying the model (11001) (see Figs. 4.3, 4.5). As a result, the impact of the dissipation processes in (11001) has been reduced, compared to the model (10001). For instance, at the absence of any atomic decay, Fig. 6.3 demonstrates that the fidelity in the model (10001) may fall to one-half of its maximum value with $\kappa/g \mapsto \frac{1}{4} \times 10^{-3}$, whereas at the same value of the photonic relaxation rate the model (11001) loses only $\sim 10\%$ of its fidelity maximum (see Fig. 6.5). This is a remarkable result since Eqs. (6.36, 6.38) tell us that the model (11001) produces more decay channels than the model (10001).

In table 6.1, we list some numerical results for all configurations that successfully map the

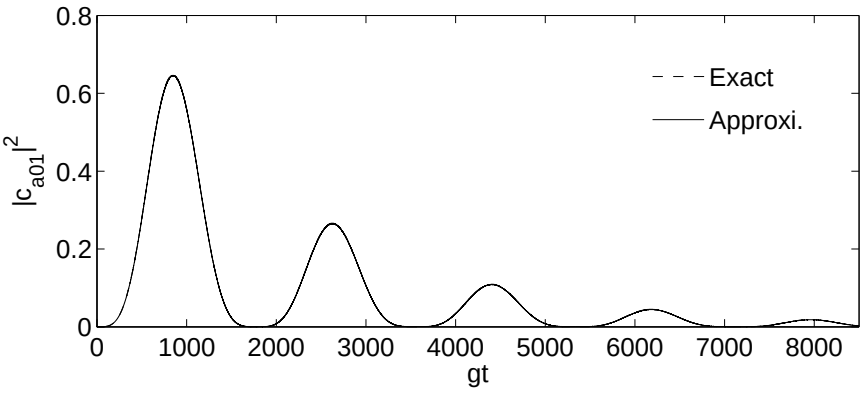

Figure 6.4: The probability $|c_{a\ 01}|^2$ of the state $|a\ 01\rangle$ in the model (11001) as a function of time. We compare the exact result provided by Eq. (6.40) with the simulation of Liouville's equation. Parameters: All coupling strengths g_i $(i = 2, 3, 4)$ are set to g, and all detunings Δ_j $(j = 2, 3)$ are set to $\Delta = 20g$. The detunings $\Delta_{1,4}$ are given by the resonance conditions (4.18), and the coupling g_1 is determined in (4.17) as $g_1 \approx \frac{g_2 g_3 g_4}{\Delta_2 \Delta_3}$. The relaxation rates κ and Γ are given as $\kappa = 0.1\bar{g}/\sqrt{2}$, and $\kappa = 2\Gamma$ (so that there is no decay in Rabi frequency).

qubit state $|a\ 10\rangle$ to $|a\ 01\rangle$. It is seen that the model (10101) is better in everything, i.e. it is faster and less sensitive to Γ, κ, and the changes in Δ_4. Unfortunately, this model fails to form the iSWAP gate (see Sec. 4.8.2). The entirely resonant model (11111), or equivalently the spin-J model (with $J = 2$), swaps the previous qubit states at $t_{int} \mapsto \pi$. This model is very insensitive to the dissipative processes, compared to other models. For example, its fidelity falls to 0.90 at the relaxation decay rates $\Gamma/g \mapsto 0.05$ or $\kappa/g \mapsto 0.02$, and it loses 0.50 of the fidelity with $\Gamma/g \mapsto 0.4$ or $\kappa/g \mapsto 0.15$.

6.4 Dissipation processes for the qubit states $|a\ 101\rangle$ and $|a\ 110\rangle$

6.4.1 Master equation method

By following the same arguments in previous sections, we can study the effect of the atomic and cavity decays on the qubit states $|a\ 101\rangle$ and $|a\ 110\rangle$, as two qubit states in the Fredkin gate. We have seen that with the absence of decays, the system can be

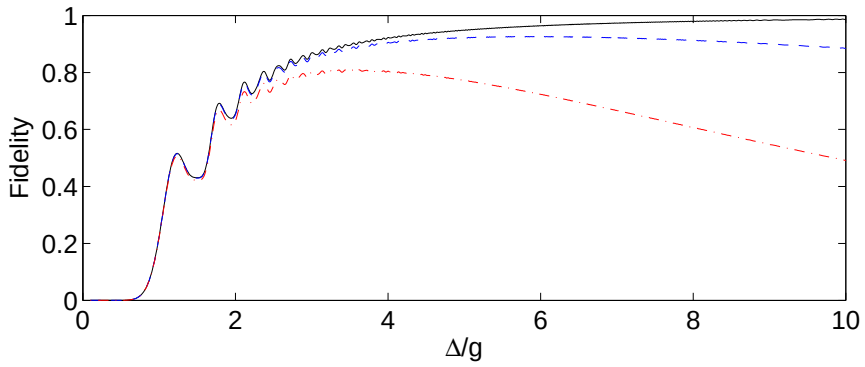

Figure 6.5: Fidelity for the model (11001) in the presence of the dissipation process. Parameters can be found in Fig. 6.4. The black, blue, and red lines respectively represent the system fidelity (where at $\Delta = 10g$) $F \sim (1, 0.9, 0.5)F_0$ with a maximum fidelity $F_0 \sim 0.9862$. The three curves corresponding to the values of the atomic decay rates $\Gamma \sim (0, 0.1, 0.75)\bar{g}/\sqrt{2}$ with $\kappa = 0$, or to the values of photonic decays $\kappa \sim (0, 0.025, 0.185)\bar{g}/\sqrt{2}$ when there is no atomic decay rate.

described completely by the wavevector $|\Psi\rangle$ in Eq. (5.3) where

$$\begin{aligned} |\Psi\rangle &= c_1\,|a\ 10,01,10\rangle + c_2\,|b\ 00,01,10\rangle + c_3\,|c\ 00,11,10\rangle \\ &+ c_4\,|d\ 00,10,10\rangle + c_5\,|e\ 10,10,10\rangle + c_6\,|f\ 10,10,00\rangle \\ &+ c_7\,|a\ 10,10,01\rangle + c_8\,|b\ 00,10,01\rangle + c_9\,|c\ 00,20,01\rangle\ . \end{aligned}$$

Recalling Liouville's operator in Eq. (6.10), one can show that the spontaneous decay rate can be described by the action of the superoperators $(\hat{J}^A + \hat{S}^A)\rho$ as

$$\begin{aligned} \hat{J}^A\,\rho &= (\Gamma_{ba} + \Gamma'_{ba})\,(\hat{\sigma}_{ab}\,\rho\,\hat{\sigma}_{ba}) + (\Gamma_{bc} + \Gamma'_{bc})\,(\hat{\sigma}_{cb}\,\rho\,\hat{\sigma}_{bc}) \\ &+ \Gamma_{dc}\,(\hat{\sigma}_{cd}\,\rho\,\hat{\sigma}_{dc}) + \Gamma_{de}\,(\hat{\sigma}_{ed}\,\rho\,\hat{\sigma}_{de}) \\ &+ \Gamma_{fe}\,(\hat{\sigma}_{ef}\,\rho\,\hat{\sigma}_{fe}) + \Gamma_{fa}\,(\hat{\sigma}_{af}\,\rho\,\hat{\sigma}_{fa})\ , \end{aligned} \tag{6.41}$$

and for the superoperator $\hat{S}^A$

$$\begin{aligned} \hat{S}^A\,\rho = &- [\frac{(\Gamma_{ba} + \Gamma'_{ba})}{2}\,(\hat{\sigma}_{ba}\,\hat{\sigma}_{ab}\,\rho + \rho\,\hat{\sigma}_{ba}\,\hat{\sigma}_{ab}) + \frac{(\Gamma_{bc} + \Gamma'_{bc})}{2}\,(\hat{\sigma}_{bc}\,\hat{\sigma}_{cb}\,\rho + \rho\,\hat{\sigma}_{bc}\,\hat{\sigma}_{cb}) \\ &+ \frac{\Gamma_{dc}}{2}\,(\hat{\sigma}_{dc}\,\hat{\sigma}_{cd}\,\rho + \rho\,\hat{\sigma}_{dc}\,\hat{\sigma}_{cd}) + \frac{\Gamma_{de}}{2}\,(\hat{\sigma}_{de}\,\hat{\sigma}_{ed}\,\rho + \rho\,\hat{\sigma}_{de}\,\hat{\sigma}_{ed}) \\ &+ \frac{\Gamma_{fe}}{2}\,(\hat{\sigma}_{fe}\,\hat{\sigma}_{ef}\,\rho + \rho\,\hat{\sigma}_{fe}\,\hat{\sigma}_{ef}) + \frac{\Gamma_{fa}}{2}\,(\hat{\sigma}_{fa}\,\hat{\sigma}_{af}\,\rho + \rho\,\hat{\sigma}_{fa}\,\hat{\sigma}_{af})\ . \end{aligned} \tag{6.42}$$

Once again, the atomic operators in the previous equations can be defined as $\hat{\sigma}_{mn} \mapsto |m\rangle\langle n|$, so as an example $\hat{\sigma}_{ab} \mapsto |a\rangle\langle b|$. Note that Γ'_{ba} and Γ'_{bc} represent the atomic decays via the over-shot state $|b\ 00,10,01\rangle$. Likewise, the photonic decay for the same system

System Model	Three-level (10101)	Four-level (11101)	(11011)
Interaction time (gt_{int})	33.6	41.7	47.12
Atomic-decay ($\Gamma \times 10^{-3}$)	$\Gamma_1 \mapsto 276.5$ $\Gamma_2 \mapsto 2195$	$\Gamma_1 \mapsto 6.8$ $\Gamma_2 \mapsto 54.5$	$\Gamma_1 \mapsto 3.01$ $\Gamma_2 \mapsto 20.87$
Photonic-decay ($\kappa \times 10^{-3}$)	$\kappa_1 \mapsto 1.8$ $\kappa_2 \mapsto 12.5$	$\kappa_1 \mapsto 1.6$ $\kappa_2 \mapsto 10.8$	$\kappa_1 \mapsto 1.4$ $\kappa_2 \mapsto 9.4$

Table 6.1: Numerical results showing the influence of the decoherence processes on the models swapping the the qubit states $|a\ 10\rangle \leftrightarrow |a\ 01\rangle$. The decay rate values (in units of g) for 90% and 50% fidelity are provided (with $\Delta/g = 15$).

can be described by

$$(\hat{J}^C + \hat{S}^C)\ \rho \ = \ \sum_{i\neq 4}^{6} \kappa_i \ \hat{a}_i\ \rho\ \hat{a}_i^\dagger \ - \sum_{i\neq 4}^{6} \frac{\kappa_i}{2}\ (\hat{a}_i^\dagger\ \hat{a}_i\ \rho + \rho\ \hat{a}_i^\dagger\ \hat{a}_i)\ . \tag{6.43}$$

Even though Liouville's space seems to be quite large in the damped system, we are still able to use the master equation in order to carry out some numerical simulations as shown in the following sections.

The population loss of the basis states in $|\Psi\rangle$ can be addressed by the previous Liouvillian operator $\hat{\mathcal{L}}\rho = (\hat{J}^A + \hat{S}^A + \hat{J}^C + \hat{S}^C)\rho$. Since the model (1001001) was found the only configuration that is able to realize the Fredkin gate (see Sec. 5.8), we may restrict our discussion on the dampings in this model. We have seen that the space of this model contains the states $\{|a\ 10, 01, 10\rangle,\ |d\ 00, 10, 10\rangle,\ |a\ 10, 10, 01\rangle\}$. It is easy to find that the decay of the upper state $|d\ 00, 10, 10\rangle$ is due to either the atomic relaxation to $|c\ 00, 10, 10\rangle$ and $|e\ 00, 10, 10\rangle$, or the cavity field relaxation to $|d\ 00, 00, 10\rangle$ and $|d\ 00, 10, 00\rangle$. The ground state $|a\ 10, 01, 10\rangle$, in turn, decays via κ to $|a\ 00, 01, 10\rangle$, $|a\ 10, 00, 10\rangle$, and $|a\ 10, 01, 00\rangle$; the damping in the ground state $|a\ 10, 10, 01\rangle$ are due to the photonic decay to $|a\ 00, 10, 01\rangle$, $|a\ 10, 00, 01\rangle$, and $|a\ 10, 10, 00\rangle$. It is clear that all states in the model (1001001) decay outside of its space.

6.4.2 The amplitude equations approach

Based on the wave-function treatment, we now study the impacts of decoherence on the system of the qubit states $|a\ 101\rangle$ and $|a\ 110\rangle$. The Hamiltonian describing the damped system (with the help of Eqs. (5.4, 6.20)) can be expressed as

$$\begin{aligned}
\hat{H}' &= -\mathrm{i}(3\kappa/2)\ \hat{\sigma}_{aa} + g_1\ (\hat{\sigma}_{ab} + \hat{\sigma}_{ba}) \\
&+ [\Delta_1 - \mathrm{i}(\kappa + \Gamma)]\ \hat{\sigma}_{bb} + g_2\ (\hat{\sigma}_{bc} + \hat{\sigma}_{cb}) \\
&+ [\Delta_2 - \mathrm{i}(3\kappa/2)]\ \hat{\sigma}_{cc} + g_3\ (\hat{\sigma}_{cd} + \hat{\sigma}_{dc}) \\
&+ [\Delta_3 - \mathrm{i}(\kappa + \Gamma)]\ \hat{\sigma}_{dd} + g_1\ (\hat{\sigma}_{de} + \hat{\sigma}_{ed}) \\
&+ [\Delta_4 - \mathrm{i}(3\kappa/2)]\ \hat{\sigma}_{ee} + g_5\ (\hat{\sigma}_{ef} + \hat{\sigma}_{fe}) \\
&+ [\Delta_5 - \mathrm{i}(\kappa + \Gamma)]\ \hat{\sigma}_{ff} + g_6\ (\hat{\sigma}_{fa'} + \hat{\sigma}_{a'f}) \\
&+ [\Delta_6 - \mathrm{i}(3\kappa/2)]\ \hat{\sigma}_{a'a'} + g_1\ (\hat{\sigma}_{a'b'} + \hat{\sigma}_{b'a'}) \\
&+ [(\Delta_1 + \Delta_6) - \mathrm{i}(\kappa + \Gamma)]\ \hat{\sigma}_{b'b'} + \sqrt{2} g_2\ (\hat{\sigma}_{b'c'} + \hat{\sigma}_{c'b'}) \\
&+ [(\Delta_2 + \Delta_6) - \mathrm{i}(3\kappa/2)\kappa]\ \hat{\sigma}_{c'c'}\ , \qquad (6.44)
\end{aligned}$$

where the atomic operators in this Hamiltonian can be defined by using

$$\begin{aligned}
\hat{\sigma}_{ab} &\equiv |a\ 10,01,10\rangle\langle b\ 00,01,10|\ , \quad \hat{\sigma}_{bc} \equiv |b\ 00,01,10\rangle\langle c\ 00,11,10|\ , \\
\hat{\sigma}_{cd} &\equiv |c\ 00,11,10\rangle\langle d\ 00,10,10|\ , \quad \hat{\sigma}_{de} \equiv |d\ 00,10,10\rangle\langle e\ 10,10,10|\ , \\
\hat{\sigma}_{ef} &\equiv |e\ 10,10,10\rangle\langle f\ 10,10,00|\ , \quad \hat{\sigma}_{fa'} \equiv |f\ 10,10,00\rangle\langle a\ 10,10,01|\ , \\
\hat{\sigma}_{a'b'} &\equiv |a\ 10,10,01\rangle\langle b\ 00,10,01|\ , \quad \hat{\sigma}_{b'c'} \equiv |b\ 00,10,01\rangle\langle c\ 00,20,01|\ . \qquad (6.45)
\end{aligned}$$

Once again, we assume all photonic decays $\kappa_i \mapsto \kappa$ (with $i = 1, 2, 3, 5, 6$), and all spontaneous emission rates are set to Γ.

We discuss below the dissipation processes in the model (1001001), as it is found in part II that this model is able to realize the Fredkin gate.

6.4.3 The model (1001001)

As mentioned in Sec. 6.4.1, there is no quantum jump event in the space of (1001001), say $\mathbb{P}$, and then we can propagate the wavefunction of the model, $|\Psi(t)\rangle = c_a(t)|a\ 10,01,10\rangle + c_d(t)|d\ 00,10,10\rangle + c_{a'}(t)|a\ 10,10,01\rangle$, with Schrödinger's equation using the Hamiltonian $\hat{H}'_{\rm eff}$ below. At the resonance case (that is, in Eqs. (5.16, 5.17) we set $\Delta^{(1)} = \Delta^{(2)} = 0$),

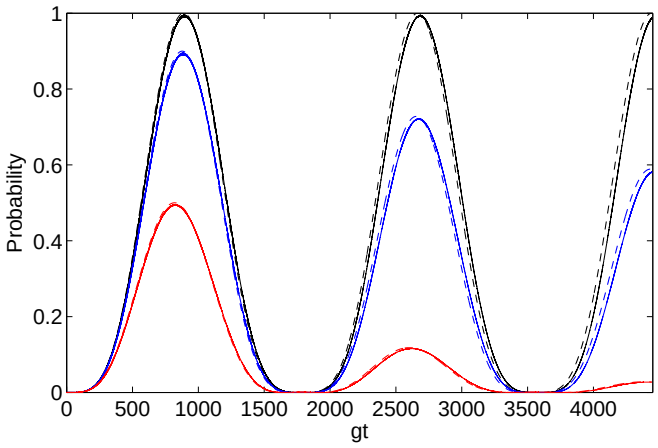

Figure 6.6: The probability of the qubit state $|a\ 110\rangle$ in the model (1001001) with non-vanishing photonic decay. Solid and dashed curves show the numerical and theoretical solutions, respectively. The coupling constants g_i $(i = 1, 2, 3, 5, 6)$ are all set to g, and the detunings $\Delta_{1,2,4,5}$ are given as $\Delta = 20g$. The effective couplings of the truncated system $g^{(1)}$ and $g^{(2)}$ are given by Eq. (5.15), and the detunings Δ_3 and Δ_6 are defined by the resonance conditions in Eqs. (5.16, 5.17). The black, blue, and red lines respectively represent (at the interaction time gt_{int}) the system probability $P \sim (100, 90, 50)\%P_0$ with a maximum probability $P_0 \sim 0.9950$. The three curves corresponding to the values of the photonic decay rates $\kappa \sim (0,\ 0.0174,\ 0.1186)\bar{g}/\sqrt{2}$ with $\Gamma \mapsto 0$.

one finds

$$\frac{d}{dt}\begin{pmatrix} c_a \\ c_d \\ c_{a'} \end{pmatrix} = \text{-i}\begin{pmatrix} -\text{i}3\kappa/2 & g^{(1)} & 0 \\ g^{(1)} & -\text{i}(\Gamma+\kappa) & g^{(2)} \\ 0 & g^{(2)} & -\text{i}3\kappa/2 \end{pmatrix}\begin{pmatrix} c_a \\ c_d \\ c_{a'} \end{pmatrix} . \tag{6.46}$$

Considering the strong coupling regime, the eigenvalues of $\hat{H}'_{\text{eff}}$ can be given as

$$\lambda_1 = -3\kappa/2\ , \quad \lambda_{2,3} = -(\frac{5\kappa+2\Gamma}{4}) \pm \text{i}\lambda\ , \tag{6.47}$$

where $\lambda = \left(\bar{g}^2 - \frac{1}{16}(\kappa - 2\Gamma)^2\right)^{1/2}$, $\bar{g} = \sqrt{(g^2_{(1)} + g^2_{(2)})}$, and $g_{(1)}$ and $g_{(2)}$ are given by Eq. (5.15). The time evolution of the coefficient c_{a110}, with the initial conditions $c_{a101}(t = 0) = 1$, $c_d(0) = 0$, and $c_{a110}(0) = 0$, reads

$$c_{a110} = \frac{g^{(1)}g^{(2)}}{\bar{g}^2}\ \exp(-\frac{3\kappa}{2}\ t)\ \{-1 + \left[\cos(\lambda t) - (\frac{\kappa-2\Gamma}{4\lambda})\ \sin(\lambda t)\right]\ \exp(\frac{\kappa-2\Gamma}{4}\ t)\} \tag{6.48}$$

The system sensitivity to the decay channels via κ and Γ can be illustrated by Figs. 6.6, 6.7. They confirm that the model (1001001) shows a higher response to the photonic decay than to the atomic decay.

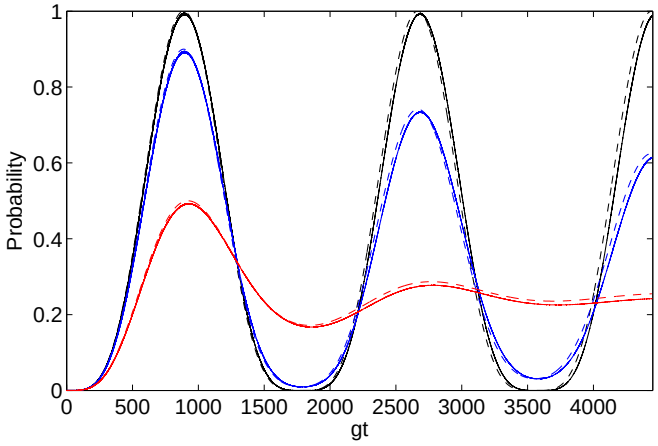

Figure 6.7: The probability of the qubit state $|a\ 110\rangle$ in the model (1001001) with non-vanishing atomic decay. The solid and dashed lines represent the numerical and analytical results, respectively. Parameters are the same as in Fig. 6.6. The black, blue and red lines respectively show (at the interaction time gt_{int}) the system probability $P \sim (100, 90, 50)\%P_0$ with a maximum probability $P_0 \sim 0.9950$. The three curves corresponding to the values of the atomic decay rates $\Gamma \sim (0,\ 0.0976,\ 0.764)\bar{g}/\sqrt{2}$ with $\kappa \mapsto 0$.

In the preceding chapters, we have observed that the model (11001) and the configuration (1001001) may have the same interaction time (see Figs. 4.5, 5.3). Under the condition $g^{(1)} = g^{(2)}$, it is easy then to prove that

$$|c_{a110}|^2 = \exp(-\kappa\ t)\ |c_{a01}|^2\ . \tag{6.49}$$

This equation informs us that (1001001) is more sensitive to the cavity decay rate κ than (11001). More generally, these models tell us that the Fredkin gate is more sensitive to the photonic relaxation κ than the iSWAP gate. Indeed, from Eqs. (6.40, 6.48) it is clear that the photonic decay rates $\kappa_{\rm F}$ in (1001001) and $\kappa_{\rm I}$ (11001) are related to each other by $3\kappa_{\rm F} = 2\kappa_{\rm I}$. This result is expected since the iSWAP gate is a two-qubit operation and the Fredkin gate is a three-qubit gate, having one more qubit with a single excitation. For a vanishing κ, on the other hand, it is shown that both models (or equivalently gates) have the same degree of sensitivity to the atomic decay rate Γ, i.e. for any value of $\Gamma \mapsto |c_{a110}|^2 = |c_{a01}|^2$. As a final line, table 6.2 shows the impacts of the dissipative processes on the models (10001) and (11001) swapping $|a\ 10\rangle$ and $|a\ 01\rangle$, and on the model (1001001) interchanging $|a\ 101\rangle$ and $|a\ 110\rangle$.

Logic gate	The iSWAP gate		The Fredkin gate
	(10001)	(11001)	(1001001)
Interaction time (gt_{int})	5314.8	500.2	499.8
Atomic-decay ($\Gamma \times 10^{-3}$)	$\Gamma_1 \mapsto$2.2 $\Gamma_2 \mapsto$15.5	$\Gamma_1 \mapsto$0.42 $\Gamma_2 \mapsto$3.25	$\Gamma_1 \mapsto$0.3 $\Gamma_2 \mapsto$3.0
Photonic-decay ($\kappa \times 10^{-3}$)	$\kappa_1 \mapsto$0.01 $\kappa_2 \mapsto$0.07	$\kappa_1 \mapsto$0.12 $\kappa_2 \mapsto$0.8	$\kappa_1 \mapsto$0.075 $\kappa_2 \mapsto$0.500

Table 6.2: A comparison between the damped models (10001), (11001), and (1001001). The detuning Δ is set to $15g$. The corresponding values of decay for 90% and 50% fidelity have been given by Γ_i and κ_i with $i = 1, 2$, respectively. (the decay rates are in units of g)

6.5 Decoherence in all photonic qubits

Previously, we have investigated the influence of the dissipative mechanisms on the qubit states $|a\ 10\rangle$ and $|a\ 01\rangle$ in the iSWAP gate, and the qubit states $|a\ 101\rangle$ and $|a\ 110\rangle$ in the Fredkin gate. Because of the presence of excitations in all qubit states in our logic gates (see tables 4.1, 5.1), all these qubits have suffered from decoherence process.

To study the effects of population decays on the remaining qubit states in either the iSWAP or the Fredkin gate, we simply follow the same probabilistic laws in previous sections in order to find the corresponding Liouvillian operator $\mathcal{L}\rho$. Note that the values of the coupling constants and the detunings always follow the models (10001) or (11001) in the iSWAP gate, and the model (1001001) in the Fredkin gate.

We are now in the position to subject all qubit states in the iSWAP and Fredkin gates to real parameters. That is, we use experimental values for the coupling strength g, the atomic decay Γ, and the photonic decay rate κ so that the performance of the dual-rail CQED gates can be practically tested. Considering the microwave cavity-QED experiment in [6], highly excited Rydberg atoms (typically ^{85}Rb) with a radiative time $\tau_{rad} \sim 30$ ms have been used to interact with a superconducting cavity with $Q \mapsto 4 \times 10^{10}$. The photon lifetime inside the cavity is in order $\tau_{ph} \sim 130$ ms, and the coupling strength is around $g/2\pi \sim 50$ kHz. Setting $\Delta = 10$ g, this corresponds to cavity-atom interaction time $t_{int} \mapsto 5$ ms in the configuration (10001), and $t_{int} \mapsto \frac{1}{\sqrt{2}}$ ms in the configurations (11001)

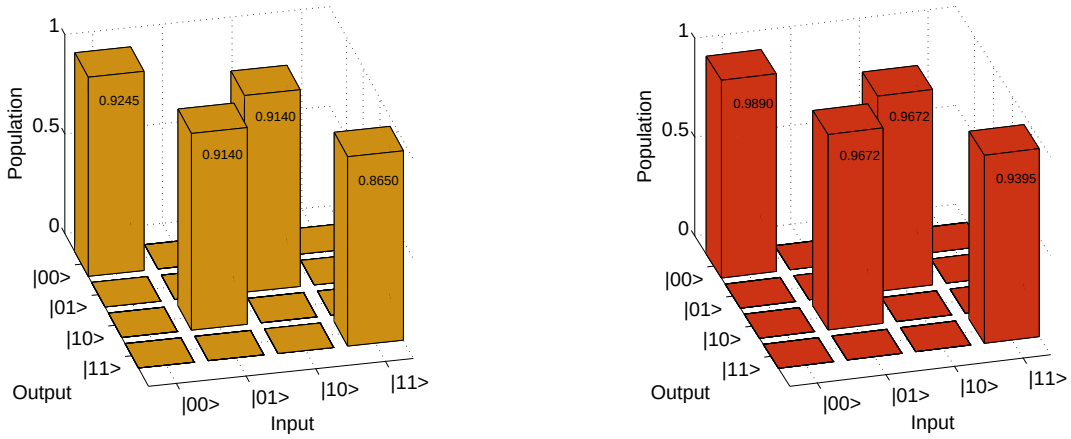

(a) (b)

Figure 6.8: Truth table of the numerically simulated iSWAP gate with $\Delta = 10\ g$ in the presence of decoherence processes. (a) in the configuration (10001). (b) in the model (11001). Parameters: the coupling constant is approximate $g/2\pi = 50$ kHz, $\Gamma/g \sim 10^{-4}$, and $\kappa/g \sim 2.5 \times 10^{-5}$.

and (1001001). The quantity τ_{ph}/t_{int} shows that the last two configurations are much better for QIP applications with the present cavity QED techniques. Figs. 6.8, 6.9 show the population loss in the iSWAP and the Fredkin gates when considering the previous parameters of g, Γ, and κ.

6.6 Summary

Based on either the master equation or the wave-function approach, the influence of dissipative mechanisms on the dual-rail cavity-QED operations, namely the iSWAP and the Fredkin gates, have been investigated.

Given the iSWAP gate to be realized by the models (10001) and (11001), this gate in the model (10001) is more sensitive to the photonic decay rates. This fact is reasonable as the gate in this model is much slower compared to the speed of the model (11001). The gate sensitivity to the atomic relaxation, on the other hand, is less in the model (10001) than in the model (11001), as a result of the presence of the excited state $|b\rangle$ in (11001).

Although the Fredkin gate by the model (1001001) and the iSWAP gate in the configuration (11001) both possess the same interaction time, the same degree of sensitivity to the atomic relaxation Γ, and the same configuration (i.e. they behave as a three-level system), the population loss in the Fredkin gate due to the photonic relaxation is higher. This is simply because the Fredkin gate is a three-qubit gate, having one more qubit with a single

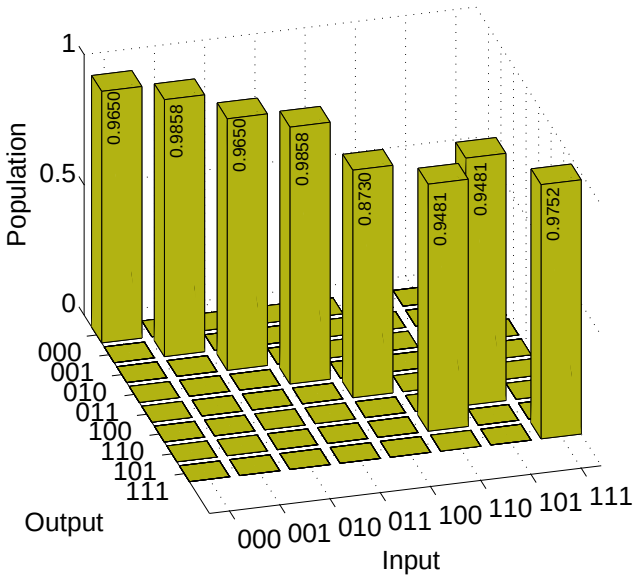

Figure 6.9: Truth table of the numerically simulated Fredkin gate in the model (1001001) with $\Delta = 10\ g$. Parameters: the coupling constant $g/2\pi \sim 50$ kHz, $\Gamma/g \sim 10^{-4}$, and $\kappa/g \sim 2.5 \times 10^{-5}$.

photon. Considering the present cavity QED techniques, the iSWAP and the Fredkin gates in the models (11001) and (1001001), respectively, can be good candidates for QIP applications.

Conclusion

Chapter 7

Summary of results

Multi-photon resonance can be a very useful technique for applications in quantum information processing. In this thesis, we use the theory of multi-photon resonance with a multi-level multi-photon Jaynes-Cummings model. Information is stored in photonic qubits and we produce a set of practical one-qubit, two-qubit, and even three-qubit gates. The effective two-level Hamiltonian procedure of Shore predicts the proper values for the sensitive detunings needed for resonance. Since Shore's theory does not ensure an entire population inversion in the systems of interest, in particular, when dealing with complex Hamiltonians, I have employed the spin-J model to provide the appropriate values for the effective couplings required so that periodic multi-photon resonances can be realized.

The main point in Shore's method is to split the eigenvalues of the RWA Hamiltonians into small and large eigenvalues. This is possible by setting large values for either certain detunings (for non-resonant systems) or the couplings (for completely resonant systems) in a number of levels. Levels with large eigenvalues can be isolated and the probabilities in the system can then be highly confined in the state space with small eigenvalues. Using one of Shore's previous methods, generally speaking, produces a long time for the transitions in the effective multi-level systems. I have successfully combined two of Shore's methods and have noticed better results can be found by generating small and fast effective systems; such an example can be found in section 5.6.

The first step in this thesis was to find fast multi-qubit gates. The multi-photon resonance theory mentioned above has been used. The results showed that the iSWAP gate can be realized by another different configuration (note that authors in [56] found that the iSWAP can be realized by a two-level configuration (10001)) and the speed of the gate can be significantly improved (see section 4.8). More precisely, the improvement in the speed of the iSWAP operation can be clearly addressed when considering the expressions

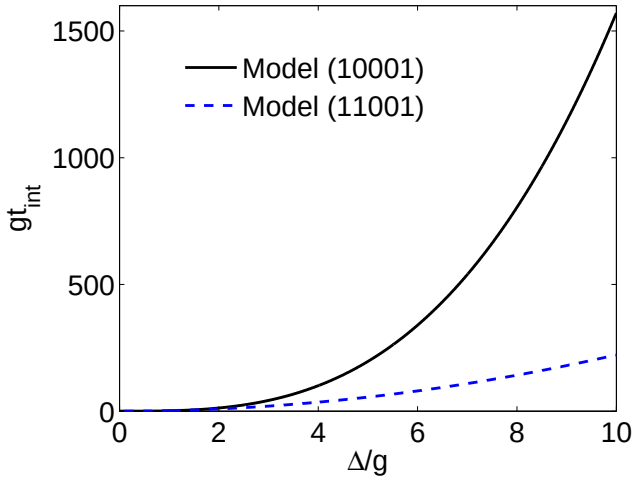

Figure 7.1: The interaction time in the models of the iSWAP gate, namely the models (10001) and (11001).

of the interaction times for the models (10001) and (11001) (see Secs. 4.3, 4.4.2). Figure 7.1 demonstrates that the operation time in the model (10001) is much longer than the interaction time needed by the model (11001). In the case of the Fredkin gate, on the other hand, we conclude that, and depending on our procedure, the configuration of the Fredkin gate realized in [56] is the only possible model (see Sec. 5.8).

Secondly, the fidelity in different configurations for both the iSWAP and Fredkin gates has been numerically measured when variations in some experimentally important parameters have been considered. It is noticed that our gates are not fragile and high fidelity can be observed. Obviously, in the Fredkin gate, which has a larger Hilbert space compared to the space of the iSWAP gate, detuning values needed for high fidelity are larger in magnitude than those ones in the iSWAP gate.

The last point in this thesis is to study the influence of the decoherence processes on the performance of the operations of interest. For this purpose, I have used Liouville's equation to address the impacts of atomic and photonic relaxations on our gates. In order to have a deep understanding I have applied the wave-function approach to the decoherence processes in the qubit states $|a\ 10\rangle$ from the iSWAP and $|a\ 101\rangle$ from the Fredkin gates. These two examples provide a good explanation for the results given by the master equation method. The main results show that for the iSWAP and Fredkin gates realized by three-level configurations, these operations can have the same sensitivity to the atomic decay rate, but the Fredkin gate is more sensitive to the photonic decay rate. Considering the present cavity-QED techniques, these gates are good candidates for applications in

QIP.

The theory of periodic multi-photon resonance developed in this thesis is a general technique and can be employed in different applications in the subject of light-matter interactions. Moreover, the dual-rail cavity-QED scheme discussed here has produced practical logic gates. The scheme proposed in this thesis may still be a challenge for the recent CQED techniques. We hope, with the current developments in resonator systems, that it may be possible to see in the near future the interaction between a multi-level atom with a multi-mode cavity field realized in the laboratory.

Part IV

Appendix

Appendix A

The quantization of a single-mode cavity field

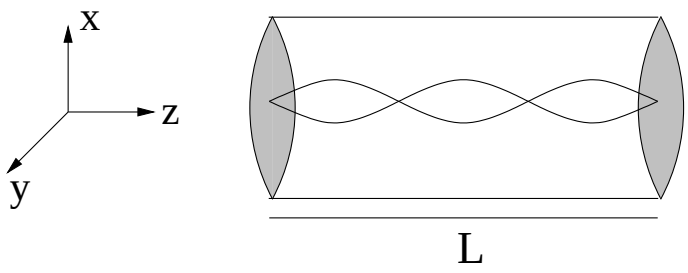

Figure A.1: One-dimensional cavity with perfectly conducting mirrors. The electric field is polarized along the x axis. The propagation of the EM field is along the z-direction.

In chapter 1, we directly introduce the expressions describing the field Hamiltonian $\hat{H}_F$ and the electric field operator $\hat{E}$ for a quantized mode in a cavity. For a completeness, we here discuss the procedure of quantization of the field.
The starting point in our discussion is the classical Maxwell equations given by [94]

$$\begin{aligned} \nabla \times \mathrm{E} &= -\frac{\partial \mathrm{B}}{\partial t} \ , \\ \nabla \times \mathrm{B} &= \mu_0 \mathrm{J} + \mu_0 \epsilon_0 \frac{\partial \mathrm{E}}{\partial \mathrm{t}} \ , \\ \nabla \ . \ \mathrm{E} &= \rho/\epsilon_0 \ , \\ \nabla \ . \ \mathrm{B} &= 0 \ , \end{aligned} \tag{A.1}$$

where E and B are the electric and the magnetic fields, and J and ρ are the densities of the currents and charges. By setting $\mathrm{J} = \rho = 0$ (i.e. at the absence of any sources of radiation) and using the second derivative [94] $\nabla \times (\nabla \times \mathrm{E}) = \nabla.(\nabla.\mathrm{E}) - \nabla^2 \mathrm{E}$, the wave

equation for the electric field can be

$$\nabla^2 \, \mathrm{E} = \mu_0 \epsilon_0 \frac{\partial^2}{\partial \, \mathrm{t}^2} \, \mathrm{E} \, . \tag{A.2}$$

Assuming the radiation field to be confined to a 1D cavity and polarized along the x-direction with the z-direction for the wave propagation (see Fig. A.1), the following solution satisfies the previous wave equation and satisfies the boundary conditions ($\mathrm{E}(\mathrm{z} = 0) = \mathrm{E}(\mathrm{z} = \mathrm{L}) = 0$)

$$\mathrm{E_x}(\mathrm{z}, \mathrm{t}) = \mathrm{E}_0 \, \sin(\omega \mathrm{t}) \, \sin(\mathrm{kz}) \, , \tag{A.3}$$

with ω and k are the frequency and the wavevector of the field. From the second Maxwell equation, the associated magnetic field can be obtained by using $\frac{\partial}{\partial z}\mathrm{B_y}(\mathrm{z}, \mathrm{t}) = -\mu_0 \epsilon_0 \frac{\partial}{\partial \mathrm{t}} \mathrm{E_x}(\mathrm{z}, \mathrm{t})$. One then finds

$$\mathrm{B_y} = \frac{\mathrm{E}_0}{\mathrm{c}} \, \cos(\mathrm{kz}) \, \cos(\omega \mathrm{t}) \, , \tag{A.4}$$

where $\mu_0 \epsilon_0 = \frac{1}{c^2}$ and $\omega = c\mathrm{k}$. The energy stored in the field inside the cavity with the volume V can be given by

$$\mathrm{U} = \frac{1}{2} \left[\int_{\mathrm{V}} \left(\epsilon_0 \, \mathrm{E_x^2}(\mathrm{z}, \mathrm{t}) + \frac{1}{\mu_0} \mathrm{B_y^2}(\mathrm{z}, \mathrm{t}) \right) \mathrm{dV} \right] . \tag{A.5}$$

Since the field is confined within the cavity, the field is said to have standing waves (i.e. we have nodes at $z = 0$ and $z = L$). Now by substituting the electric and magnetic fields in Eqs. (A.3, A.4) into Eq. (A.5) and then integrating over the cavity V, the field energy carried by either the electric field U_E or by the magnetic field U_M are

$$\mathrm{U_E} = \frac{1}{4} \epsilon_0 \mathrm{V} \mathrm{E}_0^2 \, \sin^2(\omega \mathrm{t}) \, , \quad \mathrm{U_M} = \frac{1}{4\mu_0} \mathrm{V} \mathrm{B}_0^2 \cos^2(\omega \mathrm{t}) \, . \tag{A.6}$$

Light is a wave, and the phenomena of waves can be related to the harmonic oscillators [3, 79]. One then can say that the classical field energy defined by U is formally equivalent to the energy of a harmonic oscillator. The Hamiltonian for a harmonic oscillator with a mass m and frequency ω is

$$\hat{H} = \frac{1}{2\mathrm{m}} (\mathrm{p}^2 + (\mathrm{m}\omega \mathrm{q})^2) \, , \tag{A.7}$$

where p and q are operators satisfying the commutation relation $[\mathrm{q}, \mathrm{p}] = \mathrm{i}\hbar$. By setting the one-dimensional harmonic potential (i.e. the second term in Eq. (A.7)) to be equivalent to the field energy carried by the electric field $\hat{\mathrm{U}}_\mathrm{E}$ and assuming the kinetic energy of the oscillator to be equal to the magnetic field energy $\hat{\mathrm{U}}_\mathrm{M}$, one finds (with the help of Eqs. (A.3, A.4))

$$\mathrm{E_x}(\mathrm{z}, \mathrm{t}) = \sqrt{\frac{2\mathrm{m}\omega^2}{\epsilon_0 \mathrm{V}}} \, \mathrm{q} \, \sin(\kappa \mathrm{z}) \, , \quad \mathrm{B_y}(\mathrm{z}, \mathrm{t}) = \sqrt{\frac{2\mu_0}{\mathrm{mV}}} \, \mathrm{p} \, \cos(\kappa \mathrm{z}) \, . \tag{A.8}$$

Traditionally, we define the unitless operators

$$\hat{a}^\dagger \rightarrow \frac{1}{\sqrt{2\mathrm{m}\hbar\omega}}(-\mathrm{ip} + (\mathrm{m}\omega\mathrm{q})) \ , \quad \hat{\mathrm{a}} \rightarrow \frac{1}{\sqrt{2\mathrm{m}\hbar\omega}}(\mathrm{ip} + (\mathrm{m}\omega\mathrm{q})) \ . \tag{A.9}$$

From the previous operators $\hat{a}$ and $\hat{a}^\dagger$, one finds that

$$\hat{a}^\dagger\hat{a} = \frac{1}{\hbar\omega}(\mathrm{H} - \frac{1}{2}\hbar\omega) \ , \quad (\hat{\mathrm{a}}^\dagger + \hat{\mathrm{a}}) = \frac{2\mathrm{m}\omega}{\sqrt{2\mathrm{m}\hbar\omega}}\ \mathrm{q} \ , \quad (\hat{\mathrm{a}}^\dagger - \hat{\mathrm{a}}) = -\mathrm{i}\frac{2}{\sqrt{2\mathrm{m}\hbar\omega}}\ \mathrm{p} \ . \tag{A.10}$$

The field Hamiltonian $\hat{H}_\mathrm{F}$, the electric field $\mathrm{E_x}$, and the magnetic field $\mathrm{B_y}$ for a single mode inside a cavity V are

$$\hat{H}_\mathrm{F} = \hbar(\hat{a}^\dagger\hat{a} + \frac{1}{2}) \ , \tag{A.11}$$

$$\hat{\mathrm{E}}_x(z,t) = \sqrt{\frac{\hbar\omega}{\epsilon_0 V}}\ (\hat{a}^\dagger + \hat{a})\ \sin(\kappa z) \ , \tag{A.12}$$

$$\hat{\mathrm{B}}_y(z,t) = \frac{\mathrm{i}}{c}\sqrt{\frac{\hbar\omega}{\epsilon_0 V}}(\hat{a}^\dagger - \hat{a})\ \cos(\kappa z) \ . \tag{A.13}$$

Appendix B

Single qubit unitary gate

So far, we have seen that two- and three-qubit gates can be formed in the dual-rail cavity-QED scheme. In this appendix we discuss the realization of two single-qubit gates, namely the Pauli X and Z gates.

B.1 The single-qubit phase gate

Starting with the Pauli Z gate, this gate can be easily realized by our qubits [56]. Generally speaking, the atom-cavity interaction in the Jaynes-Cummings model shows that for an atom in the ground state $|g\rangle$ interacting with a single mode having n photon (see Sec. 1.3.1)

$$|g,n\rangle \mapsto \cos(g\sqrt{n})|g,n\rangle - \mathrm{i}\sin(\mathrm{g}\sqrt{\mathrm{n}})|\mathrm{e},\mathrm{n}-1\rangle \ .$$

This is the case when the frequencies of the atomic transitions and the mode are equally matched (i.e. the resonance case $\omega_{eg} = \omega$). In the case of very large detuning ($\Delta >> g$), on the other hand, the system remains in its initial state and a phase shift can be produced as [95]

$$|g,n\rangle \mapsto e^{\mathrm{i}\Phi(\mathrm{n})}|g,n\rangle \ , \tag{B.1}$$

with $\Phi(n)$ can be expressed as [95]

$$\Phi(n) = \frac{\Delta}{2v}\int_0^L dz\left[\sqrt{1+n\left(\frac{g(z)}{\Delta/2}\right)^2}-1\right] , \tag{B.2}$$

where v is the velocity of the atom passing through a cavity, L is the cavity length, and $g(z)$ is the coupling constant which in our case is independent of z. By setting $n = 0$ nothing happens, but with a cavity being initially in the number state $|1\rangle$ (i.e. there is

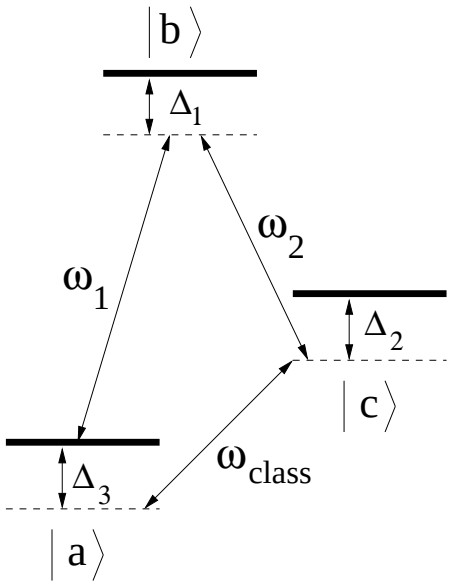

Figure B.1: The model for a single-qubit Pauli-X gate.

$n = 1$ photon) the phase gates G can be produced and the rotation operator R_z can be used (see Sec. 2.2.1).

In the case of two modes inside the cavity interacting with an atom in the ground state $|a\rangle$, such a case in the dual-rail qubits $|a\ 10\rangle$ and $|a\ 01\rangle$, the previous argument can be followed to introduce a phase shift [56]. That is, we can set a large detuning between the atom and, say the first mode, and set a very high detuning between the atom and the second mode. In this case, if the excitation is in the first mode, one finds $|a\ 10\rangle \mapsto e^{\mathrm{ig}^2\mathrm{t}/\Delta}|a\ 10\rangle$; otherwise, $|a\ 01\rangle \mapsto |a\ 01\rangle$.

B.2 The NOT gate

The single-qubit NOT gate is another operation which can be realized by our scheme [56]. Considering the model in Fig. *B.1*, we assume a de-excited three-level atom in the Λ configuration interacts with a dual-rail photonic qubit $|10\rangle$ or $|01\rangle$. The initial state, therefore, can be either $|a\ 10\rangle$ or $|a\ 01\rangle$. Then, the atom interacts with a classical field on the transition $|c\rangle \mapsto |a\rangle$. The corresponding Hamiltonian describing all such interactions, i.e. the cavity-atom interaction plus the classical field-atom interaction, can be defined as

$$\begin{aligned} \hat{H} &= \omega_a\hat{\sigma}_{aa} + \omega_b\hat{\sigma}_{bb} + \omega_c\hat{\sigma}_{cc} + \omega_1\hat{a}_1^\dagger\hat{a}_1 + \omega_2\hat{a}_2^\dagger\hat{a}_2 \\ &+ \left[g_1\hat{a}_1^\dagger\hat{\sigma}_{ab} + g_2\hat{\sigma}_{bc}\hat{a}_2 + (\Omega/2)\hat{\sigma}_{ac}e^{\mathrm{i}\omega_3\mathrm{t}} + \mathrm{H.C.}\right]. \end{aligned} \tag{B.3}$$

In the interaction picture, the RWA Hamiltonian can be reexpressed as

$$\hat{H}' = \begin{bmatrix} (\Delta_2 - \Delta_3) & \Omega/2 & 0 & 0 & 0 \\ \Omega/2 & 0 & g_1 & 0 & 0 \\ 0 & g_1 & \Delta_1 & g_2 & 0 \\ 0 & 0 & g_2 & \Delta_2 & \Omega/2 \\ 0 & 0 & 0 & \Omega/2 & \Delta_3 \end{bmatrix} , \tag{B.4}$$

where $\hat{H}'$ acts in the basis $\{|c\ 10\rangle\,|a\ 10\rangle, |b\ 00\rangle, |c\ 01\rangle, |a\ 01\rangle\}$. Now the basis states other than $|a\ 10\rangle$ and $|a\ 01\rangle$ can be adiabatically eliminated by recalling Shore's method. That is, we allow large values for $\Delta_1,\ \Delta_2$. In the language of this thesis, we assume the states $|a\ 10\rangle$ and $|a\ 01\rangle$ to be spanned by the space $\mathbb{P}$ and the remaining states to be set in the space of $\mathbb{Q}$. The resultant operators, then, can be given as

$$\hat{H}_0 = \begin{bmatrix} 0 & 0 \\ 0 & \Delta_3 \end{bmatrix} ; \hat{A} = \begin{bmatrix} (\Delta_2 - \Delta_3) & 0 & 0 \\ 0 & \Delta_1 & g_2 \\ 0 & g_2 & \Delta_2 \end{bmatrix} ; \hat{B} = \begin{bmatrix} \Omega/2 & g_1 & 0 \\ 0 & 0 & \Omega/2 \end{bmatrix} . \tag{B.5}$$

The corresponding effective detuning and coupling constant with $\Delta_{1,2} >> g_{1,2}, \Omega/2, \Delta_3$ are

$$\hat{H}_{\text{eff}} = \Delta_3 - \frac{(\Omega/2)^2\Delta_1}{(\Delta_1\Delta_2 - g_2^2)} + \frac{(\Omega/2)^2}{(\Delta_2 - \Delta_3)} + \frac{g_1^2\Delta_1}{(\Delta_1\Delta_2 - g_2^2)} \approx \Delta_3 + \frac{g_1^2}{\Delta_2} , \tag{B.6}$$

and

$$g_{\text{eff}} = \frac{(\Omega/2)g_1g_2}{(\Delta_1\Delta_2 - g_2^2)} \approx \frac{\Omega\ g_1g_2}{2\Delta_1\Delta_2} . \tag{B.7}$$

At the resonance condition, the time evolution of the initial state $|a\ 10\rangle$ or $|a\ 01\rangle$ can be given by Eq. (4.9), and with appropriate interaction time $g_{\text{eff}}t_{int}$ and a global phase the Pauli X gate can be easily realized. In Sec. 2.2.1, the exponential of the NOT gate is nothing but the rotation operator $\mathrm{R_x(g_{eff}t)}$.

Appendix C

Derivation of Eqs. (3.6) and (6.21)

C.1 Derivation of Eq. (3.6)

In Sec. 3.1 we have seen that the partition of a system $|\Psi(t)\rangle$ into two subsystems spanned by the projector operators $\mathbb{P}$ and $\mathbb{Q}$ yields $|\Psi(t)\rangle = \mathbb{P}|\Psi(t)\rangle + \mathbb{Q}|\Psi(t)\rangle$, where $\mathbb{P}+\mathbb{Q}=1$, $\mathbb{PQ}=\mathbb{QP}=0$, $\mathbb{PP}=\mathbb{P}$, and $\mathbb{QQ}=\mathbb{Q}$. By setting the space $\mathbb{P}$ to contain only the states that are either on- or near-resonance and in terms of Laplace transform

$$\mathbb{P}|\Psi(t)\rangle \;=\; \frac{1}{2\pi i}\int dz\; e^{-izt}\;\mathbb{P}\;\hat{G}(z)\;|\Psi(0)\rangle\;. \tag{C.1}$$

The effective Hamiltonian describing the system $\mathbb{P}|\Psi(t)\rangle$ can be found as follows. In order to find $\mathbb{P}G(z)$, we follow the traditional operator algebra in [54]. Since $\mathbb{P}+\mathbb{Q}=1$, one can rewrite Eq. (3.4) as

$$(z\hat{I}-\hat{H})(\mathbb{P}+\mathbb{Q})\hat{G}(z) = \mathbb{P}+\mathbb{Q}\;. \tag{C.2}$$

Then taking the effect of $\mathbb{P}$ alone from the right on the previous equation yields

$$\mathbb{P} = (z\hat{I}-\hat{H})[\mathbb{P}\hat{G}(z)\mathbb{P}+\mathbb{Q}\hat{G}(z)\mathbb{P}]\;. \tag{C.3}$$

In order to find the expression of $\mathbb{Q}\hat{G}(z)\mathbb{P}$ in the last equation, one allows $\mathbb{Q}$ acting from the left. This leads to

$$\mathbb{Q}\hat{G}(z)\mathbb{P} = -\mathbb{Q}[\mathbb{Q}(z\hat{I}-\hat{H})\mathbb{Q}]^{-1}\mathbb{Q}(z\hat{I}-\hat{H})\mathbb{P}\hat{G}(z)\mathbb{P}\;. \tag{C.4}$$

Substituting Eq. (C.4) into Eq. (C.3) gives the next expression for $\mathbb{P}\hat{G}(z)\mathbb{P}$ as

$$\mathbb{P}\hat{G}(z)\mathbb{P} = \mathbb{P}\Big(\mathbb{P}(z\hat{I}-\hat{H})\mathbb{P}-\mathbb{P}(z\hat{I}-\hat{H})\mathbb{Q}[\mathbb{Q}(z\hat{I}-\hat{H})\mathbb{Q}]^{-1}\mathbb{Q}(z\hat{I}-\hat{H})\mathbb{P}\Big)^{-1}\mathbb{P}\;. \tag{C.5}$$

Finally, by letting the operators act inside the brackets one finds that

$$\mathbb{P}(z\hat{I}-\hat{H})^{-1}=\mathbb{P}\Big(z\hat{I}-\mathbb{P}\hat{H}\mathbb{P}-\mathbb{P}\hat{H}\mathbb{Q}[z\hat{I}-\mathbb{Q}\hat{H}\mathbb{Q}]^{-1}\mathbb{Q}\hat{H}\mathbb{P}\Big)^{-1}\ . \tag{C.6}$$

This implies that $\mathbb{P}\hat{G}(z)=\hat{\tilde{G}}(z)=(z\hat{I}-\hat{H}_{\text{eff}})^{-1}$ with $\hat{H}_{\text{eff}}=\mathbb{P}\hat{H}\mathbb{P}+\mathbb{P}\hat{H}\mathbb{Q}[z\hat{I}-\mathbb{Q}\hat{H}\mathbb{Q}]^{-1}\mathbb{Q}\hat{H}\mathbb{P}$. Replacing $\hat{G}(z)$ by $\hat{\tilde{G}}(z)$ in the previous Integral transform shows that the singularities are the eigenvalues of the effective Hamiltonian $\hat{H}_{\text{eff}}$. By following [46], we define $\mathbb{P}\hat{H}\mathbb{P}=\hat{H}_0$, $\mathbb{P}\hat{H}\mathbb{Q}=\hat{B}$, and $\mathbb{Q}\hat{H}\mathbb{Q}=\hat{A}$ so that

$$\hat{H}_{\text{eff}}=\hat{H}_0+\hat{B}\ \frac{1}{(z\hat{I}-\hat{A})}\ \hat{B}^{\dagger}\ . \tag{C.7}$$

Previously, there is no consideration for the decoherence process. In chapter 6, we show that the preceding operator algebra can be expanded for a damped $\mathbb{P}|\Psi(t)\rangle$.

C.2 Derivation of Eq. (6.21)

We now seek to represent Liouville's equation in Eq. (6.9) in terms of the effective Hamiltonian $\hat{H}'$ (6.20). By recalling Liouville's equation, one then can rewrite this equation as

$$\frac{\partial}{\partial t}\rho=-\mathrm{i}(\hat{\mathrm{H}}\rho-\rho\hat{\mathrm{H}})-\frac{1}{2}\sum_{\mathrm{i}}\eta_{(\mathrm{i})}(\hat{\mathrm{L}}^{\dagger}_{(\mathrm{i})}\hat{\mathrm{L}}_{(\mathrm{i})}\rho+\rho\hat{\mathrm{L}}^{\dagger}_{(\mathrm{i})}\hat{\mathrm{L}}_{(\mathrm{i})})+\hat{\mathrm{J}}\rho\ . \tag{C.8}$$

Now we consider the following rearrangement of terms in the previous equation

$$\begin{aligned}\frac{\partial}{\partial t}\rho &= -\mathrm{i}\hat{\mathrm{H}}\rho-\frac{1}{2}\sum_{\mathrm{i}}\eta_{(\mathrm{i})}\hat{\mathrm{L}}^{\dagger}_{(\mathrm{i})}\hat{\mathrm{L}}_{(\mathrm{i})}\rho+\mathrm{i}\rho\hat{\mathrm{H}}-\frac{1}{2}\sum_{\mathrm{i}}\eta_{(\mathrm{i})}\rho\hat{\mathrm{L}}^{\dagger}_{(\mathrm{i})}\hat{\mathrm{L}}_{(\mathrm{i})}+\hat{\mathrm{J}}\rho\ ,\\ &= -\mathrm{i}(\hat{\mathrm{H}}-\mathrm{i}\frac{1}{2}\sum_{\mathrm{i}}\eta_{(\mathrm{i})}\hat{\mathrm{L}}^{\dagger}_{(\mathrm{i})}\hat{\mathrm{L}}_{(\mathrm{i})})\ \rho+\mathrm{i}\rho\ (\hat{\mathrm{H}}+\mathrm{i}\frac{1}{2}\sum_{\mathrm{i}}\eta_{(\mathrm{i})}\hat{\mathrm{L}}^{\dagger}_{(\mathrm{i})}\hat{\mathrm{L}}_{(\mathrm{i})})+\hat{\mathrm{J}}\ \rho\ .\end{aligned} \tag{C.9}$$

By defining $\hat{H}'=\hat{H}-\frac{\mathrm{i}}{2}\sum_{i}\eta_{(i)}\hat{L}^{\dagger}_{(i)}\hat{L}_{(i)}$, it is easy to find that

$$\frac{\partial}{\partial t}\rho=-\mathrm{i}(\hat{\mathrm{H}}'\ \rho-\rho\ \hat{\mathrm{H}}'^{\dagger})+\hat{\mathrm{J}}\ \rho\ . \tag{C.10}$$

This master equation is nothing but the previous Liouville's equation. However, this equation gives another insight and shows that the time evolution of a system ρ is affected by two operations: the processes in the Hamiltonian $\hat{H}'$ and the contributions by the quantum jump superoperator $\hat{J}\rho$. In the case of the quantum jump events taking place out of a system of interest, the time evolution of this system can be simply governed by the amplitude equation $\frac{\partial}{\partial t}|\Psi(t)\rangle=-\mathrm{i}\hat{\mathrm{H}}'\mathrm{t}\ |\Psi(\mathrm{t})\rangle$. This was the case in some of the quantum systems discussed in chapter 6 and analytical solutions have been found.

Appendix D

Comments on codes

All numerical solutions have been obtained by using MATLAB packages. Amongst the different Matlab functions used throughout this thesis, I want here to focus on three Matlab functions: the ode45, sparse, and interp1 functions.

The time evolution of different quantum systems was calculated by Liouville's equation in the presence or absence of decoherence processes. In order to solve the differential equations we recall the Matlab function "ode45". This solver is based on the Runge-Kutta method which requires a medium order of accuracy. In most cases, we use a tolerance in order of 10^{-3}, except when we consider the dissipation processes in the Fredkin gate where we raise the tolerance to $10^{-9} - 10^{-12}$.

Since working in Liouville space requires larger Hilbert space (if the Hilbert space dimension is N, the density matrix has N^2 elements, and its propagator is a $N^2 \times N^2$ matrix, instead of a $N \times N$ matrix for the wave function), we employ the Matlab function "sparse". This function turns a full matrix, which contains zero and non-zero elements, into the sparse form where all vanishing elements are compressed. This function helps to speed up the calculations and to save more space for memory.

In fidelity calculations, the evolution of the density matrix is carried out under the boundary conditions, and at certain values of time, the density matrix for a state of interest is picked up. To this end, we employ the Matlab function "interp1", which works as a one-dimensional data interpolation. More precisely, with a vector of the time running from zero to a maximum value and with another vector containing the corresponding density matrix for the whole system, this function finds the density matrix for a certain state at a certain time. Then, we repeat the same procedure for different values of detuning. We can use this function in calculations of FWHM, as well.

Appendix E

List of academic contributions

- A paper is submitted:
  Moteb M. Alqahtani, Mark S. Everitt, and Barry M. Garraway,"Cavity QED Photons for Quantum Information Processing", arXiv:1407.0654 [quant-ph].

- A poster is presented:
  All optical quantum logic with multi-mode cavities, International Symposium on Cavity QED, Sussex University, 11-12 June 2012.

- A seminar is given:
  Multi-photon resonances in cavity QED, Sussex University, 16 May 2014, United Kingdom.

Bibliography

[1] H. Mabuchi and A. C. Doherty. Cavity Quantum Electrodynamics: Coherence in Context. *Science*, 298(5597):1372–1377, 2002.

[2] H. Walther, B. T. H. Varcoe, B. G. Englert, and T. Becker. Cavity quantum electrodynamics. *Rep. Prog. Phys.*, 69(5):1325, 2006.

[3] C. C. Gerry and P. L. Knight. *Introductory quantum optics*. Cambridge University Press, Cambridge, 2005.

[4] S. J. van Enk, H. J. Kimble, and H. Mabuchi. Quantum Information Processing in Cavity-QED. *Quantum Information Processing*, 3(1-5):75–90, 2004.

[5] H. P. Specht, C. Nölleke, A. Reiserer, M. Uphoff, E. Figueroa, S. Ritter, and G. Rempe. A single-atom quantum memory. *Nature*, 473:190193, 2011.

[6] S. Kuhr, S. Gleyzes, C. Guerlin, J. Bernu, U. B. Hoff, S. Deléglise, S. Osnaghi, M. Brune, J. M. Raimond, S. Haroche, E. Jacques, P. Bosland, and B. Visentin. Ultrahigh finesse Fabry-Pérot superconducting resonator. *Appl. Phys. Lett.*, 90:164101, 2007.

[7] B. W. Shore and P. L. Knight. The Jaynes-Cummings model. *J. Mod. Opt.*, 40(7):1195–1238, 1993.

[8] J. M. Raimond, M. Brune, and S. Haroche. Manipulating quantum entanglement with atoms and photons in a cavity. *Rev. Mod. Phys.*, 73(3):565–582, 2001.

[9] A. Reiserer, C. Nölleke, S. Ritter, and G. Rempe. Ground-State Cooling of a Single Atom at the Center of an Optical Cavity. *Phys. Rev. Lett.*, 110(22):223003, 2013.

[10] S. Ritter, C. Nölleke, C. Hahn, A. Reiserer, A. Neuzner, M. Uphoff, M. Mücke, E. Figueroa, J. Bochmann, and G. Rempe. An elementary quantum network of single atoms in optical cavities. *Nature*, 484:195200, 2012.

[11] J. Leppäkangas, S. E. de Graaf, A. Adamyan, M. Fogelström, A. V. Danilov, T. Lindström, S. E. Kubatkin, and G. Johansson. Effects of quasiparticle tunnelling in a circuit-QED realization of a strongly driven two-level system. *J. Phys. B: At. Mol. Opt. Phys.*, 46(22):224019, 2013.

[12] E. T. Jaynes and F. W. Cummings. Comparison of quantum and semiclassical radiation theories with application to the beam maser. *Proc. IEEE*, 51(1):89–109, 1963.

[13] M. O. Scully and M.S. Zubairy. *Quantum optics*. Cambridge University Press, Cambridge, 2002.

[14] R. Loudon. *The quantum theory of light*. Oxford University Press, 3 edition, 2000.

[15] P. Lambropoulos and D. Petrosyan. *Fundamentals of quantum optics and quantum information*. Springer-Verlag Berlin Heidelberg, 2007.

[16] S. M. Barnett and P. M. Radmore. *Methods in theoretical quantum optics*. Clarendon, Oxford, 2002.

[17] B. W. Shore. *The theory of coherent atomic excitation*, volume 1. John Wiley & Sons., 1990.

[18] D. J. Griffiths. *Introduction to quantum mechanics*. Pearson Prentice Hall, 2 edition, 2005.

[19] R. J. Glauber. Coherent and Incoherent States of the Radiation Field. *Phys. Rev.*, 131(6):2766–2788, 1963.

[20] J. H. Eberly, N. B. Narozhny, and J. J. Sanchez-Mondragon. Periodic Spontaneous Collapse and Revival in a Simple Quantum Model. *Phys. Rev. Lett.*, 44(20):1323–1326, 1980.

[21] D. Deutsch. Quantum Theory, the Church-Turing Principle and the Universal Quantum Computer. *Proc. R. Soc. Lond. A*, 400(1818):97–117, 1985.

[22] D. Deutsch and R. Jozsa. Rapid Solution of Problems by Quantum Computation. *Proc. R. Soc. Lond. A*, 439(1907):553–558, 1992.

[23] P. W. Shor. Polynomial-Time Algorithms for Prime Factorization and Discrete Logarithms on a Quantum Computer. *SIAM J. Comput.*, 26(5):1484–1509, 1997.

[24] L. K. Grover. Quantum Mechanics Helps in Searching for a Needle in a Haystack. *Phys. Rev. Lett.*, 79(2):325–328, 1997.

[25] S. M. Barnett. *Quantum information.* Oxford University Press, 2009.

[26] M. A. Nielsen and I. L. Chuang. *Quantum computation and quantum information.* Cambridge University Press, Cambridge, 2000.

[27] A. Barenco, C. H. Bennett, R. Cleve, D. P. DiVincenzo, N. Margolus, P. Shor, T. Sleator, J. A. Smolin, and H. Weinfurter. Elementary gates for quantum computation. *Phys. Rev. A*, 52(5):3457–3467, 1995.

[28] D. P. DiVincenzo. Two-bit gates are universal for quantum computation. *Phys. Rev. A*, 51(2):1015–1022, 1995.

[29] D. Deutsch, A. Barenco, and A. Ekert. Universality in Quantum Computation. *Proc. R. Soc. Lond. A*, 449(1937):669–677, 1995.

[30] M. J. Bremner, C. M. Dawson, J. L. Dodd, A. Gilchrist, A. W. Harrow, D. Mortimer, M. A. Nielsen, and T. J. Osborne. Practical Scheme for Quantum Computation with Any Two-Qubit Entangling Gate. *Phys. Rev. Lett.*, 89(24):247902, 2002.

[31] J. A. Jones. Quantum Computing with NMR. *Prog. NMR Spectrosc.*, 59:91–120, 2011.

[32] P. Kok, W. J. Munro, K. Nemoto, T. C. Ralph, J. P. Dowling, and G. J. Milburn. Linear optical quantum computing with photonic qubits. *Rev. Mod. Phys.*, 79(1):135–174, 2007.

[33] T. D. Ladd, F. Jelezko, R. Laflamme, Y. Nakamura, C. Monroe, and J. L. OBrien. Quantum computers. *Nature*, 464:45–53, 2010.

[34] D. Bimberg. Quantum dots for lasers, amplifiers and computing. *J. Phys. D: Appl. Phys.*, 38(13):2055, 2005.

[35] H. Haeffner, C.F. Roos, and R. Blatt. Quantum computing with trapped ions. *Phys. Rep.*, 469:155–203, 2008.

[36] M. V. Gurudev Dutt, Jun Cheng, Bo Li, Xiaodong Xu, Xiaoqin Li, P. R. Berman, D. G. Steel, and A. S. Bracker. Stimulated and Spontaneous Optical Generation of Electron Spin Coherence in Charged GaAs Quantum Dots. *Phys. Rev. Lett.*, 94(22):227403, 2005.

[37] M. Saffman, T. G. Walker, and K. Mølmer. Quantum information with Rydberg atoms. *Rev. Mod. Phys.*, 82(3):2313–2363, 2010.

[38] T. F. Gallagher. *Rydberg atoms.* Cambridge University Press, Cambridge, 1994.

[39] J. M. Raimond, P. Facchi, B. Peaudecerf, S. Pascazio, C. Sayrin, I. Dotsenko, S. Gleyzes, M. Brune, and S. Haroche. Quantum Zeno dynamics of a field in a cavity. *Phys. Rev. A*, 86(3):032120, 2012.

[40] A. D. Boozer, A. Boca, R. Miller, T. E. Northup, and H. J. Kimble. Reversible State Transfer between Light and a Single Trapped Atom. *Phys. Rev. Lett.*, 98(19):193601, 2007.

[41] S. Brattke, B. T. H. Varcoe, and H. Walther. Generation of Photon Number States on Demand via Cavity Quantum Electrodynamics. *Phys. Rev. Lett.*, 86(16):3534–3537, 2001.

[42] B. T. H. Varcoe, S. Brattke, M. Weidinger, and H. Walther. Preparing pure photon number states of the radiation field. *Nature*, 403:743–746, 2000.

[43] M. Hofheinz, E. M. Weig, M. Ansmann, R. C. Bialczak, E. Lucero, M. Neeley, A. D. O'Connell, H. Wang, J. M. Martinis, and A. N. Cleland. Generation of Fock states in a superconducting quantum circuit. *Nature*, 454:310–314, 2008.

[44] D. Meschede, H. Walther, and G. Müller. One-Atom Maser. *Phys. Rev. Lett.*, 54(6):551–554, 1985.

[45] M. Keller, B. Lange, K. Hayasaka, W. Lange, and H. Walther. Continuous generation of single photons with controlled waveform in an ion-trap cavity system. *Nature*, 431:1075–1078, 2004.

[46] B. W. Shore. Two-level behavior of coherent excitation of multilevel systems. *Phys. Rev. A*, 24(3):1413–1418, 1981.

[47] R. J. Cook and B. W. Shore. Coherent dynamics of N-level atoms and molecules. III. An analytically soluble periodic case. *Phys. Rev. A*, 20(2):539–544, 1979.

[48] M. L. Goldberger and K. M. Watson. *Collision theory.* John Wiley & Sons., 1964.

[49] M. L. Boas. *Mathematical Methods in the Physical Sciences.* John Wiley & Sons., 2006.

[50] A. Messiah. *Quantum Mechanics.* North-Holland, 1961.

[51] B. W. Shore. Coherent manipulations of atoms using laser light. *Acta Physica Slovaca*, 58(3):243–486, 2008.

[52] Z. Białynicka-Birula, I. Białynicki-Birula, J. H. Eberly, and B. W. Shore. Coherent dynamics of N-level atoms and molecules. II. Analytic solutions. *Phys. Rev. A*, 16(5):2048–2054, 1977.

[53] V. S. Letokhov and A. A. Makarov. Leakage effect as an exciting mechanism of high vibrational levels of polyatomic molecules by a strong quasi-resonant laser ir field. *Optics Communications*, 17(3):250 – 253., 1976.

[54] B. W. Shore. *The theory of coherent atomic excitation*, volume 2. John Wiley & Sons., 1990.

[55] P. A. Ivanov, E. S. Kyoseva, and N. V. Vitanov. Engineering of arbitrary U(N) transformations by quantum Householder reflections. *Phys. Rev. A*, 74:022323., 2006.

[56] M. S. Everitt and B. M. Garraway. Multiphoton resonances for all optical quantum logic with multiple cavities. arXiv:1407.0239v1 [quant-ph].

[57] D. P. DiVincenzo. The physical implementation of quantum computation. *Fortschr. Phys.*, 48(9-11):771–783, 2000.

[58] J. Kempe, D. Bacon, D. P. DiVincenzo, and K. Whaley. Encoded University from a Single Physical Interaction. *Quantum Inf. Comp.*, 1(4):33–55, 2001.

[59] N. Schuch and J. Siewert. Natural two-qubit gate for quantum computation using the XY-interaction. *Phys. Rev. A*, 67(3):032301, 2003.

[60] T. Tanamoto, Y. X. Liu, X. Hu, and F. Nori. Efficient Quantum Circuits for One-Way Quantum Computing. *Phys. Rev. Lett.*, 102(10):100501, 2009.

[61] H. J. Briegel and R. Raussendorf. Persistent Entanglement in Arrays of Interacting Particles. *Phys. Rev. Lett.*, 86(5):910–913, 2001.

[62] R. Raussendorf and H. J. Briegel. A One-Way Quantum Computer. *Phys. Rev. Lett.*, 86(22):5188–5191, 2001.

[63] R. Raussendorf, D. E. Browne, and H. J. Briegel. Measurement-based quantum computation on cluster states. *Phys. Rev. A*, 68(2):022312, 2003.

[64] P. Walther, K. J. Resch, T. Rudolph, E. Schenck, H. Weinfurter, V. Vedral, Aspelmeyer M., and A. Zeilinger. Experimental one-way quantum computing. *Nature*, 434:169–176, 2005.

[65] I. L. Chuang and Y. Yamamoto. Simple quantum computer. *Phys. Rev. A*, 52(5):3489–3496, 1995.

[66] I. L. Chuang and Y. Yamamoto. Quantum Bit Regeneration. *Phys. Rev. Lett.*, 76(22):4281–4284, 1996.

[67] E. Knill, R. Laflamme, and G. J. Milburn. A scheme for efficient quantum computation with linear optics. *Nature*, 409:46–52, 2001.

[68] M. S. Zubairy, M. Kim, and M. O. Scully. Cavity-QED-based quantum phase gate. *Phys. Rev. A*, 68(3):033820, 2003.

[69] J. T. Chang and M. S. Zubairy. Three-qubit phase gate based on cavity quantum electrodynamics. *Phys. Rev. A*, 77(1):012329, 2008.

[70] J. Shu, X. B. Zou, Y. F. Xiao, and G. C. Guo. Quantum phase gate of photonic qubits in a cavity QED system. *Phys. Rev. A*, 75(4):044302, 2007.

[71] R. Jozsa. Fidelity for Mixed Quantum States. *Journal of Modern Optics*, 41(12):2315–2323, 1994.

[72] B. M. Garraway, B. Sherman, H. Moya-Cessa, P. L. Knight, and G. Kurizki. Generation and detection of nonclassical field states by conditional measurements following two-photon resonant interactions. *Phys. Rev. A*, 49(1):535–547, 1994.

[73] H. Lee, T. Chen, J. Li, K. Y. Yang, S. Jeon, O. Painter, and K. J. Vahala. Chemically etched ultrahigh-Q wedge-resonator on a silicon chip. *Nature Photonics*, 6:369373, 2012.

[74] S. Götzinger, L. de S. Menezes, A. Mazzei, S. Kühn, V. Sandoghdar, and O. Benson. Controlled Photon Transfer between Two Individual Nanoemitters via Shared High-Q Modes of a Microsphere Resonator. *Nano Lett.*, 6(6):11511154, 2006.

[75] E. Fredkin and T. Toffoli. Conservative logic. *International Journal of Theoretical Physics*, 21(3/4):219–253, 1982.

[76] L. Qing and L. Jian. Quantum control gates with weak cross-kerr nonlinearity. *Phys. Rev. A*, 79(2):022301, 2009.

[77] X. Q. Shao, T. Y. Zheng, X. L. Feng, C. H. Oh, and S. Zhang. One-step implementation of the genuine Fredkin gate in high-Q coupled three-cavity arrays. *JOSA B*, 31(4):697–703, 2014.

[78] P. W. Shor. Scheme for reducing decoherence in quantum computer memory. *Phys. Rev. A*, 52(4):R2493–R2496, 1995.

[79] A. M. Fox. *Quantum optics: an introduction*. Oxford University Press, 2006.

[80] W. Langbein, P. Borri, U. Woggon, V. Stavarache, D. Reuter, and A. D. Wieck. Radiatively limited dephasing in InAs quantum dots. *Phys. Rev. B*, 70(3):033301, 2004.

[81] H. J. Kimble. The quantum internet. *Nature*, 453:1023–1030, 2008.

[82] X. Li, Y. Wu, D. Steel, D. Gammon, T. H. Stievater, D. S. Katzer, D. Park, C. Piermarocchi, and L. J. Sham. An All-Optical Quantum Gate in a Semiconductor Quantum Dot. *Science*, 301(5634):809–811, 2003.

[83] G. Khitrova, H. M. Gibbs, M. Kira, S. W. Koch, and A. Scherer. Vacuum Rabi splitting in semiconductors. *Nature*, 2:81 – 90, 2006.

[84] L. Isenhower, E. Urban, X. L. Zhang, A. T. Gill, T. Henage, T. A. Johnson, T. G. Walker, and M. Saffman. Demonstration of a Neutral Atom Controlled-NOT Quantum Gate. *Phys. Rev. Lett.*, 104(1):010503, 2010.

[85] A. Gaëtan, Y. Miroshnychenko, T. Wilk, A. Chotia, M. Viteau, D. Comparat, P. Pillet, A. Browaeys, and P. Grangier. Observation of collective excitation of two individual atoms in the Rydberg blockade regime. *Nature Physics*, 5:115 – 118, 2009.

[86] G. Lindblad. On the generators of quantum dynamical semigroups. *Communications in Mathematical Physics*, 48(2):119–130, 1976.

[87] P. Goy, J. M. Raimond, M. Gross, and S. Haroche. Observation of Cavity-Enhanced Single-Atom Spontaneous Emission. *Phys. Rev. Lett.*, 50(24):1903–1906, 1983.

[88] J. Dalibard, Y. Castin, and K. Mølmer. Wave-function approach to dissipative processes in quantum optics. *Phys. Rev. Lett.*, 68(5):580–583, 1992.

[89] R. Dum, P. Zoller, and H. Ritsch. Monte Carlo simulation of the atomic master equation for spontaneous emission. *Phys. Rev. A*, 45(7):4879–4887, 1992.

[90] K. Mølmer, Y. Castin, and J. Dalibard. Monte Carlo wave-function method in quantum optics. *JOSA B*, 10(3):524–538, 1993.

[91] M. B. Plenio and P. L. Knight. The quantum-jump approach to dissipative dynamics in quantum optics. *Rev. Mod. Phys.*, 70(1):101–144, 1998.

[92] C. K. Law and H. J. Kimble. Deterministic generation of a bit-stream of single-photon pulses. *Journal of Modern Optics*, 44(11):2067–2074, 1997.

[93] S. M. Barnett and J. Jeffers. The damped Jaynes-Cummings model. *Journal of Modern Optics*, 54(13-15):2033–2048, 2007.

[94] D. J. Griffiths. *Introduction to electrodynamics*. Pearson Benjamin Cummings, 3 edition, 2008.

[95] B. G. Englert, M. Löffler, O. Benson, B. Varcoe, M. Weidinger, and H. Walther. Entangled Atoms in Micromaser Physics. *Fortschr. Phys.*, 46(6-8):897–926, 1998.